General Disclaimer

One or more of the Following Statements may affect this Document

- This document has been reproduced from the best copy furnished by the organizational source. It is being released in the interest of making available as much information as possible.

- This document may contain data, which exceeds the sheet parameters. It was furnished in this condition by the organizational source and is the best copy available.

- This document may contain tone-on-tone or color graphs, charts and/or pictures, which have been reproduced in black and white.

- This document is paginated as submitted by the original source.

- Portions of this document are not fully legible due to the historical nature of some of the material. However, it is the best reproduction available from the original submission.

Produced by the NASA Center for Aerospace Information (CASI)

HELICOPTER VIBRATION SUPPRESSION USING
SIMPLE PENDULUM ABSORBERS ON
THE ROTOR BLADE

By

G. Alvin Pierce
and
M-Nabil H. Hamouda

HELICOPTER VIBRATION SUPPRESSION USING
SIMPLE PENDULUM ABSORBERS ON
THE ROTOR BLADE

By

G. Alvin Pierce
and
M-Nabil H. Hamouda

CONTENTS

SUMMARY

A comprehensive analytical design procedure for the installation of simple pendulums on the blades of a helicopter rotor to suppress the root reactions is presented. To achieve this goal, a frequency response analysis is conducted of typical rotor blades excited by a harmonic variation of spanwise airload distributions as well as a concentrated load at the tip.

The structural modeling of the blade includes elastic degrees of freedom in flap and lead-lag bending plus torsion with a hingeless hub constraint. Simple pendulum absorbers are individually considered for both flap and lead-lag types of motion. The inertial reaction forces and moments at the pendulum hinge are formulated. On the basis of a rational ordering scheme the general nonlinear equations of motion for the rotor-pendulum system are linearized in the perturbation elastic blade displacements and pendulum angle. These linearized equations include the effects of spanwise airload distributions associated with the elastic deformations and the cyclic pitch environment of forward flight. A quasi-steady aerodynamic representation is utilized in the formation of these airloads. The solution of the system equations is based on their representation as a transfer matrix.

The numerical results presented here pertain to both uniform and nonuniform hingeless rotor blades. These results include the effect of pendulum tuning on the minimization of the hub reactions. It is found that a properly designed flapping pendulum attenuates the root out-of-plane force and moment whereas the optimum designed lead-lag pendulum attenuates the root in-plane reactions. A properly tuned pendulum can attenuate the vibratory loads by generating appropriate forces at its attachment point with the blade. These forces redistribute the loads on the blade so that only a small portion of the reactions are transmitted to the hub.

For optimum pendulum tuning the parameters to be determined are the pendulum uncoupled natural frequency, the pendulum spanwise location and its mass. It is found that the optimum pendulum frequency is in the vicinity of the excitation frequency. In the case of an off-tuned pendulum the result can be either a slight-to-moderate degradation in pendulum absorber effectiveness or a drastic increase in hub reactions. Although the uncoupled natural frequency of the pendulum is independent of the mass of the pendulum, a proper choice of the mass is required to generate an optimum force to attenuate the root reactions.

A pendulum can be tuned and its optimum mass determined by excitation with a concentrated simple harmonic load at the tip. However, it is necessary to utilize distributed airloads to accurately determine the attenuation of the root reactions. The damping at the pendulum hinge has a small effect on the hub reactions once the optimum pendulum tuning is established. For the optimum pendulum a parametric study is conducted. The parameters varied include prepitch, pretwist, precone and pendulum hinge offset.

INTRODUCTION

Vibration has always been a significant detriment to helicopters which is not surprising in view of the fact that a major percentage of a helicopter's mass consists of rotating components such as engines, rotors, gearboxes and drives. These revolve at different frequencies, though most are multiples or submultiples of the main rotor frequency, and any out-of-balance forces are easily transmitted to the light airframe. There is also the possibility of damaging beat frequencies arising in those few cases where rotational rates are not synchronous.

In addition to the inertially induced vibrations, the unsteady air loads on the main and auxiliary rotors significantly contribute to the vibratory environment. These unsteady aerodynamic reactions are caused by the local periodic dynamic pressure on the main rotor blades in forward flight and the cyclic pitch changes imposed by the rotor head. In response to these unsteady loads the elastic blades are continually deforming which induces additional unsteady aerodynamic loading.

An increasing demand for the reduction of helicopter vibration has been dictated by the expansion of flight envelopes coupled with more stringent requirements for crew and passenger comfort as well as improved reliability and maintainability.

The rotor system, which transmits the vibratory airloads to the fuselage through the rotor shaft, is one of the most significant contributors to the vibrations of the helicopter. The rotating blades create vibratory airloads containing all harmonics of the rotor rotational frequency. As the loads from the individual blades combine at the rotor hub, some harmonics cancel each other while others are additive. The loads that are additive are passed from the blades to the pylon and then to the cabin through complicated dynamic load paths. These loads are felt as vibratory forces and moments whose frequencies are integer multiples of the blade passage frequency (number of blades times rotational frequency).

Dynamic systems that reduce the vibration in helicopters may be classified into five groups:

(1)	Excitation reducers	(blade aerodynamics)
(2)	Attenuators	(blade dynamics with or without hub motion)
(3)	Absorbers	(hub dynamics)
(4)	Isolators	(pylon dynamics)
(5)	Cabin Suppressors	(fuselage dynamics)

These systems are described below and specific examples are given.

Excitation reducers are devices that either reduce aerodynamic forces on the blades, or alter the hub moments and shears by generating counter-influencing aerodynamic forces on the blades. Higher harmonic blade pitch control devices (ref. 1) fall into this category. In reference 1 a wind tunnel test has been used to evaluate higher harmonic blade pitch for the reduction of helicopter vibration. The higher harmonic pitch was obtained by higher harmonic oscillation of the swashplate. The test results indicated reduction of fuselage vibratory loads.

The attenuators are those dynamic devices that result in low hub shears and moments while the blades are subjected to specified aerodynamic excitation forces. An example of this category is a midspan or tip weight that may move the natural frequency of a mode away from exciting harmonics or reduce the modal forces at the blade root.

Absorbers are devices that are incorporated at the hub (or blade root) and absorb a large portion of the hub shears or moments causing transmittal of only the remaining forces to the mast. Examples are the simple and bifilar pendulums.

Isolators are generally integral to the pylon assembly and reduce greatly the forces and moments transmitted to the fuselage with respect to the forces applied on top of the mast.

Cabin suppressors reduce the vibration in the cabin for prescribed forces and moments applied by the pylon on the fuselage.

One of the five categories, the pendulum absorber, has proven to be quite successful as reported in references 2 to 6. Such a technique consists of mounting a simple or bifilar pendulum on each rotor blade near the hub. The blade-mounted pendulum absorbers modify the response dynamics of the blades, and reduce the

helicopter vibrational levels. All reported work has consisted of an expensive and time-consuming flight test program to establish a set of acceptable pendulum parameters. As the flight tests become more and more expensive, an analytical study is needed for pendulum design.

Murthy and Hammond (ref. 7) have studied the effect of a pendulum absorber on the natural frequencies and mode shapes of a rotor blade. A vibration analysis of rotor blades undergoing coupled flapwise bending, chordwise bending, and torsional vibrations with a spherical pendulum absorber was presented. A portion of the investigation included a reduction of the spherical pendulum to a simple flapping pendulum. It was shown that the pendulum absorber displaces original blade natural frequencies that are in the vicinity of the pendulum tuning frequency(ies). The spherical pendulum introduces two modes between the displaced original modes of the blade, whereas the simple flapping pendulum introduces one mode. Mode shape results were not presented in the report. It is worth mentioning that the equations of motion were based on the linear analysis presented by Houbolt and Brooks (ref. 8), and no damping terms were included. Also the damping at the pendulum hinge was not considered.

The principal aim of the present study is to establish comprehensive analytical design procedures and criteria for the installation of simple pendulums on the blades of a helicopter rotor to suppress the force and moment reactions at the hub during forward flight conditions.

The objectives of the present investigation can be stated as follows:

(1) Develop a mathematical model to represent the blade-pendulum system. A single nonuniform rotor blade with a hingeless hub restraint undergoing coupled flapwise bending, chordwise bending, and torsional vibrations is considered. Simple pendulum absorbers are individually treated for both flap and lead-lag types of motion. The blade is excited by an azimuthal harmonic variation of spanwise airload distributions associated with the elastic deformations and the cyclic pitch environment of forward flight.

(2) Find the dynamic response characteristics of the blade-pendulum system, using the transfer matrix method (ref. 9).

(3) Determine the optimum pendulum tuning to suppress the hub reactions. This entails the minimization of these reactions by appropriate variations of the pendulum parameters for a given excitation frequency. The pendulum parameters include the uncoupled pendulum frequency, hinge spanwise loaction and pendulum mass.

(4) Conduct a parametric study of the optimum tuned configuration. The parameters to be varied include pendulum hinge offset, precone, prepitch and pretwist. The intention of this investigation is to document the effects of these parameters on the optimum configuration previously established and thereby provide useful design criteria for future installations of pendulum absorbers.

SYMBOLS

a	airfoil lift-curve slope
$\mathscr{B}$	reference frame which rotates with speed Ω with respect to the stationary inertial frame $\mathscr{R}$
C	pendulum hinge friction coefficient, equation (35)
C_T	rotor thrust coefficient
c	blade chord

c_{do}	airfoil profile drag coefficient
E	Young's modulus of elasticity
e	mass centroid offset from elastic axis, positive when forward of the elastic axis
F_a	aerodynamic loads vector, equation (133)
$F_{y'}, F_{z'}$	components of aerodynamic forces per unit length in y', y', z' directions
G	shear modulus
g	acceleration due to gravity
$\vec{I}, \vec{J}, \vec{K}$	"fixed" unit vectors with $\vec{K}$ in direction of rotation of $\mathscr{B}$ in $\mathscr{R}$, figure A-1
$I_{y'}$	blade cross-section moment of inertia about y' axis
$I_{z'}$	blade cross-section moment of inertia about z' axis
$\vec{i}, \vec{j}, \vec{k}$	unit vectors assoicated with undeformed blade coordinate system, figure A-1
$\vec{i}', \vec{j}', \vec{k}'$	unit vectors associated with deformed blade coordinate system, figures 1, A-2
J	torsional rigidity constant
k_A	radius of gyration of blade cross section
k_m	mass radius of gyration of blade cross section
k_{m1}, k_{m2}	mass radii of gyration about η and ζ axis, respectively
L_v, L_w	components of generalized nonconservative (aerodynamic) forces in y and z directions
ℓ	length of pendulum
M	mass of the pendulum
$M_x, M_{x'}$	twisting moment about the x and x' axes
$M_y, M_{y'}$	bending moment about y and y' axes
$M_z, M_{z'}$	bending moment about z and z' axes
M_ϕ	generalized nonconservative (aerodynamic) moment about x axis
m	mass per unit length of the blade
N	time independent average normal force on the pendulum bearing, equation (35)
O	fixed point in $\mathscr{B}$ and $\mathscr{R}$ at the root of the blade, figure A-1

$[P]$	point transfer matrix of the pendulum
R	length of blade
$\mathscr{R}$	inertial reference frame
$[T(x)]$	transfer matrix of the blade from 0 to x
T_o	initial radial blade tension, equation (10)
t	time
U_R, U_T, U_P	radial, tangential, and perpendicular components of velocity for blade airfoil section
$u, v, w,$	elastic displacements in the x,y,z directions, respectively, figure A-2
V_1	wind velocity
$V_x, V_{x'}$	axial force (tension) in the x, x' directions, respectively
$V_y, V_{y'}$	shear force in the y, y' directions, respectively
$V_z, V_{z'}$	shear force in the z, z' directions, respectively
v_i	induced downwash velocity at rotor, positive downward
W	pendulum weight
X, Y, Z	inertial axis system with origin at hub centerline and Z normal to hub plane, figure A-1
x, y, z	mutually perpendicular axis system with x along the undeformed blade and y toward the leading edge, figures A-1
x', y', z'	a set of Cartesian coordinates with origin at a point along the deformed blade with x' remaining tangent to the elastic axis and y' and z' along principal axes for the cross section, figures 1, A-2
$\{Z(x,t)\}$	state vector, equation (1)
α_s	shaft angle
β_{pc}	precone angle, figure A-1
ε	small parameter of the order of the bending slopes, also airfoil section pitch angle with respect to free-stream velocity, figure 7
ζ	sectional coordinate normal to η axis at elastic axis (same as z'), figure 1, also damping ratio

η	sectional coordinate corresponding to major principal axis for a given point on the elastic axis (same as y'), figure 1
θ	pitch angle, equation (125)
θ_c	collective pitch, equation (125)
θ_{1c}, θ_{1s}	cyclic pitch components
θ_{pt}	pretwist, equation (126)
θ_t	pretwist per unit span, positive when tip angle is larger, equation (126)
λ	inflow ratio, positive upward
μ	slope of deflection curve in the plane of rotation, dv/dx
μ_f	advance ratio, $\mu_f \Omega R = V_1 \cos \alpha_s$
ν	slope of deflection curve normal to the plane of rotation, dw/dx
ρ	mass density of blade, also mass density of air
ϕ	elastic twist about the elastic axis
ψ	blade azimuth angle measured from downwind position in direction of rotation
Ω	rotational speed of the blade
ω_p	uncoupled natural frequency of the simple pendulum

Subscripts:

A	at the pendulum hinge location
P	at the pendulum mass location

Superscripts:

L	immediate left
R	immediate right
T	transpose of matrix
-1	inverse of matrix

Notations:

( )'	differentiation with respect to x, also deformed coordinate system
($\cdot$)	differentiation with respect to time
($-$)	amplitude of simple harmonic quantity

6

BLADE EQUATIONS OF MOTION

The equations of motion which are used to represent the structural dynamic characteristics of the helicopter blade are based on the development reported by Hodges and Dowell in reference 10. The mathematical model chosen to represent the rotor blade consists of a straight, slender, variably twisted, nonuniform beam which can undergo combined flapwise bending, lead-lag bending and torsion. The elastic axis, the mass axis, and the tension axis (area-centroid axis) are taken to be noncoincident. The elastic axis is inclined to the plane of rotation at a small angle in order to accommodate any built-in coning (precone). The use of an actual helicopter rotor blade as a model would be a more formidable task because of the nonhomogeneous, anisotropic structures found in typical blades.

Several orthogonal coordinate systems and coordinate transformations (Appendix A) are employed in the derivation of the equations of motion. The beam cross section is shown in figure 1 before and after deformation. The η and ζ axes are the principal axes of the cross section for the shear center. The cross section is assumed to be symmetric with respect to the η axis. The deformed beam is shown in figure 2(a) with force and moment resultants acting on the face of a cross section. The x, y, z coordinate system is the preconed undeformed system. At any point along the deformed beam, x' is tangent to the deformed elastic axis. The y' and z' are identical to the η and ζ axes, respectively, when the beam is deformed.

A mathematical ordering scheme which is consistent with the assumption of a slender beam is adopted for the purpose of systematically discarding elastic and dynamic terms which are of higher order in the equations of motion. The ordering scheme is consistent with the small deformation approximation in which the strains are negligible compared to unity and the dimensionless axial deflection u/R is generally taken to be of the same order of magnitude as the square of v/R or w/R and thus is small with respect to unity. These assumptions can be systemized by introducing ϵ, a parameter of order v/R or w/R. The ordering scheme associated with the above consideration is summarized in Table 1. Within the force and moment expressions, terms of order ϵ^2 are neglected with respect to unity. Thus, if the largest terms of the force expression are O(ϵ^n), then all terms of O(ϵ^n) are retained (first-order terms), all terms of O(ϵ^3) are retained (second-order terms), and generally terms of O(ϵ^b) are discarded.

The blade equations of motion will be written in terms of the state vector $\{Z\}$ where

$$\{Z(x,t)\}^T = \lfloor v \; w \; \phi \; \mu \; \nu \; M_x \; M_y \; M_z \; V_x \; V_y \; V_z \rfloor \tag{1}$$

It may be noted that the above state vector does not include the axial deflection, u. In order to obtain a set of linear equations for the state vector components, u must be eliminated. The components of the state vector, $\{Z\}$, can be chosen several ways, but they are chosen here such that they represent the physical quantities of deflections, slopes, moments, and shears. This is not absolutely required but highly preferable for application of the transfer matrix to obtain the dynamic response characteristics.

The equilibrium of the forces and moments that act on a differential beam element is now considered. In this consideration the element is formed by slices parallel to the yz-plane, because this choice leads to rather simple results. The forces that act on such an element are shown in figure 2(a); the moments, in figure 2(b). The quantities p_x, p_y, p_z, q_x, q_y and q_z are resultant force and moment loadings. Summation of the moments about the x-, y-, and z-directions lead to the following equilibrium conditions for moment and shear:

TABLE 1. – ORDERING SCHEME FOR ROTOR BLADE PARAMETERS

$$\frac{u}{R} = O(\epsilon^2)$$

$$\theta = O(1)$$

$$\frac{v}{R} = O(\epsilon)$$

$$\beta_{pc} = O(\epsilon)$$

$$\frac{w}{R} = O(\epsilon)$$

$$\frac{k_A}{R} = O(\epsilon)$$

$$\phi = O(\epsilon)$$

$$\frac{k_m}{R} = O(\epsilon)$$

$$\frac{x}{R} = O(1)$$

$$R(\ )' = O(1)$$

$$\frac{y}{R} = O(\epsilon)$$

$$\frac{1}{\Omega}(\ \dot{}\ ) = O(1)$$

$$\frac{z}{R} = O(\epsilon)$$

$$M'_x + V_z v' - V_y w' + q_x = 0 \qquad (2a)$$

$$M'_y - V_z + V_x w' + q_y = 0 \qquad (2b)$$

$$M'_z + V_y - V_x v' + q_z = 0 \qquad (2c)$$

$$V'_x + P_x = 0 \qquad (2d)$$

$$V'_y + P_y = 0 \qquad (2e)$$

$$V'_z + P_z = 0 \qquad (2f)$$

The applied loads p_x, p_y, p_z, q_x, q_y, q_z due to inertial and aerodynamic loadings are functions of v, w, ϕ and a longitudinal radial deformation u in the x direction. The only effective aerodynamic loading to be considered in this analysis will be forces in the y and z directions given by L_v and L_w, respectively, and moment about the x - axis given by M_ϕ. The inertia loadings, which consist of the forces and moments which oppose accelerations of the blade elements, are derived in reference 10 whereas the aerodynamic loadings L_v, L_w, and M_ϕ are left in this symbolic form. These aerodynamic loads are derived later in this text. The procedure that follows is employed in the derivation of the inertia loading which is given in reference 10. The acceleration of any mass particle on the vibrating, rotating blade is derived and the components in the x-, y- and z- directions are obtained. These component accelerations include terms for the Coriolis, transverse and centripetal accelerations along with higher order terms. The inertia force and moment loadings are then obtained by integrating over the cross section. By dropping higher order terms in accordance with the adopted ordering scheme, the following resultant loadings to second order are obtained:

$$p_x = m(\Omega^2 x + 2 \Omega \dot{v}) - m \beta_{pc} \ddot{w} \qquad (3a)$$

$$p_y = -m\ddot{v} + me\ddot{\phi} \sin\theta + m\Omega^2 [v + e \cos(\theta + \phi)] \qquad (3b)$$
$$\qquad + 2m\Omega(\beta_{pc}\dot{w} - \dot{u}) + 2m\Omega e (\dot{v}' \cos\theta + \dot{w}' \sin\theta) + L_v$$

$$p_z = -m\ddot{w} - me\ddot{\phi}\cos\theta - m\Omega^2 \beta_{pc} x - 2m\Omega\beta_{pc}\dot{v} + L_w \qquad (3c)$$

$$q_x = me(\ddot{v}\sin\theta - \ddot{w}\cos\theta) - m\Omega^2 ev\sin\theta - m\Omega^2 e\beta_{pc}x\cos\theta \qquad (3d)$$
$$\qquad \underline{-mk_m^2\ddot{\phi}} - \frac{1}{2}m\Omega^2(k_{m_2}^2 - k_{m_1}^2)\sin 2(\theta + \underline{\phi}) + \underline{M_\phi}$$

$$q_y = me(\Omega^2 x \sin(\theta + \phi) + 2\Omega\dot{v}\sin\theta) \qquad (3e)$$

$$q_z = -me(\Omega^2 x \cos(\theta + \phi) + 2\Omega\dot{v}\cos\theta) \qquad (3f)$$

The underlined higher-order terms could be dropped consistent with the ordering scheme, but this would eliminate torsional inertia. In the special case of rotor blade

configurations of very low torsional rigidity, these terms may contribute substantially to the magnitude of the torsiona' natural frequency; hence, they will be retained (ref. 10).

There are now 6 equilibrium equations, equations (2a) - (2f), and 10 unknowns, u, v, w, ϕ, M_x, M_y, M_z, V_x, V_y, and V_z. In addition, 4 force and moment deformation relations are required to express M_x, M_y, M_z, V_x in terms of u, v, w, ϕ. The force and moment resultants are expressed in terms of the deformations by resolving the distributed stresses into a resultant force and moment system acting at the elastic axis. These relations given in reference 10 are written in the deformed body axis system as

$$V_{x'} = EA\left\{u' + \frac{v'^2}{2} + \frac{w'^2}{2} + k_A^2\,\theta'\,\phi' - e_A\left[v'' \cos(\theta + \phi) + w'' \sin(\theta + \phi)\right]\right\} \qquad (4a)$$

$$M_{x'} = GJ\,\phi' + EAk_A^2(\theta + \underline{\phi})'\left(u' + \frac{v'^2}{2} + \frac{w'^2}{2}\right) + \underline{EB^*_1\theta'^2\phi'} \qquad (4b)$$

$$-EB^*_2\,\theta'(v'' \cos\theta + w'' \sin\theta)$$

$$M_{y'} = EI_{y'}\left[v'' \sin(\theta + \phi) - w'' \cos(\theta + \phi)\right] \qquad (4c)$$

$$M_{z'} = EI_{z'}\left[v'' \cos(\theta + \phi) + w'' \sin(\theta + \phi)\right] - EAe_A\left(u' + \frac{v'^2}{2} + \frac{w'^2}{2}\right) - EB^*_2\,\theta'\,\phi' \qquad (4d)$$

where B^*_1 and B^*_2 are section constants defined by

$$B^*_1 \equiv \iint\limits_A (\eta^2 + \zeta^2)^2\, d\eta\, d\zeta$$

$$B^*_2 \equiv \iint\limits_A \eta(\eta^2 + \zeta^2)\, d\eta\, d\zeta$$

and A is the blade cross-section area effective in carrying tension.

The underlined terms may be neglected according to the ordering scheme. However, as discussed before, these terms are important for configurations with low torsion stiffness. In equations (4a) - (4d), the terms which come from the warp effect are omitted due to its relative smallness for closed cross sections.

The force and moment deformation relations, equations (4a) - (4d), can be readily transformed into the undeformed body axis system using the transformation matrix of Appendix B. The resultant moments are:

10

$$M_x = GJ \phi' + EAk_A^2 (\theta + \phi)' (u' + \frac{v'^2}{2} + \frac{w'^2}{2})$$

$$+ EB_1^* \theta'^2 \phi' - EB_2^* \theta' (v'' \cos \theta + w'' \sin \theta)$$

$$- EAe_A (u' + \frac{v'^2}{2} + \frac{w'^2}{2}) (v' \sin \theta - w' \cos \theta)$$

$$+ (EI_{z'} - EI_{y'}) \left[\frac{1}{2} (v'v'' - w'w'') \sin 2 \theta + (v'w'' \right.$$

$$\left. + w'v'') \sin^2 \theta \right] + EI_{y'} v'w'' - EI_{z'} v''w' \qquad (5a)$$

$$M_y = GJ \phi'v' + EB_2^* \theta' \phi' \sin \theta + EAe_A (u' + \frac{v'^2}{2} + \frac{w'^2}{2})$$

$$\cdot \sin (\theta + \phi) - (EI_{z'} - EI_{y'}) \left[w'' \sin^2 (\theta + \phi) \right.$$

$$\left. + \frac{1}{2} v'' \sin 2 (\theta + \phi) \right] - EI_{y'} w'' \qquad (5b)$$

$$M_z = GJ \phi'w' - EB_2^* \theta' \phi' \cos \theta - EAe_A (u'$$

$$+ \frac{v'^2}{2} + \frac{w'^2}{2}) \cos (\theta + \phi) + (EI_{z'} - EI_{y'})$$

$$\cdot \frac{1}{2} \left[w'' \sin 2 (\theta + \phi) - v'' \sin^2 (\theta + \phi) \right] + EI_{z'} v'' \qquad (5c)$$

The resultant axial force in the undeformed body axis system is

$$V_x = V_{x'} - V_{y'} \left[v' \cos (\theta + \phi) + w' \sin (\theta + \phi) \right] - V_{z'} \left[-v' \sin (\theta + \phi) + w' \cos (\theta + \phi) \right]$$

11

For rotor blade applications the second and third terms on the right-hand side are negligible to second order (ref. 10); thus,

$$V_x = V_{x'} = EA \left\{ u' + \frac{v'^2}{2} + \frac{w'^2}{2} + k_A^2 \theta' \phi' - e_A \left[v'' \cos (\theta + \phi) + w'' \sin (\theta + \phi) \right] \right\} \quad (6)$$

In the above expressions all terms above second order have been neglected. As a final step the following definitions are introduced.

$$v' \equiv \mu \quad (7a)$$

$$w' \equiv \nu \quad (7b)$$

Equations (2), (5), (6), and (7) represent 12 independent equations for the 11 state variables and the elastic elongation, u. In order to obtain a set of linear equations for the state vector components, u must be eliminated. This will be accomplished by defining the time independent tension, T_0, as

$$T_0 \equiv \int_x^R m \Omega^2 x \, dx$$

In the process of linearization, the following approximations will be made

$$\left. \begin{aligned} \sin (\theta + \phi) &\cong \sin \theta + \phi \cos \theta \\ \cos (\theta + \phi) &\cong \cos \theta - \phi \sin \theta \\ \frac{1}{2} \sin 2 (\theta + \phi) &\cong \frac{1}{2} \sin 2\theta + \phi \cos 2\theta \\ \sin^2 (\theta + \phi) &\cong \sin^2 \theta + \phi \sin 2\theta \end{aligned} \right\} \quad (8)$$

Equation (6) can be rewritten as

$$u' + \frac{v'^2}{2} + \frac{w'^2}{2} = \frac{V_x}{EA} - k_A^2 \theta' \phi' + e_A \mu' \cos \theta + e_A \nu' \sin \theta \quad (9)$$

The left-hand side of equation (9) appears in equations (5) with both constant and linear coefficients. When the coefficient is constant it shall be represented as written above but with a linear coefficient it will be approximated as

$$\left(u' + \frac{v'^2}{2} + \frac{w'^2}{2} \right)_0 \cong \frac{T_0}{EA} \quad (10)$$

12

In the process of linearization, all steady-state values are neglected except the initial radial tension, and only the linear terms in the state variables are retained. These steady-state values would correspond to an equilibrium flight condition in hover. It is anticipated that these equilibrium hover values would have little effect on the dynamic response characteristics in the forward flight condition of this study. The set of linearized first-order differential equations are given below

$$v' = \mu \tag{11}$$

$$w' = \nu \tag{12}$$

$$\phi'(GJ + k_A^2 T_o + EB_1^* \theta'^2) = -k_A^2 \theta' V_x + EA(k_A^2 \theta')^2 \phi'$$

$$-EAk_A^2 \theta' e_A (\mu' \cos\theta + \nu' \sin\theta) + EB_2^* \theta'(\mu' \cos\theta$$

$$+ \nu' \sin\theta) + e_A T_o (\mu \sin\theta - \nu \cos\theta) + M_x \tag{13}$$

$$\mu'(EI_{z'} \cos^2\theta + EI_{y'} \sin^2\theta) = M_z + EB_2^* \theta' \phi' \cos\theta + e_A \cos\theta V_x$$

$$- EAk_A^2 e_A \theta' \phi' \cos\theta + EAe_A^2 (\mu' \cos^2\theta + \nu' \sin\theta \cos\theta)$$

$$- e_A T_o \phi \sin\theta - \frac{1}{2}(EI_{z'} - EI_{y'})\nu' \sin 2\theta \tag{14}$$

$$\nu'(EI_{y'} \cos^2\theta + EI_{z'} \sin^2\theta) = -M_y + EB_2^* \theta' \phi' \sin\theta + e_A V_x \sin\theta$$

$$-EAk_A^2 e_A \theta' \phi' \sin\theta + EAe_A^2 (\mu' \sin\theta \cos\theta + \nu' \sin^2\theta)$$

$$+ e_A T_o \phi \cos\theta - \frac{1}{2}(EI_{z'} - EI_{y'}) \mu' \sin 2\theta \tag{15}$$

$$M_x' = m\dot{\Omega}^2 e x(\nu \cos\theta - \mu \sin\theta) + (e_A T_o \cos\theta)'\nu - (e_A T_o \sin\theta)' \mu$$

$$+ mk_m^2 \ddot{\phi} + me\left[(\Omega^2 \nu - \ddot{\nu}) \sin\theta + \ddot{w} \cos\theta\right]$$

$$+ m\Omega^2(k_{m_2}^2 - k_{m_1}^2)\phi \cos 2\theta - M_\phi \tag{16}$$

$$M_y' = V_z - T_o \nu - 2 m\Omega e\dot{\nu} \sin\theta - m\Omega^2 ex \phi \cos\theta \tag{17}$$

13

$$M'_z = T_o \, \mu - V_y + 2 \, m \, \Omega e \dot{v} \cos \theta - m\Omega^2 ex \, \phi \sin \theta \tag{18}$$

$$V'_x = -2 \, m \, \Omega \dot{v} \tag{19}$$

$$V'_y = m\ddot{v} - me \ddot{\phi} \sin \theta - m \Omega^2 v + m \Omega^2 e \, \phi \sin \theta - 2 \, m \, \Omega \beta_{pc} \, \dot{w}$$

$$-2 \, m \, \Omega e \, \dot{\mu} \cos \theta - 2 \, m\Omega e \, \dot{v} \sin \theta - L_v \tag{20}$$

$$V'_z = m\ddot{w} + me \, \ddot{\phi} \cos \theta + 2 \, m \Omega \beta_{pc} \, \dot{v} - L_w \tag{21}$$

It may be noted that the three equations for the elastic slopes (eqs. (13), (14), and (15)) are coupled in their derivatives and must be solved simultaneously. These equations are decoupled by a straight forward application of Cramer's rule to obtain a set of linear first order differential equations in terms of the state vector so that the transfer matrix method can be applied as discussed later in this study.

Excitation of the blade is due to various simple harmonic airloads. The solution to the set of equations will be treated as individual contributions associated with each harmonic of the excitation loading. Such a solution for the nth harmonic of the state vector can be written in complex form as

$$\{ Z_n (x,t) \} = \text{Re} \left(\{ \bar{Z}_n (x) \} \, e^{i\omega t} \right) \tag{22}$$

where $\{ \bar{Z}_n(x) \}$ is the amplitude vector of the nth simple harmonic response, and

$$\omega = n \, \Omega \equiv \text{the frequency of the excitation loading}$$
$$i \equiv \sqrt{-1}$$

The above solution will be discussed in more detail with respect to the aerodynamic loading. Substituting equation (22) into equations (11) to (21) yields the following matrix equation for $\{Z\}$, the nth harmonic,

$$\{ \bar{Z} (x) \}' = \left[A (x) \right] \{ \bar{Z} (x) \} + \{ \bar{F}_a (x) \} \tag{23}$$

where $\{ \bar{F}_a \}$ is the amplitude vector of the aerodynamic loads, defined by

$$\{ \bar{F}_a \}^T \equiv \lfloor 0 \ 0 \ 0 \ 0 \ 0 \ -\bar{M}_\phi \ 0 \ 0 \ 0 \ -\bar{L}_v \ -\bar{L}_w \rfloor$$

Note that the matrix, $[A]$, includes complex terms due to retaining the linear rate terms (Coriolis intertial forces).

Evaluation of the order of magnitude of the individual elements of the complex matrix $[A]$ is made. Consistent with the adopted ordering scheme, only terms of first and second order are retained. It may be noted that in the process of decoupling eqs. (13), (14), and (15), terms of higher order are encountered. The resulting nonzero elements of $[A]$ become

$$A_{14} = 1$$

$$A_{25} = 1$$

$$A_{34} = EI_{y'}(EI_{z'} - EAe_A^2) e_A T_o \sin \theta / D$$

$$A_{35} = -A_{34} \cot \theta$$

$$A_{36} = EI_{y'}(EI_{z'} - EAe_A^2)/D$$

$$A_{37} = EI_{y'} \theta'(EAk_A^2 e_A - EB_2^*) \sin \theta / D$$

$$A_{38} = -A_{37} \cot \theta$$

$$A_{39} = EI_{y'} \theta'(EB_2^* e_A - EI_{z'} k_A^2)/D$$

$$A_{43} = -GJ e_A T_o (EI_{z'} - EA e_A^2) \sin \theta / D$$

$$A_{46} = A_{38}$$

$$A_{47} = GJ (EI_{z'} - EI_{y'} - EA e_A^2) \sin \theta \cos \theta / D$$

$$A_{48} = -A_{43} \sin \theta /(e_A T_o) + GJ EI_{y'} \cos^2 \theta / D$$

$$A_{49} = GJ EI_{y'} e_A \cos \theta / D$$

$$A_{53} = -A_{43} \cot \theta$$

$$A_{56} = -A_{37}$$

$$A_{57} = A_{43} \cos \theta \cot \theta /(e_A T_o) - GJ EI_{y'} \sin^2 \theta / D$$

$$A_{58} = -A_{47}$$

$$A_{59} = A_{49} \tan \theta$$

15

$$A_{61} = me(\Omega^2 + \omega^2)\sin\theta$$

$$A_{62} = -me\,\omega^2\cos\theta$$

$$A_{63} = -mk_m^2\,\omega^2 + m\,\Omega^2(k_{m_2}^2 - k_{m_1}^2)\cos 2\theta$$

$$A_{64} = -m\,\Omega^2\,ex\sin\theta - (e_A\,T_o\sin\theta)'$$

$$A_{65} = m\,\Omega^2\,ex\cos\theta + (e_A\,T_o\cos\theta)'$$

$$A_{71} = -2\,im\,\Omega\omega e\sin\theta$$

$$A_{73} = -m\,\Omega^2\,ex\cos\theta$$

$$A_{75} = -T_o$$

$$A_{7,11} = 1$$

$$A_{81} = -A_{71}\cot\theta$$

$$A_{83} = -m\,\Omega^2\,ex\sin\theta$$

$$A_{84} = T_o$$

$$A_{8,10} = -1$$

$$A_{91} = -2\,im\,\Omega\omega$$

$$A_{92} = -m\,\omega^2\beta_{pc}$$

$$A_{10,1} = -m(\Omega^2 + \omega^2)$$

$$A_{10,2} = -2\,im\,\Omega\omega\beta_{pc}$$

$$A_{10,3} = A_{61}$$

$$A_{10,4} = -A_{81}$$

$$A_{10,5} = A_{71}$$

$$A_{11,1} = -A_{10,2}$$

$$A_{11,2} = -m\omega^2$$

$$A_{11,3} = A_{62}$$

where

$$D = GJ\, EI_{y'}\, (EI_{z'} - EA\, e_A^2)$$

PENDULUM EQUATIONS

The pendulum configurations considered are of the simple type which are free to oscillate in the flap and lead-lag modes. The free vibration equations of motion for simple pendulums in both the flap and lead-lag degrees of freedom are developed in an identical fashion. These equations are formulated by first determining the acceleration of the pendulum mass in the inertial system and then transforming it to the deformed blade system. The absolute acceleration is used to express the inertial reaction force and moment at the pendulum hinge. Setting the reaction moment about the pendulum hinge to zero yields the equation of motion. These nonlinear equations of motion are subsequently linearized by assuming small oscillations for the pendulum about the steady-state condition. By assuming a simple harmonic solution for the linearized equation of motion of the free pendulum, the deflection of the pendulum is obtained in terms of the blade deflection. The point transfer matrix at the pendulum hinge station on the rotor blade is derived by simple equilibrium considerations of forces and moments across the pendulum after linearizing the inertial forces and moments.

Acceleration Components

The acceleration of the pendulum mass is determined with respect to an inertial reference system. This entails appropriate transformations from the inertial to the rotating system, to the preconed system, and finally to the deformed blade section. The derivation of the acceleration components is given in Appendix B. Equations (B-18) to (B-20) for these acceleration components are reproduced here as

$$a_{x'} = \ddot{\xi} - 2\Omega\,\dot{v} - \Omega^2(x+\xi) + 2\Omega\dot{\zeta}\sin\theta - 2\Omega\dot{\eta}\cos\theta \tag{24}$$

$$a_{y'} = \ddot{\eta} + (\Omega^2 x\, v + \ddot{w} + \Omega^2 \beta_{pc} x)\sin\theta + (\ddot{v} + 2\Omega\dot{\xi} - \Omega^2 v$$

$$+ \Omega^2 x\, \mu)\cos\theta - \Omega^2\eta\cos^2\theta + \frac{1}{2}\Omega^2\zeta\sin 2\theta \tag{25}$$

$$a_{z'} = \ddot{\zeta} - (\ddot{v} + 2\Omega\dot{\xi} - \Omega^2 v + \Omega^2 x \mu) \sin\theta + (\Omega^2 x \nu + \ddot{w}$$

$$+ \Omega^2 \beta_{pc} x) \cos\theta - \Omega^2 \zeta \sin^2\theta + \frac{1}{2} \Omega^2 \eta \sin 2\theta \qquad (26)$$

where (ξ, η, ζ) is a general point relative to the deformed blade coordinate system. It may be noted that the gravitational contribution to these accelerations has been neglected.

Flapping Pendulum

The blade-mounted pendulum absorber is shown in figure 3. The pendulum after deformation is shown in figure 4. The deformed coordinates of the pendulum hinge and mass can be related from figure 4 and are given by

$$\left.\begin{array}{rcl} \xi_p &=& \ell \cos\Delta \\[2ex] \eta_p &=& \eta_A \\[2ex] \zeta_p &=& \zeta_A + \ell \sin\Delta \end{array}\right\} \qquad (27)$$

where

$\ell \equiv$ the pendulum arm length

$\Delta \equiv$ rotation about $(0, \eta_A, \zeta_A)$ in the x' z' - plane

$$\frac{\ell}{R} = O(\epsilon) \qquad ; \qquad \Delta = O(1)$$

Differentiating equations (27) with respect to time yields

$$\dot{\xi}_p = -\ell \dot{\Delta} \sin\Delta \qquad (28a)$$

$$\ddot{\xi}_p = -\ell \ddot{\Delta} \sin\Delta - \ell \dot{\Delta}^2 \cos\Delta \qquad (28b)$$

18

$$\dot{\eta}_p = 0 \tag{28c}$$

$$\ddot{\eta}_p = 0 \tag{28d}$$

$$\dot{\zeta}_p = \ell\,\dot{\Delta}\,\cos\Delta \tag{28e}$$

$$\ddot{\zeta}_p = \ell(\ddot{\Delta}\cos\Delta - \dot{\Delta}^2\sin\Delta) \tag{28f}$$

Substituting the above expressions into equations (24) to (26), the acceleration components to the first order (second and higher order terms are discarded) for the flapping pendulum become

$$a_{x'_p} = -\ell\,\ddot{\Delta}\sin\Delta - \ell\,\dot{\Delta}^2\cos\Delta - 2\Omega\,\dot{v}_A - \Omega^2 x_A$$

$$- \Omega^2\ell\cos\Delta + 2\Omega\ell\,\dot{\Delta}\,\cos\Delta\,\sin\theta_A \tag{29}$$

$$a_{y'_p} = (\Omega^2 x_A\,\nu_A + \ddot{w}_A + \Omega^2\beta_{pc}\,x_A)\sin\theta_A$$

$$+ (\ddot{v}_A - 2\Omega\ell\,\dot{\Delta}\sin\Delta - \Omega^2 v_A + \Omega^2 x_A\,\mu_A)\cos\theta_A$$

$$- \Omega^2\eta_A\cos^2\theta_A + \frac{1}{2}\Omega^2(\zeta_A + \ell\sin\Delta)\sin 2\theta_A \tag{30}$$

$$a_{z'_p} = \ell\,\ddot{\Delta}\cos\Delta - \ell\,\dot{\Delta}^2\sin\Delta$$

$$- (\ddot{v}_A - 2\Omega\ell\,\dot{\Delta}\sin\Delta - \Omega^2 v_A + \Omega^2 x_A\,\mu_A)\sin\theta_A$$

$$+ (\Omega^2 x_A\,\nu_A + \ddot{w}_A + \Omega^2\beta_{pc}\,x_A)\cos\theta_A$$

$$- \Omega^2(\zeta_A + \ell\sin\Delta)\sin^2\theta_A + \frac{1}{2}\Omega^2\eta_A\sin 2\theta_A \tag{31}$$

19

These acceleration components will be used to express the inertial reaction force and moment at the pendulum hinge.

The total inertial reaction force acting on the pendulum mass, M, can be written in terms of the above acceleration components whose associated unit vectors are $\vec{i}'$, $\vec{j}'$, $\vec{k}'$ as

$$\vec{F} = -M(a_{x'_p}\vec{i}' + a_{y'_p}\vec{j}' + a_{z'_p}\vec{k}') \qquad (32)$$

The position vector of the pendulum mass with respect to the hinge point is

$$\vec{r} = \ell(\cos \Delta \vec{i}' + \sin \Delta \vec{k}') \qquad (33)$$

and the inertial moment reaction about the hinge point is

$$\vec{M} = \vec{r} \times \vec{F}$$

$$= -M\ell \begin{vmatrix} \vec{i}' & \vec{j}' & \vec{k}' \\ \cos \Delta & 0 & \sin \Delta \\ a_{x'_p} & a_{y'_p} & a_{z'_p} \end{vmatrix}$$

or

$$\vec{M} = M\ell \, a_{y'_p} \sin \Delta \vec{i}'$$
$$+ M\ell(a_{z'_p}\cos\Delta - a_{x'_p}\sin\Delta)\vec{j}'$$
$$- M\ell \, a_{y'_p}\cos\Delta \vec{k}' \qquad (34)$$

In addition to the inertial reaction moment, there is a moment due to damping at the pendulum hinge. This damping will be presumed to be of the linear viscous type. The corresponding moment reaction about the hinge can be represented as

$$\vec{M}_A = CN\Delta\vec{j}' \qquad . \qquad (35)$$

where

N ≡ steady-state normal force on the bearing due to $F_{Ax'}$ and $F_{Ay'}$

C ≡ pendulum hinge friction coefficient

Since the flapping pendulum is free to rotate about the y'-axis, the y' component of the inertial moment reaction is in equilibrium with the damping moment. Using equations (34) and (35), the equilibrium equation can be written as

$$M\ell(a_{x'_p} \sin \Delta - a_{z'_p} \cos \Delta) - CN\dot{\Delta} = 0 \qquad (36)$$

Equation (36) provides the pendulum equation of motion. The other two components of the inertial moment, the damping moment, and all three components of the force reaction provide the pendulum reactions which act on the blade at the hinge point as

$$F_{Ax'} = -Ma_{x'_p} \qquad (37)$$

$$F_{Ay'} = -Ma_{y'_p} \qquad (38)$$

$$F_{Az'} = -Ma_{z'_p} \qquad (39)$$

$$M_{Ax'} = M\ell a_{y'_p} \sin \Delta \qquad (40)$$

$$M_{Ay'} = -CN\dot{\Delta} \qquad (41)$$

$$M_{Az'} = -M\ell a_{y'_p} \cos \Delta \qquad (42)$$

Substituting for the acceleration components in equation (36), the pendulum equation can be written as

$$\ell \ddot{\Delta} - (\ddot{v}_A - \Omega^2 v_A + \Omega^2 x_A \mu_A) \sin\theta_A \cos\Delta$$

$$+ (\Omega^2 x_A v_A + \ddot{w}_A + \Omega^2 \beta_{p_C} x_A) \cos\theta_A \cos\Delta$$

$$+ \Omega^2 \ell \cos^2\theta_A \cos\Delta \sin\Delta$$

$$+ (2\Omega \dot{v}_A + \Omega^2 x_A) \sin\Delta$$

$$+ (-\Omega^2 \zeta_A \sin^2\theta_A + \tfrac{1}{2}\Omega^2 \eta_A \sin 2\theta_A) \cos\Delta = -CN\dot{\Delta}/M\ell \quad (43)$$

It may be noted that in the above equation the rotary inertia of the pendulum is neglected. This implies that the pendulum consits of mass, M, which has very small dimensions (point mass) in comparison with the pendulum arm.

The nonlinear equation of motion given by equation (43) is linearized for small angular oscillations, δ, about the steady-state equilibrium angle of the pendulum, δ_o, where

$$\Delta \equiv \delta + \delta_o \quad (44)$$

Since the perturbation angle, δ, will be fairly small as

$$\delta^2 \ll 1$$

the following approximations can be used.

$$\cos\Delta \equiv \cos\delta_o - \delta \sin\delta_o \quad (45)$$

$$\sin\delta \equiv \sin\delta_o + \delta\cos\delta_o \quad (46)$$

The steady state equilibrium angle, δ_o, is obtained from equation (43) by setting the acceleration and velocity terms to zero (assuming that the elastic deformations are zero). This process yields

$$x_A \tan\delta_o + \cos^2\theta_A \ell \sin\delta_o = \zeta_A \sin^2\theta_A - \tfrac{1}{2}\eta_A \sin 2\theta_A - \beta_{pc} x_A \cos\theta_A \quad (47)$$

In the above equation θ_A is the steady-state value of the pitch angle at x_A. It may be noted that the steady equilibrium angle, δ_o, is independent of the rotor speed. This

22

result is due to neglecting the gravitational force in equation (36). The effect of the gravitational force on the steady equilibrium angle and the uncoupled pendulum frequency is very small (ref. 7).

Substituting equations (45) and (46) into equation (43) and subtracting the steady-state relation, equation (47), from the resulting equation, the following equation of motion for the perturbation pendulum angle is obtained.

$$\ell \ddot{\delta} + \frac{CN}{M\ell} \dot{\delta} + \Omega^2 \delta \left(\frac{x_A}{\cos \delta_o} + \ell \cos^2 \theta_A \cos^2 \delta_o\right) + 2\Omega \dot{v}_A \sin \delta_o$$

$$+ \left[(\Omega^2 x_A \nu_A + \ddot{w}_A) \cos \theta_A - (\ddot{v}_A - \Omega^2 v_A + \Omega^2 x_A \mu_A) \sin \theta_A\right] \cos \delta_o$$

$$+ 2\Omega \dot{v}_A \delta \cos \delta_o - \underline{\delta \left[(\Omega^2 x_A \nu_A + \ddot{w}_A) \cos \theta_A\right.}$$

$$\underline{-(\ddot{v}_A - \Omega^2 v_A + \Omega^2 x_A \mu_A) \sin \theta_A\right] \sin \delta_o} = 0 \tag{48}$$

In equation (48) the 6th and 7th terms (underlined terms) are nonlinear. Comparison of the 7th term with the 5th term illustrates that this nonlinear term is of order $\delta \tan \delta_o$ compared to unity for the linear term. Since both δ and δ_o will be fairly small then the 7th term can be rationally neglected. Comparison of the nonlinear 6th term with the linear 4th term indicates that they are of the same order of magnitude since

$$\frac{\delta}{\tan \delta_o} = O(1)$$

Both of these terms will be fairly small. In the interest of linearization and the desire to retain an explicit damping term, the 6th term will be dropped and the 4th term retained.

The steady-state normal force on the bearing can be written as

$$N = \left[\bar{F}_{Ax'}^2 + \bar{F}_{Az'}^2\right]^{1/2} \tag{49}$$

where $\bar{F}_{Ax'}$ and $\bar{F}_{Az'}$ are the steady-state values of $F_{Ax'}$ and $F_{Az'}$, respectively. It may be noted that N is generally a time-dependent force but is approximated here by the steady-state value. Substituting for the acceleration components (eqs. (29) and (31)) in equations (37) and (39) and retaining only the steady-state terms, equation (49) becomes

$$N = M\Omega^2 (x_A + \ell \cos \delta_o) \tag{50}$$

It may be noted that high order terms are neglected. Substituting equation (50) into equation (48), the linear pendulum equation of motion becomes

$$\ell \ddot{\delta} + C\Omega^2 (\frac{x_A}{\ell} + \cos \delta_o) \dot{\delta} + \Omega^2 \left(\frac{x_A}{\cos \delta_o} + \ell \cos^2 \theta_A \cos^2 \delta_o\right)\delta$$

$$+ 2\Omega \dot{v}_A \sin \delta_o + (\ddot{w}_A + \Omega^2 x_A \nu_A) \cos \theta_A \cos \delta_o$$

$$- (\ddot{v}_A - \Omega^2 v_A + \Omega^2 x_A \mu_A) \sin \theta_A \cos \delta_o = 0 \qquad (51)$$

The uncoupled pendulum equation can be obtained from equation (51) by dropping the blade deflection terms. The resulting equation can be written as

$$\ddot{\delta} + 2\zeta\omega_p \dot{\delta} + \omega_p^2 \delta = 0 \qquad (52)$$

where

$$\omega_p = \Omega \left(\frac{x_A}{\ell \cos \delta_o} + \cos^2 \delta_o \cos^2 \theta_A\right)^{1/2} \qquad (53)$$

$$\zeta = \frac{C\Omega(x_A/\ell + \cos \delta_o)}{2\ell \left(\frac{x_A}{\ell \cos \delta_o} + \cos^2 \delta_o \sin^2 \theta_A\right)^{1/2}} \qquad (54)$$

It may be noted that the pendulum hinge coefficient, C, in equation (54) can not normally be specified, but representative values of the damping ratio, ζ , can be estimated.

The inertial reaction loads applied to the blade due to the pendulum will be considered to act at the elastic axis pendulum hinge location, $(x_A,0,0)$. These reactions will be treated as discontinuities in the tension, shear, and bending moment distributions along the blade. The values of these discontinuities can be written in terms of the component reactions as

$$\Delta M_{x'} = M_{Ax'} + \eta_A F_{Az'} - \zeta_A F_{Ay'} \tag{55}$$

$$\Delta M_{y'} = M_{Ay'} + \zeta_A F_{Ax'} \tag{56}$$

$$\Delta M_{z'} = M_{Az'} - \eta_A F_{Ax'} \tag{57}$$

$$\Delta V_{x'} = F_{Ax'} \tag{58}$$

$$\Delta V_{y'} = F_{Ay'} \tag{59}$$

$$\Delta V_{z'} = F_{Az'} \tag{60}$$

Substitution of equations (29) to (31) and equations (37) to (42) into the above equations yields

$$\Delta M_{x'}/M = (\ell \sin \Delta + \zeta_A)\Big[(\Omega^2 x_A \, \nu_A + \ddot{w}_A + \Omega^2 \beta_{pc} x_A) \sin \theta_A$$

$$+ (\ddot{v}_A - 2\Omega \ell \dot{\Delta} \sin \Delta - \Omega^2 v_A + \Omega^2 x_A \, \mu_A) \cos \theta_A$$

$$- \Omega^2 \eta_A \cos^2 \theta_A + \tfrac{1}{2}\Omega^2(\zeta_A + \ell \sin \Delta)\sin 2\theta_A\Big]$$

$$- \eta_A \Big[\ell \ddot{\Delta}\cos \Delta - \ell \dot{\Delta}^2 \sin \Delta - (\ddot{v}_A - 2\Omega \ell \dot{\Delta}\sin \Delta$$

$$- \Omega^2 v_A + \Omega^2 x_A \mu_A) \sin \theta_A + (\Omega^2 x_A \, \nu_A + \ddot{w}_A$$

$$+ \Omega^2 \beta_{pc} x_A) \cos \theta_A - \Omega^2 \zeta_A \sin^2 \theta_A$$

$$- \Omega^2 \ell \sin \Delta \sin^2 \theta_A + \tfrac{1}{2}\Omega^2 \eta_A \sin 2\theta_A\Big] \tag{61}$$

$$\Delta M_{y'}/M = \zeta_A \left[\ell \ddot{\Delta} \sin \Delta + \ell \dot{\Delta}^2 \cos \Delta + 2\Omega \dot{v}_A + \Omega^2 x_A \right.$$

$$\left. + \Omega^2 \ell \cos \Delta - 2\Omega \ell \dot{\Delta} \cos \Delta \sin \theta_A \right]$$

$$- C \Omega^2 (x_A + \ell \cos \Delta) \dot{\Delta} \tag{62}$$

$$\Delta M_{z'}/M = - \eta_A \left[\ell \ddot{\Delta} \sin \Delta + \ell \dot{\Delta}^2 \cos \Delta + 2\Omega \dot{v}_A \right.$$

$$\left. + \Omega^2 x_A + \Omega^2 \ell \cos \Delta - 2\Omega \ell \dot{\Delta} \cos \Delta \sin \theta_A \right]$$

$$- \ell \cos \Delta \left[(\Omega^2 x_A \nu_A + \ddot{w}_A + \Omega^2 \beta_{pc} x_A) \sin \theta_A \right.$$

$$+ (\ddot{v}_A - 2\Omega \ell \dot{\Delta} \sin \Delta - \Omega^2 v_A + \Omega^2 x_A \mu_A) \cos \theta_A$$

$$\left. - \Omega^2 \eta_A \cos^2 \theta_A + \frac{1}{2} \Omega^2 (\zeta_A + \ell \sin \Delta) \sin 2\theta_A \right] \tag{63}$$

$$\Delta V_{x'}/M = \ell \ddot{\Delta} \sin \Delta + \ell \dot{\Delta}^2 \cos \Delta + 2\Omega \dot{v}_A$$

$$+ \Omega^2 x_A + \Omega^2 \ell \cos \Delta - 2\Omega \ell \dot{\Delta} \cos \Delta \sin \theta_A \tag{64}$$

$$\Delta V_{y'}/M = -(\Omega^2 x_A \nu_A + \ddot{w}_A + \Omega^2 \beta_{pc} x_A) \sin \theta_A$$

$$- (\ddot{v}_A - 2\Omega \ell \dot{\Delta} \sin \Delta - \Omega^2 v_A + \Omega^2 x_A \mu_A) \cos \theta_A$$

$$+ \Omega^2 \eta_A \cos^2 \theta_A - \frac{1}{2} \Omega^2 (\zeta_A + \ell \sin \Delta) \sin 2\theta_A \tag{65}$$

$$\Delta\,V_{z'}/M \;=\; -\ell\,\ddot{\Delta}\cos\Delta + \ell\,\dot{\Delta}^2\sin\Delta + (\ddot{v}_A - 2\Omega\,\ell\,\dot{\Delta}\sin\Delta$$

$$-\,\Omega^2\,v_A + \Omega^2\,x_A\,\mu_A)\sin\theta_A - (\Omega^2 x_A\,v_A + \ddot{w}_A$$

$$+\,\Omega^2\,\beta_{pc}\,x_A)\cos\theta_A + \Omega^2\,z_A\sin^2\theta_A$$

$$+\,\Omega^2\,\ell\,\sin\Delta\sin^2\theta_A - \tfrac{1}{2}\,\Omega^2\,\eta_A\,\sin 2\,\theta_A \tag{66}$$

where M is the pendulum mass.

Using the adopted ordering scheme given by Table 1 and equation (28), the orders of magnitude of the above expressions are as follow

$$\left.\begin{aligned}
\Delta M_{x'}/M &\;\sim\; O(\epsilon^2)\\[4pt]
\Delta M_{y'}/M &\;\sim\; O(\epsilon)\\[4pt]
\Delta M_{z'}/M &\;\sim\; O(\epsilon)
\end{aligned}\right\} \tag{67}$$

$$\left.\begin{aligned}
\Delta V_{x'}/M &\;\sim\; O(1)\\[4pt]
\Delta V_{y'}/M &\;\sim\; O(\epsilon)\\[4pt]
\Delta V_{z'}/M &\;\sim\; O(\epsilon)
\end{aligned}\right\} \tag{68}$$

For inclusion in the blade equations, the shear and moment reactions must be transformed into the undeformed x, y, z system using the transformation matrix of Appendix B. The transformations consistent with the above orders of magnitude are

$$\Delta\,M_x/M = (\Delta M_{x'}/M) - (\Delta M_{y'}/M)(\mu_A\cos\theta_A + \nu_A\sin\theta_A)$$

$$+ (\Delta M_{z'}/M)(\mu_A\sin\theta_A - \nu_A\cos\theta_A) \tag{69}$$

$$\Delta M_y/M = (\Delta M_{y'}/M)(\cos\theta_A - \phi_A\sin\theta_A) - (\Delta M_{z'}/M)(\sin\theta_A + \phi_A\cos\theta_A) \tag{70}$$

$$\Delta M_z/M = (\Delta M_{y'}/M)(\sin\theta_A + \phi_A\cos\theta_A) + (\Delta M_{z'}/M)(\cos\theta_A - \phi_A\sin\theta_A) \tag{71}$$

where only $O(\epsilon^2)$ terms and larger are retained. Similarly

$$\Delta V_x / M = \Delta V_{x'} / M \tag{72}$$

$$\Delta V_y / M = (\Delta V_{x'}/M)\ \mu_A + (\Delta V_{y'}/M) \cos \theta_A - (\Delta V_{z'}/M) \sin \theta_A \tag{73}$$

$$\Delta V_z / M = (\Delta V_{x'}/M)\ \nu_A + (\Delta V_{y'}/M) \sin \theta_A + (\Delta V_{z'}/M) \cos \theta_A \tag{74}$$

where only $O(\epsilon)$ terms and larger are retained.

Substituting equations (61) to (66) into equations (69) to (74) and retaining only the linear time dependent terms (to be compatible with the completed time dependent blade equations), the shear and moment reactions in the undeformed preconed system are obtained after making use of equations (44) to (46).

$$
\begin{aligned}
\Delta M_x / M =\ & \left[(\ell \sin \delta_o + \zeta_A) \sin \theta_A - \eta_A \cos \theta_A \right] \ddot{w}_A \\[2mm]
& + \left[(\ell \sin \delta_o + \zeta_A) \cos \theta_A + \eta_A \sin \theta_A \right] \left[\ddot{v}_A - 2\Omega \ell \dot{\delta} \sin \delta_o \right. \\[2mm]
& \left. - \Omega^2 v_A + \Omega^2 x_A \mu_A + \Omega^2 \ell \delta \cos \delta_o \sin \theta_A \right] \\[2mm]
& + \ell \delta \cos \delta_o \left[\Omega^2 \beta_{pc} x_A \sin \theta_A - \Omega^2 \eta_A \cos^2 \theta_A \right. \\[2mm]
& \left. + \Omega^2 (\zeta_A + \ell \sin \delta_o) \sin \theta_A \cos \theta_A \right] - \eta_A \ell \ddot{\delta} \cos \delta_o \\[2mm]
& - \Omega^2 x_A (\eta_A \sin \theta_A + \zeta_A \cos \theta_A) \mu_A \\[2mm]
& + \ell \sin \delta_o \Omega^2 x_A \nu_A \sin \theta_A
\end{aligned}
\tag{75}
$$

28

$$\Delta M_y/M = (\eta_A \sin \theta_A + \zeta_A \cos \theta_A)\left[\ell \ddot{\delta} \sin \delta_0 + 2\Omega \dot{v}_A\right.$$

$$\left. - \Omega^2 \ell \delta \sin \delta_0 - 2\Omega \ell \dot{\delta} \cos \delta_0 \sin \theta_A\right]$$

$$+ \ell \cos \delta_0 \sin \theta_A \left[(\Omega^2 x_A \nu_A + \ddot{w}_A) \sin \theta_A\right.$$

$$+ (\ddot{v}_A - 2\Omega \ell \dot{\delta} \sin \delta_0 - \Omega^2 v_A + \Omega^2 x_A \mu_A) \cos \theta_A$$

$$\left. + \Omega^2 \ell \delta \cos \delta_0 \sin \theta_A \cos \theta_A\right] - \Omega^2 \ell \delta \sin \delta_0 \sin \theta_A$$

$$\cdot \left[\beta_{pc} x_A \sin \theta_A - \eta_A \cos^2 \theta_A + (\zeta_A\right.$$

$$\left. + \ell \sin \delta_0) \sin \theta_A \cos \theta_A\right] + \Omega^2 x_A (\eta_A \cos \theta_A$$

$$- \zeta_A \sin \theta_A) \; \phi_A - C \Omega^2 \dot{\delta}(x_A + \ell \cos \delta_0) \cos \theta_A \qquad (76)$$

$$\Delta M_z/M = (-\eta_A \cos \theta_A + \zeta_A \sin \theta_A)\left[\ell \ddot{\delta} \sin \delta_0\right.$$

$$\left. + 2\Omega \dot{v}_A - \Omega^2 \ell \delta \sin \delta_0 - 2\Omega \ell \dot{\delta} \cos \delta_0 \sin \theta_A\right]$$

$$- \ell \cos \delta_0 \cos \theta_A \left[(\Omega^2 x_A \nu_A + \ddot{w}_A) \sin \theta_A\right.$$

$$+ (\ddot{v}_A - 2\Omega \ell \dot{\delta} \sin \delta_0 - \Omega^2 v_A + \Omega^2 x_A \mu_A) \cos \theta_A$$

$$\left. + \Omega^2 \ell \ddot{\delta} \cos \delta_0 \sin \theta_A \cos \theta_A\right]$$

$$+ \Omega^2 \ell \delta \sin \delta_0 \cos \theta_A \left[\beta_{pc} x_A \sin \theta_A\right.$$

$$\left. - \eta_A \cos^2 \theta_A + (\zeta_A + \ell \sin \delta_0) \sin \theta_A \cos \theta_A\right]$$

$$+ \Omega^2 x_A (\eta_A \sin \theta_A + \zeta_A \cos \theta_A) \; \phi_A$$

$$- C \Omega^2 \dot{\delta}(x_A + \ell \cos \delta_0) \sin \theta_A \qquad (77)$$

$$\Delta V_x / M = \ell \ddot{\delta} \sin \delta_0 + 2 \Omega \dot{v}_A - \Omega^2 \ell \, \delta \sin \delta_0 - 2 \Omega \ell \dot{\delta} \cos \delta_0 \sin \theta_A \quad (78)$$

$$\Delta V_y / M = -\ddot{v}_A + 2 \Omega \ell \dot{\delta} \sin \delta_0 + \Omega^2 v_A$$

$$- \Omega^2 \ell \, \delta \cos \delta_0 \sin \theta_A + \ell \ddot{\delta} \cos \delta_0 \sin \theta_A \quad (79)$$

$$\Delta V_z / M = -\ddot{w}_A - \ell \ddot{\delta} \cos \delta_0 \cos \theta_A \quad (80)$$

Since these discontinuous load reactions contain the time dependent pendulum angle, it must be related to the elastic displacements for its elimination. This can be accomplished by using the linearized pendulum equation (eq. (51). By seeking the simple harmonic motion of the form

$$\delta(t) = \bar{\delta} e^{i \omega t} \quad (81)$$

and corresponding harmonic solutions for the state variables, the pendulum deflection can be written as

$$\bar{\delta} = v_A \delta_v + w_A \delta_w + \mu_A \delta_\mu + \nu_A \delta_\nu \quad (82)$$

where

$$\delta_v = -\left[(\Omega^2 + \omega^2) \cos \delta_0 \sin \theta_A + 2 i \Omega \omega \sin \delta_0 \right] / a \quad (83)$$

$$\delta_w = \omega^2 \cos \delta_0 \cos \theta_A / a \quad (84)$$

$$\delta_\mu = \Omega^2 x_A \cos \delta_0 \sin \theta_A / a \quad (85)$$

$$\delta_\nu = -\Omega^2 x_A \cos \delta_0 \cos \theta_A / a \quad (86)$$

30

$$a = \ell(\omega_p^2 - \omega^2) + iC\,\Omega^2\omega\left(\frac{x_A}{\ell} + \cos\,\delta_o\right) \tag{87}$$

where C can be determined from the estimated damping ratio of equation (54) as

$$C = \frac{2\,\ell\zeta\left(\dfrac{x_A}{\ell\cos\,\delta_o} + \cos^2\,\delta_o\,\cos^2\,\theta_A\right)^{1/2}}{\Omega\,(x_A/\ell + \cos\,\delta_o)}$$

The discontinuous load reactions associated with the presence of the pendulum are used to relate the bending moment and shear force state variables on the right side (outboard) of x_A to those on the left side (inboard). These state variables are indicated in figure 5. The state variables are related as

$$\left.\begin{array}{ll}
M_x^R = M_x^L - \Delta M_x & V_x^R = V_x^L - \Delta V_x \\[2mm]
M_y^R = M_y^L - \Delta M_y & V_y^R = V_y^L - \Delta V_y \\[2mm]
M_z^R = M_z^L - \Delta M_z & V_z^R = V_z^L - \Delta V_z
\end{array}\right\} \tag{88}$$

All other state variables must be continuous across the point x_A.

Substituting for the shear and moment reactions, given by equations (75) to (80), with the explicit time dependency, the above relations can be described by

$$\left\{z^R\right\} = \left[P\right]\left\{z^L\right\} \tag{89}$$

where $[P]$ is a "point" transfer matrix. The elements of $[P]$ are all zero except for

$$P_{ij} = 1 \qquad\qquad (i = j)$$

$$P_{61} = M\left[(\ell\sin\,\delta_o + \zeta_A)\cos\,\theta_A + \eta_A\sin\,\theta_A\right](\Omega^2 + \omega^2) - \delta_v M_{x\delta}$$

$$P_{62} = M\left[(\ell\sin\,\delta_o + \zeta_A)\sin\,\theta_A - \eta_A\cos\,\theta_A\right]\omega^2 - \delta_w M_{x\delta}$$

$$P_{64} = -M\,\ell\sin\,\delta_o\,\cos\,\theta_A\,\Omega^2 x_A - \delta_\mu M_{x\delta}$$

$$P_{65} = -M\,\ell\sin\,\delta_o\,\sin\,\theta_A\,\Omega^2 x_A - \delta_v M_{x\delta}$$

$$P_{71} = -M\left[(\eta_A \sin\theta_A + \zeta_A \cos\theta_A)2i\omega\Omega \right.$$

$$\left. -\ell\cos\delta_o \sin\theta_A \cos\theta_A(\omega^2 + \Omega^2)\right] - \delta_v M_{y\delta}$$

$$P_{72} = M\omega^2\ell\cos\delta_o \sin^2\theta_A - \delta_w M_{y\delta}$$

$$P_{73} = -M(\eta_A \cos\theta_A - \zeta_A \sin\theta_A)\Omega^2 x_A$$

$$P_{74} = -M\Omega^2 x_A \ell\cos\delta_o \sin\theta_A \cos\theta_A - \delta_\mu M_{y\delta}$$

$$P_{75} = -M\Omega^2 x_A \ell\cos\delta_o \sin^2\theta_A - \delta_\nu M_{y\delta}$$

$$P_{81} = -M\left[\ell\cos\delta_o \cos^2\theta_A(\omega^2 + \Omega^2)\right.$$

$$\left. -(\eta_A \cos\theta_A - \zeta_A \sin\theta_A)2i\omega\Omega\right] - \delta_v M_{z\delta}$$

$$P_{82} = -M\omega^2\ell\cos\delta_o \cos\theta_A \sin\theta_A - \delta_w M_{z\delta}$$

$$P_{83} = -M(\eta_A \sin\theta_A + \zeta_A \cos\theta_A)\Omega^2 x_A$$

$$P_{84} = M\Omega^2 x_A \ell\cos\delta_o \cos^2\theta_A - \delta_\mu M_{z\delta}$$

$$P_{85} = M\Omega^2 x_A \ell\cos\delta_o \cos\theta_A \sin\theta_A - \delta_\nu M_{z\delta}$$

$$P_{91} = -2M i\omega\Omega - \delta_v V_{x\delta}$$

$$P_{92} = -\delta_w V_{x\delta}$$

$$P_{94} = -\delta_\mu V_{x\delta}$$

$$P_{95} = -\delta_\nu V_{x\,\delta}$$

$$P_{10,1} = -M(\omega^2 + \Omega^2) - \delta_\nu V_{y\,\delta}$$

$$P_{10,2} = -\delta_w V_{y\,\delta}$$

$$P_{10,4} = -\delta_\mu V_{y\,\delta}$$

$$P_{10,5} = -\delta_\nu V_{y\,\delta}$$

$$P_{11,1} = -\delta_\nu V_{z\,\delta}$$

$$P_{11,2} = -M\omega^2 - \delta_w V_{z\,\delta}$$

$$P_{11,4} = -\delta_\mu V_{z\,\delta}$$

$$P_{11,5} = -\delta_\nu V_{z\,\delta}$$

where

$$M_{x\,\delta} = M\Big\{ \Big[(\ell \sin \delta_o + \zeta_A) \cos \theta_A + \eta_A \sin \theta_A\Big](\Omega \cos \delta_o \sin \theta_A$$

$$-i\omega \sin \delta_o) 2\Omega \ell - \ell \eta_A \cos \delta_o (\Omega^2 - \omega^2)$$

$$+ \Omega^2 \beta_{pc} \ell \, x_A \cos \delta_o \sin \theta_A \Big\} \tag{90}$$

$$M_{y\delta} = -M\Bigg\{(\eta_A \sin \theta_A + \zeta_A \cos \theta_A) \ell \sin \delta_o (\omega^2 + \Omega^2)$$

$$+ \Big[(\ell \sin \delta_o + \zeta_A) \sin \theta_A - \eta_A \cos \theta_A\Big]$$

$$\cdot \Omega^2 \ell \sin \delta_o \sin \theta_A \cos \theta_A + (x_A \beta_{pc} \sin \delta_o$$

$$- \ell \cos^2 \delta_o \cos \theta_A) \Omega^2 \ell \sin^2 \theta_A + \Big[(\ell \sin \delta_o$$

$$+ \zeta_A) \cos \theta_A + \eta_A \sin \theta_A\Big] 2i\omega\Omega \ell \cos \delta_o \sin \theta_A$$

$$+ iC \Omega^2 \omega (x_A + \ell \cos \delta_o) \cos \theta_A\Bigg\} \qquad (91)$$

$$M_{z\delta} = M\Bigg\{(\eta_A \cos \theta_A - \zeta_A \sin \theta_A) \ell \sin \delta_o (\omega^2 + \Omega^2)$$

$$+ \Big[(\ell \sin \delta_o + \zeta_A) \sin \theta_A - \eta_A \cos \theta_A\Big]$$

$$\cdot \Omega^2 \ell \sin \delta_o \cos^2 \theta_A + (x_A \beta_{pc} \sin \delta_o$$

$$- \ell \cos^2 \delta_o \cos \theta_A) \Omega^2 \ell \cos \theta_A \sin \theta_A + \Big[(\eta_A \cos \theta_A$$

$$- \zeta_A \sin \theta_A) \sin \theta_A + \ell \sin \delta_o \cos^2 \theta_A\Big]$$

$$\cdot 2i\omega\Omega \ell \cos \delta_o - iC\Omega^2 \omega (x_A + \ell \cos \delta_o) \sin \theta_A\Bigg\} \qquad (92)$$

34

$$V_{x\delta} = -M\left[\ell \sin \delta_o (\omega^2 + \Omega^2) + 2 l \omega \Omega \ell \cos \delta_o \sin \theta_A\right] \tag{93}$$

$$V_{y\delta} = -M\left[\ell \cos \delta_o \sin \theta_A (\omega^2 + \Omega^2) - 2 l \omega \Omega \ell \sin \delta_o\right] \tag{94}$$

$$V_{z\delta} = M\omega^2 \ell \cos \delta_o \cos \theta_A \tag{95}$$

Lead-Lag Pendulum

The lead-lag pendulum after deformation is shown in figure 6. The equations of motion for the lead-lag pendulum can be derived by following the procedure used in the flapping pendulum case. This process yields the following equations for the lead-lag pendulum:

The relation between the pendulum mass and hinge in deformed coordinates

$$\left.\begin{aligned}
\xi_p &= \ell \cos \Delta \\[4pt]
\eta_p &= \eta_A + \ell \sin \Delta \\[4pt]
\zeta_p &= \zeta_A
\end{aligned}\right\} \tag{96}$$

Pendulum angle

$$\Delta \equiv \delta_o + \delta \tag{97}$$

where

$\delta_o \equiv$ steady-state equilibrium angle

$\delta \equiv$ time dependent perturbation angle

The equation for determination of the steady-state equilibrium angle, becomes

$$x_A \tan \delta_o + \ell \sin^2 \theta_A \sin \delta_o = -\tfrac{1}{2} \zeta_A \sin 2\theta_A + \eta_A \cos^2 \theta_A - \beta_{pc} x_A \sin \theta_A \tag{98}$$

The pendulum deflection in terms of the blade deflections

$$\bar{\delta} = v_A \delta_v + w_A \delta_w + \mu_A \delta_\mu + \nu_A \delta_\nu \tag{99}$$

where

$$\delta_v = \left[(\Omega^2 + \omega^2) \cos \delta_o \cos \theta_A - 2i\omega\Omega \sin \delta_o\right]/a \qquad (100)$$

$$\delta_w = \omega^2 \cos \delta_o \sin \theta_A/a \qquad (101)$$

$$\delta_\mu = -\Omega^2 x_A \cos \delta_o \cos \theta_A/a \qquad (102)$$

$$\delta_\nu = -\Omega^2 x_A \cos \delta_o \sin \theta_A/a \qquad (103)$$

$$a = \ell(\omega_p^2 - \omega^2) + i C\Omega^2\omega \left(\frac{x_A}{\ell} + \cos \delta_o\right) \qquad (104)$$

$$\omega_p^2 = \Omega^2\left(\frac{x_A}{\ell \cos \delta_o} + \cos^2 \delta_o \sin^2 \theta_A\right) \qquad (105)$$

$$C = \frac{2 \ell \zeta \left(\frac{x_A}{\ell \cos \delta_o} + \cos^2 \delta_o \sin^2 \theta_A\right)^{1/2}}{\Omega (x_A/\ell + \cos \delta_o)} \qquad (106)$$

$$\delta = \bar{\delta} e^{i\omega t} \qquad (107)$$

The nonzero elements of the point transfer matrix become

$$P_{ij} = 1 \quad (i = j)$$

$$P_{61} = M\left[\zeta_A \cos \theta_A + (\eta_A + \ell \sin \delta_o) \sin \theta_A\right](\omega^2 + \Omega^2) - \delta_v M_{x\delta}$$

$$P_{62} = M\left[\zeta_A \sin \theta_A - (\eta_A + \ell \sin \delta_o) \cos \theta_A\right]\omega^2 - \delta_w M_{x\delta}$$

$$P_{64} = -M \ell \sin \delta_o \sin \theta_A \Omega^2 x_A - \delta_\mu M_{x\delta}$$

36

$$P_{65} = M\ell \sin \delta_o \cos \theta_A \; \Omega^2 x_A - \delta_\nu M_{x \delta}$$

$$P_{71} = -M\left[(\eta_A \sin \theta_A + \zeta_A \cos \theta_A) 2i\omega\Omega + \ell \cos \delta_o \cos \theta_A \right.$$
$$\left. \cdot \sin \theta_A(\omega^2 + \Omega^2)\right] - \delta_\nu M_{y \delta}$$

$$P_{72} = M\ell \cos \delta_o \cos^2 \theta_A \omega^2 - \delta_w M_{y \delta}$$

$$P_{73} = -M(\eta_A \cos \theta_A - \zeta_A \sin \theta_A) \Omega^2 x_A$$

$$P_{74} = M\ell \cos \delta_o \cos \theta_A \sin \theta_A \Omega^2 x_A - \delta_\mu M_{y \delta}$$

$$P_{75} = -M\ell \cos \delta_o \cos^2 \theta_A \Omega^2 x_A - \delta_\nu M_{y \delta}$$

$$P_{81} = -M\left[\ell \cos \delta_o \sin^2 \theta_A(\omega^2 + \Omega^2) \right.$$
$$\left. -(\eta_A \cos \theta_A - \zeta_A \sin \theta_A) 2i\omega\Omega\right] - \delta_\nu M_{z \delta}$$

$$P_{82} = M\omega^2 \ell \cos \delta_o \sin \theta_A \cos \theta_A - \delta_w M_{z \delta}$$

$$P_{83} = -M(\eta_A \sin \theta_A + \zeta_A \cos \theta_A) \Omega^2 x_A$$

$$P_{84} = M\Omega^2 x_A \ell \cos \delta_o \sin^2 \theta_A - \delta_\mu M_{z \delta}$$

$$P_{85} = -M\Omega^2 x_A \ell \cos \delta_o \sin \theta_A \cos \theta_A - \delta_\nu M_{z \delta}$$

$$P_{91} = -2Mi \omega\Omega - \delta_\nu V_{x \delta}$$

$$P_{92} = -\delta_w V_{x \delta}$$

$$P_{94} = -\delta_\mu V_{x \delta}$$

$$P_{95} = -\delta_\nu V_{x \delta}$$

$$P_{10,1} = -M(\omega^2 + \Omega^2) - \delta_v V_{y\,\delta}$$

$$P_{10,2} = -\delta_w V_{y\,\delta}$$

$$P_{10,4} = -\delta_\mu V_{y\,\delta}$$

$$P_{10,5} = -\delta_\nu V_{y\,\delta}$$

$$P_{11,1} = -\delta_v V_{z\,\delta}$$

$$P_{11,2} = -M\omega^2 - \delta_w V_{z\,\delta}$$

$$P_{11,4} = -\delta_\mu V_{z\,\delta}$$

$$P_{11,5} = -\delta_\nu V_{z\,\delta}$$

where

$$
\begin{aligned}
M_{x\,\delta} = -M \Big\{ &\big[\zeta_A \cos\theta_A + (\eta_A + \ell \sin\delta_o) \sin\theta_A \big] \\
&\cdot (\Omega \cos\delta_o \cos\theta_A + i\omega \sin\delta_o) \, 2\Omega\ell \\
&- \ell\,\zeta_A \cos\delta_o (\Omega^2 - \omega^2) + \Omega^2 \beta_{pc}\, \ell x_A \cos\delta_o \cos\theta_A \Big\} \quad (108)
\end{aligned}
$$

$$
\begin{aligned}
M_{y\,\delta} = -M \Big\{ &(\eta_A \sin\theta_A + \zeta_A \cos\theta_A) \ell \sin\delta_o (\omega^2 + \Omega^2) \\
&+ \big[-\zeta_A \sin\theta_A + (\eta_A + \ell \sin\delta_o) \cos\theta_A \big] \Omega^2 \ell \sin\delta_o \sin\theta_A \cos\theta_A \\
&+ (x_A \beta_{pc} \sin\delta_o - \ell\cos^2\delta_o \sin\theta_A) \Omega^2 \ell \cos^2\theta_A \\
&- \big[(\eta_A + \ell \sin\delta_o) \sin\theta_A + \zeta_A \cos\theta_A \big] 2i\,\omega\Omega\,\ell\cos\delta_o \cos\theta_A \\
&- iC\Omega^2\omega (x_A + \ell \cos\delta_o) \sin\theta_A \Big\} \quad (109)
\end{aligned}
$$

38

$$M_{z\delta} = M\left\{(\eta_A \cos\theta_A - \zeta_A \sin\theta_A)\, \ell \sin\delta_o\,(\omega^2 + \Omega^2)\right.$$

$$+ \left[\zeta_A \sin\theta_A - (\eta_A + \ell \sin\delta_o)\cos\theta_A\right]\Omega^2 \ell \sin\delta_o \sin^2\theta_A$$

$$-(x_A \beta_{pc} \sin\delta_o - \ell \cos^2\delta_o \sin\theta_A)\,\Omega^2 \ell \cos\theta_A \sin\theta_A$$

$$- \left[(\eta_A \cos\theta_A - \zeta_A \sin\theta_A)\cos\theta_A - \ell \sin\delta_o \sin^2\theta_A\right]$$

$$\left. \cdot 2i\omega\Omega\,\ell \cos\delta_o - iC\,\Omega^2\omega\,(x_A + \ell \cos\delta_o)\cos\theta_A\right\} \qquad (110)$$

$$V_{x\delta} = -M\left[\ell \sin\delta_o\,(\omega^2 + \Omega^2) - 2i\omega\Omega\,\ell \cos\delta_o \cos\theta_A\right] \qquad (111)$$

$$V_{y\delta} = M\left[\ell \cos\delta_o \cos\theta_A\,(\omega^2 + \Omega^2) + 2i\omega\Omega\,\ell \sin\delta_o\right] \qquad (112)$$

$$V_{z\delta} = M\omega^2 \ell \cos\delta_o \sin\theta_A \qquad (113)$$

AERODYNAMIC FORCES

This section is concerned with the calculation of the aerodynamic loads on a helicopter rotor blade in forward flight. Due to the complexity of the flow field involved and the interaction of different effects in the flow, a completely general solution to the problem has not been obtained. There are a large number of approximate methods available. These methods range in complexity from simple blade element representations to lifting surface models with freely distorted vortex wakes, with associated ranges in computational expense, accuracy and detail of the solution. Commonly used is an approach based on a combination of simple momentum theory and the blade element description. This method is adopted for the present study. The method takes no note of the reverse flow and stall.

The aerodynamic forces are formulated from two-dimensional, incompressible, quasi-steady, strip theory in which only the velocity components perpendicular to the spanwise axis of the deformed blade are assumed to influence the aerodynamic loading. Account is taken of the varying freestream velocity associated with the rotating blade by employing Greenberg's extension (ref. 11) of Theodorsen's unsteady theory for determining the aerodynamic lift and pitching moment acting on the blade. The resulting expressions are specialized to the case of quasi-steady flow by setting Theodorsen's circulation function to unity. Simple momentum theory is used to calculate the steady flow induced by the rotor. The expressions for the aerodynamic loading are based on the analysis reported in reference 12.

In Theodorsen's theory a two-dimensional airfoil is assumed to be pivoted about an axis which may be distinct, in general, from the aerodynamic center. The airfoil is pitched at an angle $\epsilon(t)$ to the freestream flowing at constant velocity V. The airfoil is vertically displaced with velocity h (t) as shown in figure 7. Greenberg (ref. 11) has extended Theodorsen's theory for a varying free-stream velocity V(t). The lift and moment acting on an element section of the blade may be expressed in terms of the circulatory and noncirculatory components as

$$L = L_C + L_{NC}$$
$$M = M_C + M_{NC}$$
$$(114)$$

With the airfoil pivot axis (analogous to the rotor blade elastic axis) at the airfoil quarter chord (the airfoil aerodynamic center) the relations for the aerodynamic loads per unit length may be written as (ref. 12).

$$L_{NC} = \frac{1}{2} \rho a \frac{c^2}{4} \left(-\dot{U}_p + \frac{c}{4}\ddot{\epsilon} \right) \qquad (115a)$$

$$L_C = \frac{1}{2} \rho acU \left(-U_p + \frac{c}{2}\dot{\epsilon} \right) \qquad (115b)$$

$$M_{NC} = -\frac{1}{2} \rho ac \left(\frac{c}{4}\right)^2 \left(-\dot{U}_p - U_T\dot{\epsilon} + \frac{3c}{8}\ddot{\epsilon} \right) \qquad (115c)$$

$$M_C = -\frac{1}{2} \rho ac \left(\frac{c}{4}\right)^2 2U_T\dot{\epsilon} \qquad (115d)$$

The profile drag force acts parallel to U and is given by

$$D = \frac{1}{2} \rho ac \frac{c_{do}}{a} U^2 \qquad (116)$$

The components of the aerodynamic forces in the deformed coordinate system can be written as

$$F_{y'} = -L_C \sin \alpha - D \cos \alpha$$
$$F_{z'} = L_C \cos \alpha + L_{NC} - D \sin \alpha$$
$$(117)$$

where

$$\sin \alpha = U_p/U$$

$$\cos \alpha = U_T/U$$

$$U \simeq \sqrt{U_T^2 + U_p^2}$$

Substituting equations (115a), (115b) and (116) into equations (117) yields

$$F_{y'} = \frac{1}{2} \rho \, ac \left[U_p^2 - \frac{c}{2} U_p \, \dot{\epsilon} - \frac{c_{do}}{a} U_T^2 \right]$$

$$F_{z'} = \frac{1}{2} \rho \, ac \left[-U_p U_T + \frac{c}{2} \, \dot{\epsilon} \, U_T - \frac{c}{2} \dot{U}_p + \left(\frac{c}{4}\right)^2 \ddot{\epsilon} \right]$$

(118)

From equations (115c) and (115d) the pitching moment can be written as

$$M_{x'} (=M_\phi) = -\frac{1}{2} \rho \, ac \left(\frac{c}{4}\right)^2 \left[U_T \dot{\epsilon} - \dot{U}_p + \frac{3c}{8} \ddot{\epsilon} \right]$$

(119)

where

$U_p, U_T \equiv$ relative velocity components in the deformed coordinate system (fig. 7)

$\dot{\epsilon} \equiv$ angular velocity of the blade about the x' - axis

$$V(t) \simeq \sqrt{U_T^2 + U_p^2}$$

The assumed orders of magnitude of the quantities used in deriving the aerodynamic loads are

$$\frac{U_p}{U_T} = O(\epsilon)$$

$$\frac{c_{do}}{a} = O(\epsilon^2)$$

$$\frac{c}{R} = O(\epsilon)$$

$$\frac{v_i}{\Omega R} = O(\epsilon)$$

$$\theta = O(\epsilon)$$

The aerodynamic forces in the undeformed coordinate system are obtained by using the transformation given by equation (A-4). To second order, the aerodynamic loads can be written as

$$
\left.
\begin{aligned}
L_v\ (=F_y) &= & F_{y'} - F_{z'}\,(\theta + \phi) \\[2mm]
L_w\ (=F_z) &= & F_{y'}\,(\theta + \phi) + F_{z'} \\[2mm]
M_x &= & M_{x'}
\end{aligned}
\right\}
\tag{120}
$$

In equations (118) and (119) the blade aerodynamic loads are expressed in terms of U_T, U_p, and $\dot{\varepsilon}$. In order to use the expressions for blade aerodynamic loads in the blade equations of motion, U_T, U_p, and $\dot{\varepsilon}$ must be expressed in terms of the blade bending and torsion deflections v, w, and ϕ. The blade velocity is easily expressed in the x, y, z coordinate system. The deformed blade coordinate transformation, which relates the x,y, z and x', y', z' coordinate systems, is given by equation (A-4). This is used to express the U_T and U_p velocity components in terms of v, w, and ϕ.

The total flow velocity seen by a point on the elastic axis can be written from reference 12 as

$$
\begin{aligned}
\vec{V} = \ & (\mu_f \Omega R \cos\psi + \Omega R \lambda \, \beta_{pc} - \dot{u} + \Omega v)\,\vec{i} \\[3mm]
& + (\Omega \beta_{pc}\, w - \dot{v} - \Omega(x + u) - \mu_f \Omega R \sin\psi)\,\vec{j} \\[3mm]
& + (\Omega R \lambda - \mu_f \Omega R \beta_{pc} \cos\psi - \dot{w} - \Omega \beta_{pc} v)\,\vec{k}
\end{aligned}
\tag{121}
$$

where

$$
\mu_f = \frac{V \cos\alpha_s}{\Omega R}
$$

$$
\lambda = \frac{V \sin\alpha_s - v_i}{\Omega R}
$$

and the aerodynamic velocity components are shown in figure 8.

The tangential and perpendicular velocity components, U_T and U_p, are obtained from equation (121) using $[T]$ from equation (A-4). To second order in the dependent variables they have the form

$$U_T = \mu_f \, \Omega R \, v' \cos \psi + \Omega x + \mu_f \, \Omega R \sin \psi + \dot{v} \qquad (122)$$

$$U_p = \mu_f \, \Omega R \, w' \cos \psi - \mu_f \, \Omega R \, v' \theta \cos \psi$$

$$- (\mu_f \, \Omega R \sin \psi + \Omega x)(\theta + \phi) - \dot{v}\theta$$

$$+ \mu_f \, \Omega R \, \beta_{pc} \cos \psi - \Omega R \lambda + \dot{w} + \Omega \beta_{pc} v \qquad (123)$$

It may be noted that the nonlinear terms are neglected.

The angular velocity about the x' axis, $\dot{\varepsilon}$, is now considered. It can be regarded as being composed of three parts: the first part due to the rigid-body angular velocity of the hub in space, the second part due to the control inputs, and the third due to the angular velocity associated with the elastic deformations. The total sectional pitching velocity can be written as (ref. 12.)

$$\dot{\varepsilon} = \Omega \, (\beta_{pc} + w' + \theta_{1c} \sin \psi - \theta_{1s} \cos \psi) + \dot{\phi} \qquad (124)$$

It may be noted that the total geometric pitch angle, θ , is given by

$$\theta = \theta_{pt} + \theta_c - \theta_{1c} \cos \psi - \theta_{1s} \sin \psi \qquad (125)$$

where θ_{pt} is the built-in twist angle (pretwist), θ_c is the collective pitch angle measured at the tip, and θ_{1c} and θ_{1s} are the first harmonic cyclic pitch components. The built-in twist is a linear linear function of x and may be written as

$$\theta_{pt} = - \theta_t (R - x) \qquad (126)$$

The induced veloctiy, v_i, is calculated by equating the integral thrust to the thrust from momentum theory using the relations

$$v_i = \frac{C_T \Omega R}{2 \sqrt{\mu_f^2 + \lambda^2}} \qquad (127)$$

$$C_T = \frac{b}{2\pi} \; \frac{1}{\pi \rho \Omega^2 R^4} \int_0^{2\pi} \int_0^R L_{w_o} \, dx \, d\psi \qquad (128)$$

where L_{w_o} is the steady-state value of L_w.

Substituting equations (118) and (119) into equations (120) and using expressions for U_T, U_P, and $\dot{\epsilon}$, given by equations (122) to (124), the aerodynamic loads to second order can be written as

$$
L_v = \frac{1}{2}\rho\, ac \left[-(\Omega x + \mu_f \Omega R \sin\psi)\theta + 2(\mu_f \Omega R \beta_{pc} \cos\psi \right.
$$

$$
\left. -\Omega R \lambda) \right] \dot{w} + \frac{1}{2}\rho\, ac \left[-(\Omega x + \mu_f \Omega R \sin\psi) \right.
$$

$$
\left. \cdot (\mu_f \Omega R \beta_{pc} \cos\psi - \Omega R \lambda) \right] \phi + \frac{1}{2}\rho\, ac \left[-(\Omega x \right.
$$

$$
\left. + \mu_f \Omega R \sin\psi)\theta + 2(\mu_f \Omega R \beta_{pc} \cos\psi - \Omega R \lambda) \right]
$$

$$
\cdot \mu_f \Omega R \cos\psi\, v + \frac{1}{2}\rho\, ac \left[-(\Omega x + \mu_f \Omega R \sin\psi) \right.
$$

$$
\cdot (\mu_f \Omega R \beta_{pc} \cos\psi - \Omega R \lambda)\theta - \frac{c_{do}}{a}(\Omega x
$$

$$
\left. + \mu_f \Omega R \sin\psi)^2 + (\mu_f \Omega R \beta_{pc} \cos\psi - \Omega R \lambda)^2 \right] \qquad (129)
$$

$$L_W = \frac{1}{2}\rho\, ac\left[-(\Omega x + \mu_f \Omega R \sin\psi)\,\Omega\,\beta_{pc}\right] v$$

$$+ \frac{1}{2}\rho\, ac\left[2(\Omega x + \mu_f \Omega R \sin\psi)\,\theta - (\mu_f \Omega R \beta_{pc}\cos\psi\right.$$

$$\left. - \Omega R\lambda)\right]\dot{v} + \frac{1}{2}\rho\, ac\left[-(\Omega x + \mu_f \Omega R \sin\psi)\,\dot{w} - \frac{c}{4}\ddot{w}\right]$$

$$+ \frac{1}{2}\rho\, ac\left[-(\Omega x + \mu_f \Omega R \sin\psi)^2\right.$$

$$\left. + \frac{c}{4}\mu_f\,\Omega^2 R\cos\psi\right]\phi + \frac{1}{2}\rho\, ac\left[\frac{3c}{4}(\Omega x\right.$$

$$\left. + \mu_f \Omega R \sin\psi)\right]\dot{\phi} + \frac{1}{2}\rho\, ac\left[2(\Omega x\right.$$

$$\left. + \mu_f \Omega R \sin\psi)\,\theta - (\mu_f \Omega R \beta_{pc}\cos\psi - \Omega R\lambda)\right]$$

$$\cdot(\mu_f \Omega R \cos\psi)\,\mu + \frac{1}{2}\rho\, ac\left[-(\Omega x\right.$$

$$\left. + \mu_f \Omega R \sin\psi)\,\mu_f \Omega R \cos\psi + \frac{c}{2}\Omega(\Omega x\right.$$

$$\left. + \mu_f \Omega R \sin\psi) + \frac{c}{4}\mu_f\,\Omega^2 R \sin\psi\right]v$$

$$+ \frac{1}{2}\rho\, ac\left[-\frac{c}{4}\mu_f\,\Omega R \cos\psi\right]\dot{v}$$

$$+ \frac{1}{2}\rho\, ac\left[-(\mu_f \Omega R\,\beta_{pc}\cos\psi - \Omega R\lambda) + (\mu_f \Omega R \sin\psi\right.$$

$$\left. + \Omega x)\,\theta\right](\Omega x + \mu_f \Omega R \sin\psi)$$

$$+ \frac{1}{2}\rho\, ac\left[\frac{c}{2}(\Omega\beta_{pc} + \frac{3}{2}\dot{\theta})(\Omega x + \mu_f \Omega R \sin\psi)\right.$$

$$\left. + \frac{c}{4}\mu_f\,\Omega^2 R \cos\psi\,\theta + \frac{c}{4}\mu_f\,\Omega^2 R\,\beta_{pc}\sin\psi\right] \qquad (130)$$

$$M_\phi = -\frac{1}{2}\rho\, ac\,(\tfrac{c}{4})^2 \left[-\ddot{w} + \mu_f\,\Omega^2\,R\cos\psi\,\phi \right.$$

$$+ 2(\Omega x + \mu_f\,\Omega R \sin\psi)\,\dot{\phi} + (\Omega^2 x + 2\mu_f\,\Omega^2 R\sin\psi)\,\nu$$

$$\left. - \mu_f\,\Omega\,R\cos\psi\,\dot{\nu} \right]$$

$$-\frac{1}{2}\rho\, ac\,(\tfrac{c}{4})^2 \left[(\Omega x + \mu_f\,\Omega R\sin\psi) \right.$$

$$\cdot (\Omega\,\beta_{pc} + 2\dot{\theta}) + \mu_f\,\Omega^2\,R\,\theta\cos\psi$$

$$\left. + \mu_f\,\Omega^2\,R\,\beta_{pc}\sin\psi \right] \qquad (131)$$

The above expressions can be rewritten in matrix form as (retaining only time-dependent terms)

$$\{F_a\} = \left[B(x,t)\right]\{Z(x,t)\} + \left[C(x,t)\right]\{\dot{Z}(x,t)\} + \left[D(x,t)\right]\{\ddot{Z}(x,t)\}$$

$$+ \sum_{n=1}^{3} \left[B_c(x,t)\right]_n \{Z(x,t)\}\cos n\psi$$

$$+ \sum_{n=1}^{3} \left[C_c(x,t)\right]_n \{\dot{Z}(x,t)\}\cos n\psi$$

$$+ \sum_{n=1}^{3} \left[B_s(x,t)\right]_n \{Z(x,t)\}\sin n\psi$$

$$+ \sum_{n=1}^{3} \left[C_s(x,t)\right]_n \{\dot{Z}(x,t)\}\sin n\psi$$

$$+ \sum_{n=1}^{3} \{P_c(x)\}_n \cos n\psi + \sum_{n=1}^{3} \{P_s(x)\}_n \sin n\psi \qquad (132)$$

where $\{Z\}$ is the state vector, defined by equation (1), and

$$\{F_a\}^T \equiv \lfloor 0 \quad 0 \quad 0 \quad 0 \quad 0 \quad -M_\phi \quad 0 \quad 0 \quad 0 -L_v -L_w \rfloor \qquad (133)$$

The nonzero elements of the elastic-deformation-independent aerodynamic load vector, P, are:

For $n = 1$;

$$P_{c6} = \frac{1}{2} \rho \, ac \left(\frac{c}{4}\right)^2 \Omega \left[-2\Omega x \, \theta_{1s} + \mu_f \, \Omega R (\theta_t + \theta_c) \right]$$

$$P_{c10} = -\frac{1}{2} \rho ac \, \Omega R \left[-2 \beta_{pc} \mu_f \Omega R\lambda - (\theta_t + \theta_c) \beta_{pc} \mu_f \Omega x \right.$$

$$\left. + \frac{1}{4} \beta_{pc} \mu_f^2 \, \Omega R \, \theta_{1s} - \lambda \Omega x \, \theta_{1c} \right]$$

$$P_{c11} = -\frac{1}{2} \rho \, ac \, \Omega R \left[-\beta_{Pc} \mu_f \Omega x + \frac{c}{4} (\theta_t + \theta_c) \mu_f \Omega \right.$$

$$\left. - \frac{3c}{4} \Omega \left(\frac{x}{R}\right) \theta_{1s} - \left(\frac{\Omega x^2}{R} + \frac{1}{4} \mu_f^2 \, \Omega R\right) \theta_{1c} \right]$$

$$P_{s6} = \frac{1}{2} \rho ac \left(\frac{c}{4}\right)^2 \Omega \left[2\Omega x \, \theta_{1c} + 2\Omega \beta_{pc} \mu_f R \right]$$

$$P_{s10} = -\frac{1}{2} \rho \, ac \, \Omega R \left[-2 \frac{c_{do}}{a} \mu_f \Omega x + (\theta_t + \theta_c) \mu_f \Omega R\lambda \right.$$

$$\left. - \lambda \Omega x \, \theta_{1s} + \frac{1}{4} \beta_{pc} \mu_f^2 \Omega R \, \theta_{1c} \right]$$

$$P_{s11} = -\frac{1}{2} \rho ac \, \Omega R \left[\frac{3c}{4} \beta_{pc} \, \Omega \mu_f + \lambda \Omega \mu_f R \right.$$

$$\left. + 2 (\theta_t + \theta_c) \mu_f \Omega x - \left(\frac{\Omega x^2}{R} + \frac{3}{4} \mu_f^2 \, \Omega R\right) \theta_{1s} \right.$$

$$\left. + \frac{3c}{4} \Omega \left(\frac{x}{R}\right) \theta_{1c} \right]$$

For $n = 2$;

$$P_{c6} = \frac{1}{2} \rho\, ac \left(\frac{c}{4}\right)^2 \Omega \left(\frac{-3}{2} \mu_f \Omega R\, \theta_{1c}\right)$$

$$P_{c10} = -\frac{1}{2} \rho\, ac\, \Omega R \left[\frac{1}{2} \frac{c_{do}}{a} \mu_f^2 \Omega R + \frac{1}{2} \beta_{pc}^2 \mu_f^2 \Omega R\right.$$

$$\left. + \frac{1}{2} \lambda \mu_f \Omega R\, \theta_{1s} + \frac{1}{2} \beta_{pc} \mu_f \Omega x\, \theta_{1c}\right]$$

$$P_{c11} = -\frac{1}{2} \rho\, ac\, \Omega R \left[-\frac{1}{2}(\theta_t + \theta_c) \mu_f^2 \Omega R + \Omega \mu_f x\, \theta_{1s}\right.$$

$$\left. - \frac{c}{2} \mu_f \Omega\, \theta_{1c}\right]$$

$$P_{s6} = \frac{1}{2} \rho\, ac \left(\frac{c}{4}\right)^2 \Omega \left(\frac{-3}{2} \mu_f \Omega R\, \theta_{1s}\right)$$

$$P_{s10} = -\frac{1}{2} \rho\, ac\, \Omega R \left[-\frac{1}{2}(\theta_t + \theta_c) \beta_{pc} \mu_f^2 \Omega R + \frac{1}{2}\beta_{pc} \mu_f \Omega x\, \theta_{1s}\right.$$

$$\left. - \frac{1}{2} \lambda \mu_f \Omega R\, \theta_{1c}\right]$$

$$P_{s11} = -\frac{1}{2} \rho\, ac\, \Omega R \left[-\frac{1}{2} \beta_{pc} \mu_f^2 \Omega R - \frac{1}{2} c \mu_f \Omega\, \theta_{1s} - \Omega \mu_f x\, \theta_{1c}\right]$$

For $n = 3$;

$$P_{c10} = -\frac{1}{2} \rho\, ac\, \Omega R \left(-\frac{1}{4} \beta_{pc} \mu_f^2 \Omega R\, \theta_{1s}\right)$$

$$P_{c11} = -\frac{1}{2} \rho\, ac\, \Omega R \left(\frac{1}{4} \mu_f^2 \Omega R\, \theta_{1c}\right)$$

$$P_{s10} = -\frac{1}{2} \rho\, ac\, \Omega R \left(\frac{1}{4} \beta_{pc} \mu_f^2 \Omega R\, \theta_{1c}\right)$$

$$P_{s11} = -\frac{1}{2} \rho\, ac\, \Omega R \left(\frac{1}{4} \mu_f^2 \Omega R\, \theta_{1s}\right)$$

48

The first seven terms in equation (132) represent the aerodynamic loads due to elastic deformations. The coefficients of the corresponding matrices are given in Appendix C.

The aerodynamic loads as represented by equation (132) are to be included in the blade equations of motion. It may be recalled that the solution to these equations is treated as individual contributions associated with each harmonic of the excitation loading. Such a solution may be written in a complex form as, equation (22),

$$\left\{ Z_n(x, t) \right\} = \text{Re}\left(\left\{ \bar{Z}_n(x) \right\} e^{i\omega t} \right) \tag{134}$$

where

$$\omega = n\Omega \qquad\qquad (n = 1, 2, 3) \tag{135}$$

In the aerodynamic loads expression (eq. (132)) the fourth to the seventh terms contain functions of the azimuth angle (rotational speed). Due to the existence of these terms, the above solution (eq. (134) can not be applied. Instead, the state vector should be written as

$$\left\{ Z(x, t) \right\} = \text{Re}\left(\sum_{n=-\infty}^{\infty} \left\{ \bar{Z}_n(x) \right\} e^{in\Omega t} \right) \tag{136}$$

In this case the resulting equations must be solved simultaneously for all harmonics. Even if only three harmonics are considered for the state vector (eq. (136)) obtaining the corresponding solution is very complicated. An approximate method is used to determine the aerodynamic forces by neglecting the fourth to the seventh terms in equation (132). These terms are of lower order than the corresponding terms in the blade equations of motion and thus may be neglected according to the adopted ordering scheme. Although the first three terms of equation (132) may also be neglected according to the ordering scheme, they are retained here. These aeroelastic terms will be the only representation of coupling between the elastic deformations and the aerodynamic loading.

With the fourth to the seventh terms in equation (132) neglected the solution given by equation (134) can be applied. Substituting equation (134) into equation (132) yields the following complex notation for the nth harmonic of the aerodynamic load.

$$\left\{ \bar{F}_a \right\} = \left[A_a \right] \left\{ \bar{Z} \right\} + \left\{ \bar{P} \right\} \tag{137}$$

where

$\left\{ \bar{F}_a \right\} \equiv$ amplitude vector of the aerodynamic load

$\left\{ \bar{P} \right\} \equiv$ amplitude vector of the elastic-deformation-independent aerodynamic force

and

$$\{\bar{P}\} = \{P_c\} - i \{P_s\} \tag{138}$$

$$[A_a] = [B(x, \omega)] + i\omega [C(x, \omega)] - \omega^2 [D(x,\omega)] \tag{139}$$

From equation (139) and Appendix C, the nonzero elements of $[A_a]$ are

$$A_{a62} = \frac{1}{2} \rho\, ac\, (\tfrac{c}{4})^2\, \omega^2$$

$$A_{a63} = \frac{1}{2} \rho\, ac\, (\tfrac{c}{4})^2\, (2i\omega\Omega\, x)$$

$$A_{a65} = \frac{1}{2} \rho\, ac\, (\tfrac{c}{4})^2\, \Omega^2 x$$

$$A_{a10,2} = -\frac{1}{2} i\, \rho ac\, \omega \left[-\Omega x\,(\theta_c + \theta_t) + \frac{1}{2}\,\mu_f\,\Omega R\,\theta_{1s} - 2\Omega R\,\lambda \right]$$

$$A_{a10,3} = -\frac{1}{2}\, \rho\, ac\, \Omega^2\, x\, R\, \lambda$$

$$A_{a10,5} = -\frac{1}{2}\, \rho\, ac\, (\tfrac{1}{2}\,\Omega^2 x\,\mu_f\, R\,\theta_{1c} + \Omega^2\,\mu_f^2\, R^2\,\beta_{pc})$$

$$A_{a11,1} = -\frac{1}{2}\, \rho\, ac\, (-\Omega^2 x\,\beta_{pc})$$

$$-\frac{1}{2} i\rho\, ac\, \omega \left[2\Omega x\,(\theta_c + \theta_t) - \mu_f\,\Omega R\,\theta_{1s} + \Omega R\,\lambda \right]$$

$$A_{a11,2} = -\frac{1}{2}\, \rho ac\, (-i\omega\Omega\, x + \tfrac{c}{4}\,\omega^2)$$

$$A_{a11,3} = -\frac{1}{2}\, \rho ac\, (-\Omega^2 x^2 - \frac{1}{2}\,\mu_f^2\,\Omega^2 R^2 + \tfrac{3c}{4}\,i\omega\Omega\, x)$$

$$A_{a11,4} = -\frac{1}{2}\, \rho ac\, (-\Omega^2 x\,\mu_f\, R\,\theta_{1c} - \frac{1}{2}\,\Omega^2\,\mu_f^2\, R^2\,\beta_{pc})$$

$$A_{a11,5} = -\frac{1}{2} \rho ac \left(\frac{c}{2} \Omega^2 x\right)$$

The induced velocity, v_i, is obtained by substituting the steady-state value of L_w from equation (130) into equations (127) and (128). The resulting equation is

$$v_i = \mu_f \tan \alpha_s - \lambda = \frac{a_n(6\lambda + C_n)}{\sqrt{\mu_f^2 + \lambda^2}} \qquad (140)$$

where

$$\mu_f = \frac{V \cos \alpha_s}{\Omega R} \qquad (141)$$

$$a_n = \frac{1}{48} \frac{bc}{\pi R} a \qquad (142)$$

$$C_n = (4 + 6\mu_f^2) \theta_c - (1 + 3\mu_f^2) \theta_t R - 6\mu_f \theta_{1s}$$

$$+ \frac{c}{R} (3\beta_{pc} + 3\mu_f \theta_{1c}) \qquad (143)$$

Equation (140) is an algebraic equation in λ.

TRANSFER MATRIX METHOD

System Equations

The blade equations of motion are given in a matrix form by equation (23) for the nth harmonic of frequency ω as

$$\{\bar{Z}(x)\}' = [A(x)] \{\bar{Z}(x)\} + \{\bar{F}_n(x)\} \qquad (144)$$

The boundary conditions corresponding to a hingeless rotor blade are idealized in this analysis as being cantilevered at the hub ($x = 0$) and free at the tip ($x = R$).

Hub: $$\left\{ \bar{Z}_d (0) \right\} = \left\{ 0 \right\}$$ (145)

Tip: $$\left\{ \bar{Z}_f (R) \right\} = \left\{ 0 \right\}$$ (146)

where

$$\left\{ \bar{Z}_d (x) \right\}^T = \lfloor \bar{v} \quad \bar{w} \quad \bar{\phi} \quad \bar{\mu} \quad \bar{\nu} \rfloor$$ (147)

$$\left\{ \bar{Z}_f (x) \right\}^T = \lfloor \bar{M}_x \quad \bar{M}_y \quad \bar{M}_z \quad \bar{V}_x \quad \bar{V}_y \quad \bar{V}_z \rfloor$$ (148)

Equation (144) represents a set of 11 linear first-order ordinary nonhomogeneous differential equations. It may be noted that $\lfloor A \rfloor$ is a complex matrix due to inclusion of the linear damping terms. The desired solution is obtained by the fomulation of a field transfer matrix which relates the state variables between any two points along the blade.

Transfer Matrix

The concept of the transfer matrix has been thoroughly discussed by Pestel and Leckie in reference 13. The backward transfer matrix $\lfloor T(x) \rfloor$ is defined by

$$\left\{ Z(x) \right\} = \left[T(x) \right] \left\{ Z(0) \right\}$$ (149)

which relates the state vector at two stations.

It is often possible to determine the transfer matrix by using simple statics. Such techniques are described in reference 13. These techniques prove satisfactory for simple lumped parameter or lower order uniform continuous systems, but become cumbersome when used for nonuniform and higher order systems because of the required algebraic manipulation. Murthy (ref. 9) has presented a systematic approach which eliminates much of the algebra and results directly in differential equations for the elements of the transfer matrix. The state vector usually satisfies the differential equation

$$\frac{d}{dx} \left\{ Z(x) \right\} = \left[A(x) \right] \left\{ Z(x) \right\}$$ (150)

Differentiating equation (149) with respect to x gives

52

$$\frac{d}{dx}\left\{Z(x)\right\} = \frac{d}{dx}\left[T(x)\right]\left\{Z(0)\right\} \tag{151}$$

From equation (149) it is obvious that

$$\left\{Z(0)\right\} = \left[T(x)\right]^{-1}\left\{Z(x)\right\} \tag{152}$$

Substituting this into equation (151) the following equation can be obtained

$$\frac{d}{dx}\left\{Z(x)\right\} = \frac{d}{dx}\left[T(x)\right]\left[T(x)\right]^{-1}\left\{Z(x)\right\} \tag{153}$$

Equating equations (150) and (153) gives

$$\left[\left[A(x)\right] - \frac{d}{dx}\left[T(x)\right]\left[T(x)\right]^{-1}\right]\left\{Z(x)\right\} = \left\{0\right\} \tag{154}$$

Since equation (154) must be satisfied for all values of x and all values of Z it follows that

$$\left[A(x)\right] = \frac{d}{dx}\left[T(x)\right]\left[T(x)\right]^{-1}$$

Then post multiplying both sides by $\left[T(x)\right]$ yields

$$\frac{d}{dx}\left[T(x)\right] = \left[A(x)\right]\left[T(x)\right] \tag{155}$$

Therefore, the transfer matrix is given directly by the solution to equation (155). By letting x go to zero in equation (149) the initial condition of the transfer matrix becomes the identity matrix.

$$\left[T(0)\right] = \left[I\right] \tag{156}$$

If equation (155) is solved as a coupled set of first-order differential equations, then equation (156) provides a sufficient number of initial conditions.

The transfer matrix of the blade without a pendulum can be obtained by integration of equation (155) together with the initial conditions of equation (156). The tension

coefficient, T, appearing in matrix $[A]$ is given by

$$T = \Omega^2 \int_x^R mx_1 \, dx_1 \qquad (157)$$

When a pendulum is attached to the blade the transfer matrix at any spanwise location is obtained as follows. Let x_A be the spanwise location of the pendulum hinge:

Case 1. $\qquad 0 \leq x \leq x_A^L$

The transfer matrix in this case is obtained by the direct integration of equation (155) together with the initial conditions given by equation (156) similar to the case of the blade without the pendulum, but the tension coefficient is given by the following equation instead of the one given by equation (157).

$$T = \Omega^2 \int_x^R mx_1 \, dx_1 + M \Omega^2 (x_A + \ell \cos \delta_o) \qquad (158)$$

Case 2. $\qquad x_A^R \leq x \leq R$

Let $[T_1]$ be the transfer matrix of the blade at $x = x_A^L$; this matrix can be obtained from Case 1 as described above. Recall that $[P]$ (see eq. (89)) is the point transfer matrix of the pendulum. Let $[T_2(x)]$ be the transfer matrix of the blade from x_A^R to x. This matrix is obtained by the integration of equation (155) with the initial conditions given by equation (156) from x_A^R to x. While integrating this equation the tension coefficient given by equation (157) should be used instead of the one given by equation (158). By the product rule of transfer matrices, the transfer matrix of the system at any spanwise location for this case is given by

$$[T(x)] = [T_2(x)][P][T_1] \qquad (159)$$

Once the system transfer matrix is obtained, the state vector at any spanwise location can be determined.

System Dynamic Response

It has been shown how the transfer matrix can be used to solve the homogeneous

differential equations. An application of such a solution is to find the natural frequencies and mode shapes of an elastic system (ref. 14). Once they are known it is possible to solve the most general cases of forced undamped vibrations, whether they are transient or steady-state in character, either for discrete or continuous systems, through the normal mode approach. On the other hand the steady-state response caused by a harmonic excitation is more readily solved with the aid of a particular integral of the nonhomogeneous differential equation without making use of the normal modes and natural frequencies (ref. (13)).

The procedure adopted here for the steady-state response of forced vibrations with harmonic excitation is usually called the "exter led" transfer matrix approach for undamped systems and the "complex extended" t*ansfer matrix approach for damped systems. The procedure is valid for any linear damping since normal modes are not introduced. The restr ctions are that the response is steady and excitations are harmonic. With the knowledge of the system's response to harmonic inputs, the response to any arbitrary input can be computed by synthesizing the arbitrary forcing function from an aggregate of infinitesimal harmonic forces.

The blade-pendulum equation of motion was given by equation (23) as

$$\left\{ \bar{Z}(x) \right\}' = \left[A(x) \right] \left\{ \bar{Z}(x) \right\} + \left\{ \bar{F}_a(x) \right\} \qquad (160)$$

By definition of the transfer matrix, the solution for the homogeneous part of equation (160) can be written as

$$\left\{ \bar{Z}_h(x) \right\} = \left[T(x) \right] \left\{ \bar{Z}(0) \right\} \qquad (161)$$

The particular solution of equation (160) can be written as

$$\left\{ \bar{Z}_p(x) \right\} = \int_0^x \left[T(x, s) \right] \left\{ \bar{F}_a(s) \right\} \, ds \qquad (162)$$

where $\left[T(x,s) \right]$ is the transfer matrix of the system from s to x (in contrast to $\left[T(x) \right]$, the transfer matrix from 0 to x). By the product rule of transfer matrices the following relation can be written

$$\left[T(x) \right] = \left[T(x, s) \right] \left[T(s) \right] \qquad (163)$$

From equations (162) and (163) the particular solution can be written as

$$\left\{ \bar{Z}_p(x) \right\} = \left[T(x) \right] \int_0^x \left[T(s) \right]^{-1} \left\{ \bar{F}_a(s) \right\} \, ds \qquad (164)$$

The complete solution of equation (160) can be obtained by adding equations (161) and (164).

$$\left\{\bar{Z}(x)\right\} = \left[T(x)\right]\left\{\bar{Z}(0)\right\} + \left[T(x)\right]\int_0^x \left[T(s)\right]^{-1}\left\{\bar{F}_a(s)\right\}\,ds \qquad (165)$$

Equation (165) gives the amplitude vector of the simple harmonic response. The vector $\left\{\bar{Z}(0)\right\}$ is not completely known, but it can be determined from the boundary conditions of the system.

To determine the vector $\left\{\bar{Z}(0)\right\}$, first rewrite equation (165) as

$$\left\{\begin{array}{c}\bar{Z}_d(x)\\ \text{---}\\ \bar{Z}_f(x)\end{array}\right\} = \left[\begin{array}{c|c}T_a(x) & T_b(x)\\ \hline T_c(x) & T_d(x)\end{array}\right]\left\{\begin{array}{c}\bar{Z}_d(0)\\ \text{---}\\ \bar{Z}_f(0)\end{array}\right\}$$

$$+ \left[\begin{array}{c|c}T_a(x) & T_b(x)\\ \hline T_c(x) & T_d(x)\end{array}\right]\int_0^x\left[\begin{array}{c|c}S_a(s) & S_b(s)\\ \hline S_c(s) & S_d(s)\end{array}\right]\left\{\begin{array}{c}\bar{F}_d(s)\\ \text{---}\\ \bar{F}_f(s)\end{array}\right\}ds$$

$$(166)$$

where

$$\left\{\bar{Z}_d\right\}^T \equiv \lfloor \bar{v}\ \ \bar{w}\ \ \bar{\phi}\ \ \bar{\mu}\ \ \bar{\nu}\rfloor$$

$$\left\{\bar{Z}_f\right\}^T \equiv \lfloor \bar{M}_x\ \ \bar{M}_y\ \ \bar{M}_z\ \ \bar{V}_x\ \ \bar{V}_y\ \ \bar{V}_z\rfloor$$

$$\left\{\bar{F}_d\right\} \equiv \left\{0\right\} \qquad (167)$$

$$\left\{\bar{F}_f\right\}^T \equiv \lfloor -\bar{M}_\phi\ \ 0\ \ 0\ \ 0\ \ -\bar{L}_v\ \ -\bar{L}_w\rfloor \qquad (168)$$

$$\left[S(s)\right] \equiv \left[T(s)\right]^{-1} \qquad (169)$$

The boundary conditions corresponding to a hingeless rotor blade are

$$\left\{\bar{Z}_d(0)\right\} = \left\{0\right\} \qquad (170)$$

$$\left\{\bar{Z}_f(R)\right\} = \left\{0\right\} \qquad (171)$$

Substituting equations (167) and (170) into equation (166) yields

$$\left\{ \frac{\bar{Z}_d(x)}{\bar{Z}_f(x)} \right\} = \left[\frac{T_b(x)}{T_d(x)} \right] \left\{ \bar{Z}_f(0) \right\}$$

$$+ \left[\begin{array}{c|c} T_a(x) & T_b(x) \\ \hline T_c(x) & T_d(x) \end{array} \right] \int_0^x \left[\frac{S_b(s)}{S_d(s)} \right] \left\{ \bar{F}_f(s) \right\} ds \qquad (172)$$

From equation (172)

$$\left\{ \bar{Z}_f(R) \right\} = \left[T_d(R) \right] \left\{ \bar{Z}_f(0) \right\} + \left[T_c(R) \mid T_d(R) \right] \int_0^R \left[\frac{S_b(s)}{S_d(s)} \right] \left\{ \bar{F}_f(s) \right\} ds \qquad (173)$$

Substituting the boundary condition of equation (171) into equation (173) yields

$$\left\{ \bar{Z}_f(0) \right\} = - \left[T_d(R) \right]^{-1} \left[T_c(R) \mid T_d(R) \right] \int_0^R \left[\frac{S_b(s)}{S_d(s)} \right] \left\{ \bar{F}_f(s) \right\} ds \qquad (174)$$

Equation (172) gives the response state vector of a hingeless rotor blade due to a simple harmonic load. The hub constraint reactions, $\left\{ \bar{Z}_f(0) \right\}$, which appear in equation (172) can be obtained from equation (174). It may be noted that the transfer matrix and all state variables are complex due to inclusion of the linear damping terms in the system equations of motion.

The transfer matrix, by definition, is independent of the boundary conditions. Having determined the transfer matrix, the boundary conditions can be simply imposed to determine the response state vector as shown above for the case of a hingeless blade. So all the problems corresponding to various boundary conditions can be analyzed easily. Another advantage of the method is that it provides for the continuous integration of the equations. In the present study the Runge-Kutta procedure is utilized to solve the differential equations governing the elements of the transfer matrix (eq. (155)). One distinguishing advantage of the transfer matrix is that the hub constraint reactions are obtained as a direct result (eq. (174)). The extended transfer matrix approach is valid for any linear damping since normal modes are not considered. The number of stations at which the transfer matrix is determined depends only on the step size of the integration. The incremental step size can be selected arbitrarily and then the result compared with that obtained for a smaller increment. In this way an optimal value for the step size is obtained.

RESULTS AND DISCUSSION

The object of this study is to establish a comprehensive analytical design procedure for the installation of simple pendulums on the blades of a helicopter rotor to suppress the force and moment reactions at the hub during forward flight conditions. This procedure will correspond to a process of optimization with the ultimate object of

minimizing the root shear and moment. The minimization of these reactions will be accomplished by a systematic variation of the pendulum parameters (both geometrical and inertial). In this section numerical results are presented together with a discussion of their significance. The numerical results presented pertain to both uniform and nonuniform hingeless rotor blades. The properties of these blades are given in Appendix D.

Simple Flapping Pendulum

The first part of this section compares the root reactions from this study with the results of Murthy (ref. 15) for an undamped analysis. This comparison is made solely to verify the correctness of the computer program. The remainder of this section contains: 1) a detailed discussion of the numerical results for a 4/Rev concentrated load at the tip; and, 2) the results for excitation by a harmonic variation of spanwise airload in forward flight.

Analysis verification. - By dropping the damping terms in the blade and pendulum equations of motion the case of undamped dynamic response can be recovered. The undamped root reactions of a uniform rotor configuration (Appendix D) are presented in Table 2 together with the results of reference 15. The reactions with a properly tuned simple pendulum are also shown in Table 2. The excitation force for all these results is a concentrated out-of-plane simple harmonic load at the tip of the blade with a frequency equal to 4/Rev. It is apparent from the data presented in Table 2 that the present analysis provides results which agree with the work of reference 15 for a uniform rotor blade without damping. The computer code has also been verified by duplicating published data of normal vibration modes for hingeless and articulated rotor blades (ref. 16).

Concentrated load excitation. - The force vector for a concentrated out-of-plane load can be written as (see eq. (168))

$$\{\bar{F}_f\}^T = \lfloor 0 \ 0 \ 0 \ 0 \ 0 \ -\bar{F}_c \rfloor \qquad (175)$$

where $\bar{F}_c$ is the amplitude of the applied load. The concentrated harmonic force at the tip has the following characteristics:

Magnitude. . . . . .2224 N

Frequency. 4/REV

Both the uniform and nonuniform blades are considered for this particular excitation.

The root reactions of the uniform blade with a flapping simple pendulum are computed. It may be noted that all state variables are complex due to inclusion of the linear damping terms. The results for the vertical shear amplitude at the hub are plotted in figure 9. The pendulum weight is 66.726 N (10% of the blade total weight). Damping at the pendulum hinge is neglected. The effect of this damping on pendulum tuning is discussed later in this section.

The tuning of the pendulum is changed by varying the spanwise location of the pendulum for a fixed value of the uncoupled pendulum frequency. It may be noted from equation (53) that the uncoupled natural frequency of the pendulum is mainly dependent on (1) rotational speed of the blade, (2) spanwise location of the pendulum, and (3) its

TABLE 2. - CORRELATION OF UNDAMPED ROOT REACTIONS

Source	M_x, Nm	M_y, Nm	M_z, Nm	V_y, N	V_z, N
No Pendulum Attached					
Reference 15	-139	1536	-648	-1054	3256
Present	-146	1535	-648	-1051	3254
With Pendulum Attached[a]					
Reference 15	-5	58	-576	-983	-0.5
Present	-23	53	-606	-973	-2.8

[a] $\omega_p = 144$ rad/s; $x_A = 1.651$ m ; $\zeta_A = 0.2032$ m

length. The simple pendulum considered here swings in the flapping plane and hence can generate significant out-of-plane shear force and moment at its point of connection with the blade. These facts can be observed from the results of figure 9. The root normalized vertical shear (the shear reaction with the pendulum attached to the blade divided by that value without the pendulum) is altered significantly by the pendulum. For instance, when the pendulum is located at 15.2% of the span, the root normalized vertical shear is attenuated to 2.9% for a pendulum frequency equal to 146 rad/sec (3.87/Rev), while it is amplified to 2579% for a pendulum frequency equal to 160 rad/sec (4.24/Rev). The latter case shows that an improperly tuned pendulum might amplify the root reactions rather than attenuate them, and the system would be better off without the pendulum.

From the results of figure 9, it can be observed that the pendulum of frequency 146 rad/sec (3.87/Rev) located at 18% of the span is a proper design because it attenuates the hub vertical shear to 1.3%. The out-of-plane moment at the hub is reduced to 14.2%. This choice of pendulum also attenuates the in-plane force and moment at the hub to 4.2% and 22.8%, respectively.

The effect of pendulum mass on the vertical reaction is illustrated in figure 10 as a function of spanwise location. The results are for a simple flapping pendulum of frequency 146 rad/sec. It can be observed from these results that if the weight of the pendulum is 66.726 N (at x_A = 18% span) then the normalized vertical shear at the hub is 1.3%. If the weight of the pendulum is reduced by two thirds (located at 18% span) then the normalized vertical shear at the hub is 39.3%. This variation of the pendulum weight will be referred to as the weight ratio, where in this instance the weight ratio is 33%. This result indicates that even though the uncoupled natural frequency of the pendulum is independent of the mass of the pendulum, a proper choice of the mass is also required to generate an optimum force to attenuate the root reactions.

It can be observed from figure 9 that the minimum normalized vertical shear for any pendulum frequency occurs when the pendulum is located near 18% of the span. These values are replotted for different uncoupled pendulum frequencies in figure 11. Comparison of the hub vertical shear with pendulum absorber to the hub shear with no absorber shows the pendulum absorber to be effective in reducing hub out-of-plane reaction for tunings between 3.82 and 4.00/Rev. It can be recalled that the optimum tuning is 3.87/Rev. The steep gradient of the hub shear with pendulum tunings beyond optimum indicates decreasing effectiveness of the pendulum absorber and for tunings above 4/Rev the pendulum absorber becomes detrimental. Figure 11 demonstrates that in the case of an off-tuned pendulum, it is apparent that the result can be either a slight-to-moderate degradation in pendulum absorber effectiveness or a drastic increase in hub reaction depending upon the direction of tuning variation from the optimum pendulum natural frequency.

Similar results have been obtained in reference 4. In this reference a semi-empirical analysis, using in-flight measured flap bending moment data, was developed to study the pendulum effectiveness in reducing 4/Rev blade root vertical shear. The Boeing Vertol 347 aircraft was used for the flight test. It is a tandem-rotor helicopter with fully articulated 4 bladed rotors. The vertical 4/Rev pendulum absorbers were installed on all blades of both rotors at 16% blade radius. Comparison of the predicted hub motion with the pendulum absorber showed that the pendulum absorber is effective for tunings between 3.4 and 4.0/Rev. Test results indicated that a 3.95/Rev is an optimum tuning. For this optimum tuning the vertical hub shears were reduced by 80 to 90% on both forward and aft rotors. However, the vibratory blade root chordwise bending was increased by 25% with the pendulum installed.

The elastic deflections and structural load reactions for the present uniform blade

corresponding to the optimum flapping pendulum (3.87/Rev at 18%) are shown in figure 12 together with values obtained without the pendulum. The chordwise and flapwise deflections are normalized with respect to the chord (c=0.7m). It may be recalled that all the deflections and forces are complex. The phase angles for the deflections are found to be either 0° or 180° as presented in figure 12. However, the phase angles for the moments and forces are not exactly 0° or 180° at a few blade stations, and therefore it is appropriate to plot only the magnitude of these forces and moments.

It can be observed from figure 12 that the pendulum causes a spanwise redistribution of the structural loads such that the hub reactions are attenuated. Figure 12 shows that the optimum pendulum decreases the loads inboard of the pendulum and increases the loads outboard of the pendulum. It can also be observed that the maxima of the deflections, twisting moment, and vertical shear are higher than the corresponding quantities without the pendulum. This is the penalty one must pay for achieving the drastic reductions in the root reactions. The vertical shear is characterized by a large change at the pendulum attachment point due to the vertical inertial reaction of the flapping pendulum mass. This vertical reaction, which is imposed at the pendulum attachment point, is the basis of the blade-mounted flapping pendulum concept which has the purpose of attenuating the root force and moment reactions.

In general, a properly tuned pendulum can attenuate the vibratory loads in two ways: (1) by eliminating the resonant responses of the blade by displacing the initial natural frequencies that are in the vicinity of the excitation frequency, and (2) by generating appropriate forces at its attachment point with the blade. These forces redistribute the loads on the blade so that the root forces are attenuated as discussed above.

Figure 13 shows the hub vertical shear for pendulum tuning of the nonuniform blade. The blade rotor speed and precone angle are equal to 289 rpm and 0.1 rad, respectively. The pendulum weight is 133.452 N (13.8% of the blade total weight). The results indicate that a pendulum with uncoupled natural frequency of 3.85/Rev located at 22% of the span is a proper design because it attenuates the hub vertical shear to 2.2% and the out-of-plane moment to 3.4%. This choice of pendulum attenuates the root in-plane force to 47.6%. However the root in-plane moment is amplified by 75%. This adverse effect can be reduced by offsetting the pendulum hinge (η_A) from the elastic axis. The effect of the pendulum hinge offset is discussed later in this section.

For the optimum pendulum ($\omega_p = 3.85/\text{Rev}$ and $x_A = 22\%$ span) the root forces are computed for different values of the pendulum mass. The results are shown in figure 14. It can be observed that a 50% weight ratio (66.72 N) is an optimum choice. For this weight the normalized vertical shear at the hub is practically zero as compared to 2.2% with a pendulum of weight 133.452 N. This demonstrates, once again, that a proper choice of pendulum mass is required to minimize the root forces.

In the above analysis the damping at the pendulum hinge is neglected. However, it is necessary to study the effect of the pendulum damping on the root reactions once the optimum pendulum tuning is established. The hub shears and moments are computed for different damping ratios, and these results are presented in figure 15. It can be observed from these results that damping of the pendulum due to friction in the pivot bearing has a very small effect on the hub reactions.

Once the optimum tuning configuration and mass effectiveness are established, a parametric study is conducted. The parameters to be varied include prepitch, pretwist, precone and pendulum hinge offsets. The parametric survey is conducted for the nonuniform blade with the optimum tuned pendulum ($\omega_p = 3.85/\text{Rev}$ and $x_A = 22\%$ span). The pendulum mass is 133.452 N for this study.

Figure 16 shows the effect of root collective pitch (prepitch) on the hub reactions. The pretwist angle for these results is equal to $-9°$. The prepitch has a small effect on the hub vertical shear. It significantly affects the hub in-plane force and moment, which are both increased by increasing the root collective pitch. The out-of-plane moment is affected moderately by changing the collective pitch. The effect of collective pitch on the twisting moment (not shown in figure 16) is negligible.

The effect of the built-in twist angle (pretwist) on the hub reactions of the blade-mounted flapping pendulum is shown in figure 17. The root collective pitch for these results is equal to $13°$. Figure 17 shows that the pretwist has a small effect on the hub vertical shear. Unlike the effect of the collective pitch, the pretwist has a significant effect on the root out-of-plane moment. However, for typical rotor blades (negative pretwist) the root out-of-plane moment is still attenuated to less than 10%. It can be observed from figure 17 that the in-plane force and moment are both increased by decreasing the blade pretwist. The pretwist has negligible effect on the twisting moment. It can be concluded that the flapping pendulum effectiveness in attenuating the root out-of-plane moment, and the in-plane force and moment is reduced by decreasing the blade pretwist.

The root reactions of the blade are computed for various precone angles, and these results are presented in figure 18. It can be observed that the blade precone has no significant influence on the hub reactions. Thus, the flapping pendulum effectiveness in attenuating the blade root reactions is not affected by changing the precone angle.

The results from varying the pendulum hinge chordwise offset, η_A, are shown in figure 19. It may be recalled that the optimum flapping pendulum is tuned with its hinge located at the shear center of the blade cross section ($\eta_A = 0$, $\zeta_A = 0$). It can be argued that this is an impractical location since the shear center is usually inside the airfoil envelope. The pendulum chordwise hinge offset has a small effect on both the root out-of-plane force and moment as shown in figure 19. Both the in-plane force and moment are decreased by increasing the chordwise offset. The effect of chordwise offset on twisting moment at the hub is negligible.

Figure 20 shows the root forces for different values of the pendulum hinge vertical offset, ζ_A. It can be concluded from figure 20 that the vertical offset, ζ_A, has only a slight effect on the hub reactions. Although not illustrated in figure 20 its effect on twisting moment is negligible.

Aerodynamic load excitation. - The dynamic excitation of the rotor blade is provided by a quasi-steady representation of the spanwise airload distribution associated with the cyclic pitch environment of forward flight. As previously discussed the aerodynamic loads induced by the elastic deformations are also included. The aerodynamic load distributions consist of lift, drag, and pitching moment. Values of the aerodynamic parameters used to calculate the airloads are presented in Table 3.

As previously discussed the unsteady aerodynamic forces which occur in forward flight are due to time dependent variations in velocity, angle of attack, and elastic deflections encountered by the rotating blade. The quasi-steady representation provides 1/Rev, 2/Rev, and 3/Rev excitation airloads. The amplitude of the airloads decreases as the harmonic order increases. For each of the three harmonics, the amplitude of the vertical force is much larger than the amplitude of the in-plane force.

For airloads which are identical on each rotor blade, the only loads and moments which the blades may transmit to the rotor hub are those which are integral multiples (N) of the number of blades (ref. 17). The N/Rev rotor hub loads are the greatest contributors to helicopter vibration. The source of N/Rev hub loads are N-1, N, N+1 rotor blade airload harmonics. Therefore one solution for reducing N/Rev vibration is to cancel or eliminate these harmonics of blade loading. As discussed above, the quasi-

TABLE 3. – VALUES OF AERODYNAMIC PARAMETERS FOR THE NONUNIFORM BLADE IN FORWARD FLIGHT

Advance ratio, μ_f 0.3

Shaft angle, α_s, deg . . . . -5

Cosine cyclic pitch coefficient, θ_{1c}, deg . . . . -1.5

Sine cyclic pitch coefficient, θ_{1s}, deg 3.0

Collective pitch, θ_c, deg 13

Pretwist, θ_{pt}, deg . . . . -9

Airfoil lift-curve slope, a, per rad 2π

Profile drag coefficient, c_{do} 0.01

Precone angle, β_{pc}, rad 0.1

Blade rotational speed, Ω, rpm 289

steady representation of the airloads contains only three harmonics. In the present analysis, the effectiveness of the flapping pendulum in reducing the blade root forces due to 2/Rev and 3/Rev airloads is discussed. Throughout the following, unless stated otherwise, all numerical results pertain to the nonuniform blade.

The root reactions of the nonuniform blade with a flapping pendulum are computed for a 2/Rev spanwise airload distribution. The results for the vertical shear at the hub are plotted in figure 21. The pendulum weight is 133.452 N. From the hub reactions it is observed that the pendulum of uncoupled natural frequency 2.02/Rev located at 22% of the span is a proper design because it attenuates the hub vertical shear to 22% and the out-of-plane moment to 31%. This choice of pendulum attenuates the in-plane moment by only 4% and amplifies the in-plane force by 66%. However for the 2/Rev airload the in-plane hub force is small compared to the hub vertical shear.

For the optimum pendulum tuning ($\omega_p = 2.02/Rev$ and $x_A = 22\%$ span) the root reactions are computed for different values of the pendulum mass and the results are presented in figure 22. It can be observed that a 94.53 N pendulum weight (0.71 weight ratio) is a proper choice because it attenuates the hub shear to 2.9 %. It also attenuates the hub out-of-plane moment to 17%.

To establish the importance of representing the excitation as a distributed loading the responses due to the distributed airload are compared with corresponding responses associated with a concentrated harmonic force applied at the tip with the same frequency. Figure 23 shows the results for a 2/Rev concentrated out-of-plane force at the tip. It can be noticed from figure 23 that the flapping pendulum effect on the hub vertical shear is similar to the results obtained for the 2/Rev spanwise airload distribution (fig. 21). For specific values of the pendulum frequency and spanwise location, the pendulum attenuates or amplifies the root vertical shear the same way for both the distributed airload and the concentrated load. It is observed that an optimum tuning occurs at 22% spanwise location with pendulum frequency equal to 2.02/Rev. This optimum tuning attenuates the vertical shear and the out-of-plane moment to 17 and 38%, respectively. It amplifies the in-plane force by 63%. It may be recalled that the optimum pendulum for the 2/Rev distributed airloads also occurs at $x_A = 22\%$ span, $\omega_p = 2.02/Rev$, and $W = 94.53$ N.

The pendulum mass optimization for the 2/Rev concentrated load is shown in figure 24. It can be observed that a 100.09 N pendulum weight (0.75 weight ratio) is a proper choice because it attenuates the hub shear to 8%. It also attenuates the root out-of-plane moment to 26%.

For the 2/Rev concentrated load at the tip, discussed above, the elastic-aerodynamic coupling is not included. However, it is important to study the effect of these terms when the blade is excited by a concentrated load. Figure 25 shows the results for a 2/Rev concentrated load at the tip with the aerodynamic coupling terms included, as well as the results without these terms (W = 133.45 N). It can be noted from figure 25 that for both cases the root vertical shear has the same characteristics. However, the amount of attenuation is different. Figure 25 shows that, for the case with aerodynamic coupling the optimum tuning occurs at $x_A = 26\%$ span and $\omega_p = 2.02/Rev$. This choice of pendulum attenuates the root out-of-plane shear and moment to 38% and 84%, respectively. The results of varying the pendulum mass indicate that the reaction attenuation varies only by 1.0%. The results also show that a 133.45 N is a proper choice. Comparing the pendulum tuning for the 2/Rev distributed airloads, the 2/Rev concentrated load, and the 2/Rev concentrated load with aerodynamic coupling, it can be concluded that a pendulum tuned for a concentrated simple harmonic load acting at the blade tip can serve the purpose of a distributed simple harmonic loading at the same frequency as far as the pendulum tuning and mass

optimization is concerned. However, it is necessary to utilize appropriate distributed airloads to accurately determine the attenuation of the root reactions.

Figure 26 shows the effect of pendulum tuning on the root vertical shear for 3/Rev spanwise airload distribution. The results of figure 26 indicate that a flapping pendulum of frequency 3.10/Rev located at 26% of the span is an optimum tuning. This choice of pendulum attenuates the root vertical shear and the out-of-plane moment to 4.2 and 26.8%, respectively. It attenuates the root in-plane moment only to 97%. However, the in-plane force at the hub is amplified by 44%. This adverse effect is the penalty being paid for achieving the drastic reductions in the root out-of-plane force and moment.

The root reactions are computed for various masses of the optimum pendulum. Results for the vertical shear are presented in figure 27. These data show that a 155.69 N pendulum weight (1.17 weight ratio) is a proper choice. For this weight the vertical shear and out-of-plane moment are attenuated to 3.3 and 25.2%, respectively.

The above results for a simple flapping pendulum on the nonuniform blade are summarized in Table 4.

Simple Lead-Lag Pendulum

As discussed in the previous section, the simple flapping pendulum can be tuned to achieve significant reductions in the root out-of-plane forces. To significantly attenuate the in-plane forces a simple lead-lag pendulum is needed. In this section, the effect of mounting a lead-lag pendulum on a rotor blade is discussed. The excitation loads to be considered are 4/Rev concentrated load at the blade tip and 2/Rev and 3/Rev spanwise distributed airloads. Throughout the following all numerical results pertain to the nonuniform blade.

Concentrated load excitation. - The root reactions of the nonuniform blade with a simple lead-lag pendulum are computed. The results for the in-plane force amplitude at the hub are plotted in figure 28. The study of the effect of the pendulum tuning on the root in-plane reaction is of prime importance since the lead-lag pendulum attenuates mainly the in-plane forces. The pendulum weight is equal to 133.452 N. From the results it can be observed that the pendulum of uncoupled natural frequency 3.85/Rev located at 26% of the span is a proper design because it attenuates the hub in-plane force to 5% and the in-plane moment to 44.6%. This choice of pendulum also attenuates the root vertical shear and the out-of-plane moment to 20.6 and 16.8%, respectively. In principle, it is feasible to design a lead-lag simple pendulum to achieve significant reductions in the hub in-plane force and moment without producing an adverse effect on the out-of-plane forces.

For the optimum lead-lag pendulum ($\omega_p = 3.85$/Rev and $x_A = 26\%$ span) the root forces are computed for different values of the pendulum mass. The results are shown in figure 29. It can be observed from figure 29 that if the pendulum weight ratio is reduced from 1.0 to 0.3, then the normalized in-plane force at the hub increases from 5% to 39%. This result indicates that even though the uncoupled natural frequency of the lead-lag pendulum is independent of the mass of the pendulum, a proper choice of the mass is required to minimize the root forces. It may be recalled that this conclusion was also observed for the simple flapping pendulum.

It is appropriate, at this stage, to compare the results for the optimum tuned flapping and lead-lag pendulums. Shown in Table 5 are the optimum pendulum parameters for both the flap and lead-lag pendulum configurations. Also shown in this table are the normalized root forces of the nonuniform blade due to a 4/Rev concentrated load at the tip. From Table 5 it can be observed that for both the flap and lead-lag pendulums the uncoupled frequencies are the same. Also the uncoupled

TABLE 4.- OPTIMUM FLAPPING PENDULUMS
FOR NONUNIFORM BLADE

Type of Excitation	Natural frequency, ω_p, per Rev	Spanwise location, x_A, percent span	Pendulum weight, W, N(lb)	Normalized out-of-plane shear, V_z, percent	Normalized out-of-plane moment, M_y, percent
2/Rev Concentrated no aeroelastic terms	2.02	22	100.09 (22.50)	8.0	26.0
2/Rev Concentrated with aeroelastic terms	2.02	26	133.45 (30.00)	38.0	84.0
2/Rev Distributed with aeroelastic terms	2.02	22	94.53 (21.25)	2.9	17.0
3/Rev Distributed with aeroelastic terms	3.10	26	155.69 (35.00)	3.3	25.2
4/Rev Concentrated no aeroelastic terms	3.85	22	66.72 (15.00)	0.2	5.8

TABLE 5. – ROOT REACTIONS FOR OPTIMUM FLAP AND LEAD – LAG PENDULUMS AT 4/REV

Normalized root reaction, percent	Flapping pendulum[a]	Lead – lag pendulum[b]
M_x	139.0	85.0
M_y	5.8	16.8
M_z	172.0	44.6
V_y	43.6	5.0
V_z	0.2	20.6

[a] ω_p = 3.85/Rev ; x_A = 22% span ; W = 66.72 N

[b] ω_p = 3.85/Rev ; x_A = 26% span ; W = 133.45 N

frequency (3.85/Rev) is in the vicinity of the external load frequency (4/Rev). It may be concluded that, in general, the optimum pendulum frequency depends mainly on the excitation frequency. This observation is due to the fact that the optimum tuned pendulum attenuates the hub reactions by eliminating the resonant responses of the blade (in addition to generating an appropriate reaction force at the hinge). The optimum pendulum eliminates these resonant responses by displacing the natural frequencies that are in the vicinity of the excitation frequency, and since the pendulum is more effective in altering the blade frequencies adjacent to the uncoupled pendulum frequency (ref. 7), then the uncoupled pendulum frequency must be close to the excitation frequency. As expected, the flapping pendulum significantly attenuates the hub vertical shear, whereas the lead-lag pendulum reduces the hub in-plane force drastically as shown in Table 5. Finally, it can be observed from Table 5 that for this particular blade the flapping pendulum produces an adverse effect on the twisting and in-plane moments, whereas the lead-lag pendulum attenuates the twisting and out-of-plane moments.

The spanwise variations of deflections and forces for the nonuniform blade corresponding to the optimum lead-lag pendulum, which is located at 26% span, are shown in figure 30 together with the values obtained without the pendulum. The lead-lag and flapwise deflections are normalized with respect to the chord (c = 0.53 m). Only the magnitude of the forces and moments are plotted. It can be observed from figure 30 that the lead-lag pendulum redistributes the structural loads of the blade such that the hub forces are attenuated. The pendulum decreases the loads inboard of its location and increases the loads outboard. Figure 30 shows that the lead-lag deflection of the blade-pendulum system is significantly reduced. Also, it can be observed that the in-plane force, V_v, is characterized by a large change at the lead-lag pendulum attachment point due to the intertial reaction of the lead-lag pendulum mass. It may be recalled that the flapping pendulum produces a large change in the vertical shear. These reactions at the attachment point redistribute the loads on the blades in such a way that only a small portion of the shears and moments are transmitted to the hub.

A parametric study is conducted for the optimum lead-lag pendulum (ω_p = 3.85/Rev and x_A = 26% span). The parameters varied include prepitch, pretwist, precone, and pendulum hinge offsets.

Figure 31 shows the effect of the root collective pitch (prepitch) on the hub reactions. The pretwist angle for these results is equal to $-9°$. It can be observed from figure 31 that increasing the prepitch decreases the hub in-plane force to a minimum value after which it increases. The in-plane hub moment is increased by increasing the prepitch (in the normal range). Figure 31 shows that the prepitch has a negligible effect on both the out-of-plane shear and moment at the hub.

The effect of pretwist on the hub reactions is shown in figure 32. The root collective pitch for these results is equal to $13°$. Figure 32 shows that both the hub in-plane force and moment are increased by decreasing the blade pretwist. Thus, the lead-lag pendulum effectiveness in attenuating the root in-plane force and moment is reduced by decreasing the blade pretwist. It can be observed from figure 32 that the effect of the pretwist on both the out-of-plane force and moment at the hub is small.

The root reactions as a function of the blade precone angle are computed, and the results are presented in figure 33. It can be observed that the precone angle has no significant influence on the hub reactions. It may be recalled that the same conclusion was observed for the flapping pendulum.

The results from varying the lead-lag pendulum hinge chordwise offset (η_A) are shown in figure 34. It may be noted that the optimum lead-lag pendulum is tuned with its hinge located at the shear center of the blade cross section (η_A = 0, ζ_A = 0). It can

68

be observed from figure 34 that the pendulum hinge chordwise offset has only a slight effect on both the hub in-plane force and moment. However, both the hub out-of-plane force and moment are decreased sigificantly to practically zero, after which they are increased, by increasing the chordwise offset.

Figure 35 shows the root reactions for different values of the lead-lag pendulum hinge vertical offset, ζ_A. This offset has a small effe   n the root in-plane moment. However, the in-plane force at the hub is increased by   sing the vertical offset as shown in figure 35. Also, both the root out-of-plane force and moment are increased by increasing the lead-lag pendulum hinge offset, ζ_A. It can also be noted that both the chordwise and vertical offsets have a negligible effect on the hub twisting moment reaction.

Aerodynamic load excitation. - The root reactions of the nonuniform blade with a lead-lag pendulum are computed for a 3/Rev spanwise airload distribution. The results for the root in-plane force are shown in figure 36. It can be observed from figure 36 that for this particular load the lead-lag pendulum attenuates the root in-plane force only by a small amount. However, the root in-plane force is small for all three harmonics of the spanwise airload distribution. The lead-lag pendulum of uncoupled frequency 3.10/Rev located at 19% of the span is a proper choice because it attenuates the hub in-plane force to 65%. However, it amplifies the other root reactions by 5 to 25%.

The effect of lead-lag pendulum tuning on the root in-plane force for a 2/Rev spanwise airload distribution and a 2/Rev concentrated out-of-plane load is shown in figures 37 and 38. It can be observed from these figures that for specific values of the pendulum frequency and spanwise location, the pendulum attenuates or amplifies the root in-plane force the same way for both the distributed airload and the concentrated load. The pendulum of frequency 2.01/Rev located at 9% span attenuates the root in-plane force to 60% for the distributed airload and 42% for the concentrated load at the tip. As concluded earlier, for the flapping pendulum, a pendulum can be tuned for a concentrated simple harmonic load at the tip as well as by a distributed simple harmonic loading of the same frequency.

CONCLUDING REMARKS

Comprehensive analytical design procedures for the installation of simple pendulums on the blades of a helicopter rotor to suppress the root reactions were developed. To achieve this goal, a frequency response analysis of typical rotor blades excited by a harmonic variation of spanwise airload distributions as well as a concentrated load at the tip was conducted. A single nonuniform rotor blade with hingeless hub restraint undergoing coupled flapwise bending, chordwise bending, and torsional vibrations was considered. The equations of motion of both flap and lead-lag pendulums were derived. Expressions for the aerodynamic loads associated with the elastic deformations and the cyclic pitch environment of forward flight were presented. The transfer matrix method was used to determine the optimum pendulum tuning and mass to suppress the hub reactions. Lastly, the effects of various structural dynamic properties of the blade on the optimum pendulum configuration were established.

The results of the study indicate that the following conclusions can be drawn.

(1) In general, it is feasible to design a simple pendulum to suppress the vibratory loads at the hub of a rotor blade. Further:

(i) A properly designed flapping plane simple pendulum attenuates the root out-of-plane force and moment significantly. In principle, the reductions in the root out-of-plane reactions can be achieved without producing adverse effects on the root in-plane

forces. However, in some of the cases investigated, the hub in-plane forces are amplified with the flapping pendulum. This is a design penalty which results from reducing the out-of-plane reactions.

(ii) An optimum lead-lag pendulum design attenuates the root in-plane force and moment.

(iii) For the cases investigated, the flapping plane simple pendulum is more effective in attenuating the root out-of-plane reactions than the lead-lag pendulum in suppressing the in-plane forces at the hub.

(2) A properly tuned pendulum can attenuate the vibratory loads in two ways: (1) by eliminating the resonant responses of the blade by displacing the initial frequencies that are in the vicinity of the excitation frequency, and (2) by generating appropriate forces at its attachment point with the blade. These forces redistribute the loads on the blade so that only a small portion of the shears and moments are transmitted to the hub.

(3) For optimum tuning, the parameters to be determined are the pendulum uncoupled natural frequency, the pendulum spanwise location, and its mass. Further:

(i) The pendulum uncoupled natural frequency is a function of the (a) rotational speed of the blade, (b) spanwise location of the pendulum, (c) its length, (d) steady-state deflection of the pendulum, and (e) blade pitch angle at the pendulum hinge location.

(ii) The optimum pendulum frequency is in the vicinity of the excitation frequency. In general, both the flapping plane pendulum and the lead-lag pendulum have the same optimum frequency for the same excitation frequency. In the case of an off-tuned pendulum the results range from a slight-to-moderate degradation in pendulum absorber effectiveness to a drastic increase in hub vibration.

(iii) The uncoupled natural frequency of the pendulum is independent of the mass of the pendulum, and a proper choice of the mass is required to generate an optimum force to minimize the root reactions.

(4) A pendulum can be tuned and its optimum mass determined by excitation with a concentrated simple harmonic load at the tip. However, it is necessary to utilize appropriate distributed airloads to accurately determine the attenuation of the root reactions.

(5) Damping at the pendulum hinge has a very small effect on the hub reactions once the optimum pendulum tuning is established.

(6) The parametric study for a 4/Rev flapping plane pendulum and a 4/Rev lead-lag pendulum indicates:

(i) Blade precone has no significant effect on the hub reactions for both types of pendulum.

(ii) The effect of collective pitch on the hub vertical shear is small, but has an appreciable effect on the hub out-of-plane moment for a flapping plane pendulum. For the lead-lag pendulum the collective pitch has a negligible effect on both the hub out-of-plane force and moment. Increasing the collective pitch, the hub in-plane force and moment are significantly raised in the case of the flapping pendulum, whereas they are lowered to a minimum value after which they are increased in the case of a lead-lag pendulum.

(iii) The pendulum effectiveness in attenuating the hub in-plane force and moment is reduced by decreasing the blade pretwist for both types of pendulum. In the case of the flapping pendulum, pretwist has a significant effect on the hub out-of-plane moment.

(iv) The pendulum hinge chordwise offset has a small effect on the hub out-of-plane reactions in the case of a flapping plane pendulum. Also, for this type of pendulum the hub in-plane reactions are slightly decreased by increasing the chordwise

offset. In the case of a lead-lag pendulum, the hinge chordwise offset has only a slight effect on the root in-plane reactions, whereas the out-of-plane forces are significantly decreased by increasing the chordwise offset.

(v) The pendulum hinge offset normal to the chord has only a slight effect on the hub reactions for the flapping plane pendulum. In the case of a lead-lag pendulum, the hub in-plane force and both the out-of-plane force and moment are increased by increasing the hinge offset. But the hinge offset has only a small effect on the hub in-plane moment.

(vi) For both the flapping and lead-lag pendulum configurations the pendulum hinge offset in both the chordwise and normal directions had a negligible effect on the twisting moment reaction at the hub.

APPENDIX A

COORDINATE SYSTEMS AND TRANSFORMATIONS

Several coordinate systems are used in deriving the blade and pendulum equations of motion. Those which are common to both the dynamic and aerodynamic aspects of the derivation are shown in figures A-1 and A-2. The orthogonal axes system X, Y, Z (fig. A-1) and associated unit vectors $\vec{I}$, $\vec{J}$, $\vec{K}$ are fixed in an inertial frame $\mathscr{R}$. It is assumed that the rotor hub has neither translational nor angular motion. Orthogonal axes x_p, y, Z are fixed in a reference frame $\mathscr{B}$ which rotates with respect to $\mathscr{R}$ at constant angular velocity $\Omega \vec{K}$. Point O, which is common to both the inertial and rotating frames, is located at the root of the beam. The x axis, which lies along the elastic axis of the undeformed beam, is inclined to the plane of rotation (and to the x_p axis) by the precone angle β_{pc}. The orthogonal axes x, y, z and the corresponding unit vectors $\vec{i}$, $\vec{j}$, $\vec{k}$, therefore, are also fixed in $\mathscr{B}$. Beam bending deformations shown in figure A-2 for $\theta = 0$ are described by the displacements of the elastic axis u, v, w parallel to $\vec{i}$, $\vec{j}$, $\vec{k}$ respectively.

The transformation between the X, Y, Z coordinates of the inertial reference frame, $\mathscr{R}$, and the x_p, y, Z coordinates of the rotating reference frame, $\mathscr{B}$, is given by

$$\begin{bmatrix} X \\ Y \\ Z \end{bmatrix} = \begin{bmatrix} \cos \Omega t & -\sin \Omega t & 0 \\ \sin \Omega t & \cos \Omega t & 0 \\ 0 & 0 & 1 \end{bmatrix} \begin{bmatrix} x_p \\ y \\ Z \end{bmatrix} \tag{A-1}$$

Rotation of the x_p, y, Z coordinate system by the precone angle β_{pc} about the y axis yields the x, y, z undeformed coordinate system. These two systems are related by the following transformation.

$$\begin{bmatrix} x_p \\ y \\ z \end{bmatrix} = \begin{bmatrix} \cos \beta_{pc} & 0 & -\sin \beta_{pc} \\ 0 & 1 & 0 \\ \sin \beta_{pc} & 0 & \cos \beta_{pc} \end{bmatrix} \begin{bmatrix} x \\ y \\ z \end{bmatrix} \tag{A-2}$$

For small values of the precone angle equation (A-2) can be approximated as

$$\begin{bmatrix} x_p \\ y \\ z \end{bmatrix} = \begin{bmatrix} 1 & 0 & -\beta_{pc} \\ 0 & 1 & 0 \\ \beta_{pc} & 0 & 1 \end{bmatrix} \begin{bmatrix} x \\ y \\ z \end{bmatrix} \tag{A-3}$$

The relationship between the deformed x', y', z' coordinates and the undeformed x, y, z coordinates illustrated in figure A-2 has been developed in reference 10. A transformation matrix, $[T]$, which relates their respective unit vectors $\vec{i}'$, $\vec{j}'$, $\vec{k}'$ and $\vec{i}$, $\vec{j}$, $\vec{k}$, can be defined as

$$\begin{bmatrix} \vec{i} \\ \vec{j} \\ \vec{k} \end{bmatrix} = [T]^T \begin{bmatrix} \vec{i'} \\ \vec{j'} \\ \vec{k'} \end{bmatrix} \qquad\qquad (A\text{-}4)$$

where the transformation matrix to first order (second and higher order terms are discarded) is given by

$$[T] = \begin{bmatrix} 1 & v' & w' \\ -v' \cos(\theta+\phi) - w' \sin(\theta+\phi) & \cos(\theta+\phi) & \sin(\theta+\phi) \\ v' \sin(\theta+\phi) - w' \cos(\theta+\phi) & -\sin(\theta+\phi) & \cos(\theta+\phi) \end{bmatrix}$$
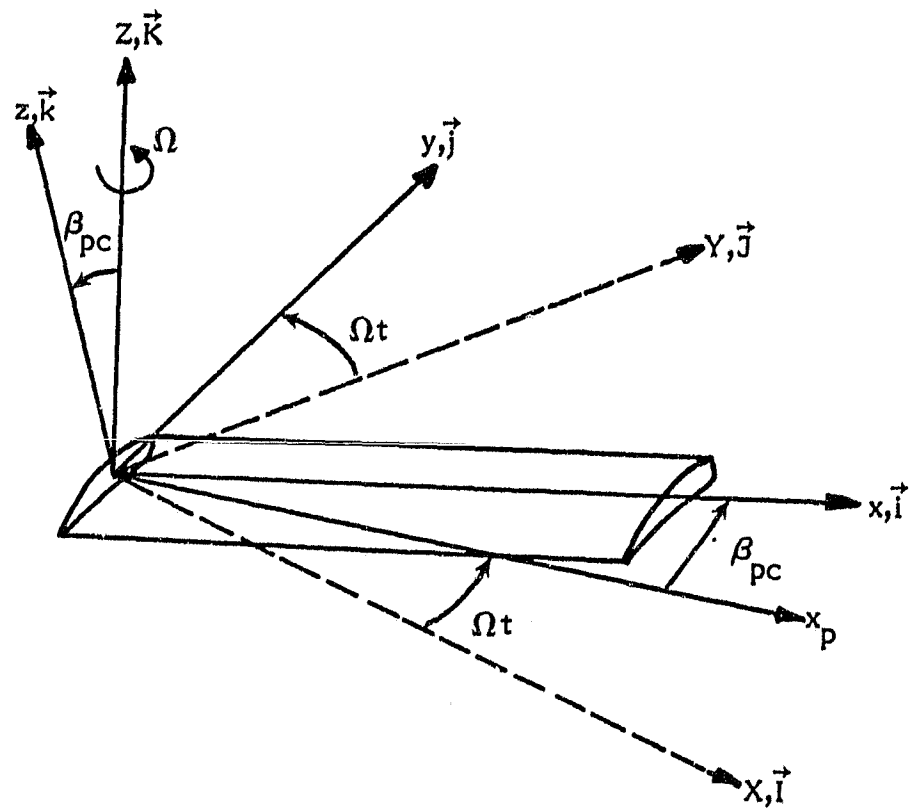
Figure A-1. - Undeformed coordinate system.
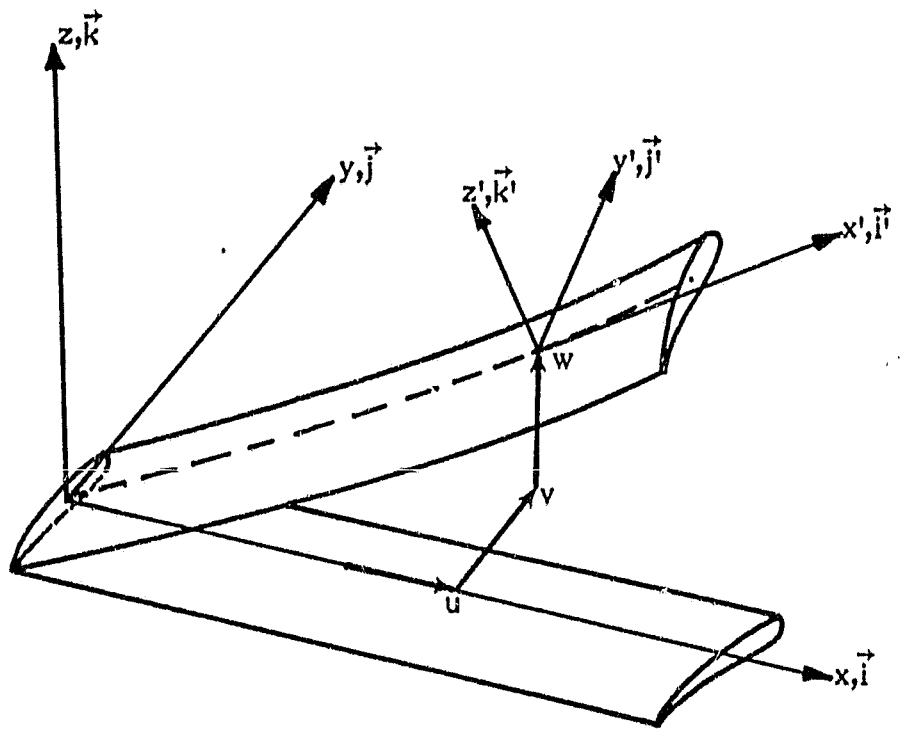
Figure A-2. - Blade elastic displacements.

APPENDIX B

ACCELERATION COMPONENTS

The purpose of this appendix is to formulate the components of absolute acceleration as measured in the deformed coordinate system for a general point (x_1, y_1, z_1) in the undeformed system. It is desired to use the deformed coordinate system since it is easier to formulate the pendulum equilibrium equations in this system. These acceleration components are to be described in terms of section coordinates and the elastic blade displacements and rotations to the first order.

A position vector in the inertial reference system can be written as

$$\vec{r} = X\vec{I} + Y\vec{J} + Z\vec{K} \tag{B-1}$$

and the corresponding acceleration components are

$$a_X = \ddot{X} \quad ; \quad a_Y = \ddot{Y} \quad ; \quad a_Z = \ddot{Z} \tag{B-2}$$

The components of acceleration in the rotating, nonpreconed system can be obtained from the component transformations in equation (A-1) as

$$\left.\begin{aligned}
a_{xp} &= \ddot{X} \cos \Omega t + \ddot{Y} \sin \Omega t \\
a_y &= \ddot{Y} \cos \Omega t - \ddot{X} \sin \Omega t \\
a_z &= \ddot{Z}
\end{aligned}\right\} \tag{B-3}$$

Substitution of equation (B-3) into equation (A-3) yields the acceleration components in the undeformed system which is rotating at a small precone angle as illustrated in figure A-1. These components become

$$\left.\begin{aligned}
a_x &= \ddot{X} \cos \Omega t + \ddot{Y} \sin \Omega t + \ddot{Z} \beta_{pc} \\
a_y &= \ddot{Y} \cos \Omega t - \ddot{X} \sin \Omega t \\
a_z &= \ddot{Z} - (\ddot{X} \cos \Omega t + \ddot{Y} \sin \Omega t) \beta_{pc}
\end{aligned}\right\} \tag{B-4}$$

The position vector of equation (B-1) can be written for a general point (x_1, y_1, z_1) in the undeformed system by successive applications of equations (A-1) and (A-3) as

$$\vec{r} = (x_1 \cos \Omega t - y_1 \sin \Omega t - z_1 \beta_{pc} \cos \Omega t) \vec{I}$$

$$+ (x_1 \sin \Omega t + y_1 \cos \Omega t - z_1 \beta_{pc} \sin \Omega t) \vec{J}$$

$$+ (x_1 \beta_{pc} + z_1) \vec{K} \tag{B-5}$$

The second time derivative of the components of equation (B-5) are

$$\ddot{X} = \ddot{x}_1 \cos \Omega t - \ddot{y}_1 \sin \Omega t - \ddot{z}_1 \ \beta_{pc} \cos \Omega t \qquad (B-6)$$

$$-2 \Omega \dot{x}_1 \sin \Omega t - 2 \Omega \dot{y}_1 \cos \Omega t + 2 \Omega \dot{z}_1 \ \beta_{pc} \sin \Omega t$$

$$- \Omega^2 x_1 \cos \Omega t + \Omega^2 y_1 \sin \Omega t + \Omega^2 z_1 \ \beta_{pc} \cos \Omega t$$

$$\ddot{Y} = \ddot{x}_1 \sin \Omega t + \ddot{y}_1 \cos \Omega t - \ddot{z}_1 \ \beta_{pc} \sin \Omega t \qquad (B-7)$$

$$+2 \Omega \dot{x}_1 \cos \Omega t - 2 \Omega \dot{y}_1 \sin \Omega t - 2 \Omega \dot{z}_1 \ \beta_{pc} \cos \Omega t$$

$$- \Omega^2 x_1 \sin \Omega t - \Omega^2 y_1 \cos \Omega t + \Omega^2 z_1 \ \beta_{pc} \sin \Omega t$$

$$\ddot{Z} = \ddot{x}_1 \ \beta_{pc} + \ddot{z}_1 \qquad (B-8)$$

Substituting these derivatives into the acceleration components of equation (B-4) and neglecting second degree terms in the precone angle yields

$$\left. \begin{array}{l} a_x = \ddot{x}_1 - 2 \Omega \dot{y}_1 - \Omega^2 x_1 + \Omega^2 z_1 \ \beta_{pc} \\[2mm] a_y = \ddot{y}_1 + 2 \Omega \dot{x}_1 - 2 \Omega \dot{z}_1 \ \beta_{pc} - \Omega^2 y_1 \\[2mm] a_z = \ddot{z}_1 + 2 \Omega \dot{y}_1 \ \beta_{pc} + \Omega^2 x_1 \ \beta_{pc} \end{array} \right\} \qquad (B-9)$$

In the deformed body, the coordinates x_1, y_1, z_1 of the general point in the undeformed coordinate system can be expressed in terms of the elastic deflections u, v, w, ϕ and the section coordinates ξ, η, ζ (same as x', y', z') with the aid of equation (A-4) as

$$\begin{bmatrix} x_1 \\ y_1 \\ z_1 \end{bmatrix} = \begin{bmatrix} x + u \\ v \\ w \end{bmatrix} + [T]^T \begin{bmatrix} \xi \\ \eta \\ \zeta \end{bmatrix} \qquad (B-10)$$

These coordinates become

$$x_1 = x + u + \xi - v' \left[\eta \cos(\theta + \phi) - \zeta \sin(\theta + \phi) \right]$$

$$-w' \left[\eta \sin(\theta + \phi) + \zeta \cos(\theta + \phi) \right] \qquad (B-11)$$

$$y_1 = v + v' \xi + \eta \cos(\theta + \phi) - \zeta \sin(\theta + \phi) \qquad \text{(B-12)}$$

$$z_1 = w + w' \xi + \eta \sin(\theta + \phi) + \zeta \cos(\theta + \phi) \qquad \text{(B-13)}$$

When these coordinates and their time derivatives are substituted into equation (B-9) the acceleration components to first order become

$$a_x = \ddot{\xi} - 2\Omega\dot{v} - \Omega^2(x + \xi)$$

$$+ 2\Omega\dot{\zeta} \sin(\theta + \phi) - 2\Omega\dot{\eta} \cos(\theta + \phi) \qquad \text{(B-14)}$$

$$a_y = \ddot{v} + 2\Omega\dot{\xi} - \Omega^2 v$$

$$+ (\Omega^2\zeta - \ddot{\zeta}) \sin(\theta + \phi) - (\Omega^2\eta - \ddot{\eta}) \cos(\theta + \phi)$$
$$\text{(B-15)}$$

$$a_z = \ddot{w} + \Omega^2 \beta_{pc}(x + \xi)$$

$$+ \ddot{\eta} \sin(\theta + \phi) + \ddot{\zeta} \cos(\theta + \phi) \qquad \text{(B-16)}$$

In the above acceleration expressions, the coordinates ξ, η, ζ are of a general point off the blade. These acceleration components in the undeformed system can be transformed into the deformed system components by again applying the transformation of equation (A-4) as

$$\begin{bmatrix} a_{x'} \\ a_{y'} \\ a_{z'} \end{bmatrix} = [T] \begin{bmatrix} a_x \\ a_y \\ a_z \end{bmatrix} \qquad \text{(B-17)}$$

The final acceleration components in the deformed system can be further simplified by applying the trigonometric approximations of equation (8) to yield

$$a_{x'} = \ddot{\xi} - 2\Omega\dot{v} - \Omega^2(x + \xi) + 2\Omega\dot{\zeta} \sin\theta$$

$$-2\Omega\dot{\eta} \cos\theta \qquad \text{(B-18)}$$

78

$$a_{y'} = \ddot{\eta} + (\Omega^2 x \nu + \ddot{w} + \Omega^2 \beta_{pc} x) \sin \theta$$

$$+ (\ddot{v} + 2 \Omega \dot{\xi} - \Omega^2 v + \Omega^2 x \mu) \cos \theta$$

$$- \Omega^2 \eta \cos^2 \theta + 1/2 \ \Omega^2 \zeta \sin 2 \theta \qquad \text{(B-19)}$$

$$a_{z'} = \ddot{\zeta} - (\ddot{v} + 2 \Omega \dot{\xi} - \Omega^2 v + \Omega^2 x \mu) \sin \theta$$

$$+ (\Omega^2 x \nu + \ddot{w} + \Omega^2 \beta_{pc} x) \cos \theta$$

$$- \Omega^2 \zeta \sin^2 \theta + 1/2 \ \Omega^2 \eta \sin 2 \theta \qquad \text{(B-20)}$$

APPENDIX C

AERODYNAMIC COUPLING COEFFICIENTS

In equation (132) the elastic deformations-dependent aerodynamic loads are expressed in a matrix form. The nonzero elements of these matrices are

$$B_{65} = \frac{1}{2}\rho ac \left(\frac{c}{4}\right)^2 \Omega^2 x$$

$$B_{10,3} = -\frac{1}{2}\rho ac \, \Omega^2 x R \lambda$$

$$B_{10,5} = -\frac{1}{2}\rho ac \left(\frac{1}{2}\Omega^2 x \, \mu_f R \, \theta_{1c} + \Omega^2 \mu_f^2 \, R^2 \beta_{pc}\right)$$

$$B_{11,1} = -\frac{1}{2}\rho ac \left(-\Omega^2 x \, \beta_{pc}\right)$$

$$B_{11,3} = -\frac{1}{2}\rho ac \left(-\Omega^2 x^2 - \frac{1}{2}\mu_f^2 \, \Omega^2 R^2\right)$$

$$B_{11,4} = -\frac{1}{2}\rho ac \left(-\Omega^2 x \, \mu_f R \, \theta_{1c} - \frac{1}{2}\Omega^2 \mu_f^2 R^2 \beta_{pc}\right)$$

$$B_{11,5} = -\frac{1}{2}\rho ac \left(-\frac{c}{2}\Omega^2 x\right)$$

$$C_{63} = \frac{1}{2}\rho ac \left(\frac{c}{4}\right)^2 (2\Omega x)$$

$$C_{10,2} = -\frac{1}{2}\rho ac \left[-\Omega x (\theta_c + \theta_t) + \frac{1}{2}\mu_f \Omega R \, \theta_{1s} - 2\Omega R \lambda\right]$$

$$C_{11,1} = -\frac{1}{2}\rho ac \left[2\Omega x (\theta_c + \theta_t) - \mu_f \Omega R \, \theta_{1s} + \Omega R \lambda\right]$$

$$C_{11,2} = -\frac{1}{2}\rho ac \left(-\Omega x\right)$$

$$C_{11,3} = -\frac{1}{2}\rho ac \left(\frac{3c}{4}\Omega x\right)$$

$$D_{62} = -\frac{1}{2}\rho ac \left(\frac{c}{4}\right)^2$$

$$D_{11,2} = \frac{1}{2}\rho ac \left(\frac{c}{4}\right)$$

80

For n = 1:

$$B_{c63} = \frac{1}{2} \rho ac \left(\frac{c}{4}\right)^2 \mu_f \Omega^2 R$$

$$B_{c10,3} = -\frac{1}{2} \rho ac \left(-\Omega^2 x \mu_f R \beta_{pc}\right)$$

$$B_{c10,5} = -\frac{1}{2} \rho ac \left[-\Omega^2 x (\theta_c + \theta_t) \mu_f \Omega R + \frac{1}{4} \Omega^2 \mu_f^2 R^2 \theta_{1s} \right.$$
$$\left. -2 \Omega^2 \mu_f R^2 \lambda\right]$$

$$B_{c11,3} = -\frac{1}{2} \rho ac \left(\frac{c}{4} \mu_f \Omega^2 R\right)$$

$$B_{c11,4} = -\frac{1}{2} \rho ac \left[2\Omega^2 x (\theta_c + \theta_t) \mu_f R - \frac{1}{2} \Omega^2 \mu_f^2 R^2 \theta_{1s} \right.$$
$$\left. + \Omega^2 \mu_f R^2 \lambda\right]$$

$$B_{c11,5} = -\frac{1}{2} \rho ac \left(\Omega^2 x \mu_f R\right)$$

$$C_{c65} = \frac{1}{2} \rho ac \left(\frac{c}{4}\right)^2 \mu_f \Omega R$$

$$C_{c10,2} = -\frac{1}{2} \rho ac \left(\Omega x \theta_{1c} + 2 \mu_f \Omega R \beta_{pc}\right)$$

$$C_{c11,1} = -\frac{1}{2} \rho ac \left(-2 \Omega x \theta_{1c} - \mu_f \Omega R \beta_{pc}\right)$$

$$C_{c11,5} = -\frac{1}{2} \rho ac \left(-\frac{c}{4} \Omega \mu_f R\right)$$

$$B_{s65} = \frac{1}{2} \rho ac \left(\frac{c}{4}\right)^2 \left(2 \Omega^2 \mu_f R\right)$$

$$B_{s10,3} = -\frac{1}{2} \rho ac \left(\Omega^2 \mu_f R^2 \lambda\right)$$

$$B_{s10,5} = -\frac{1}{2} \rho ac \left(\frac{1}{4} \Omega^2 \mu_f^2 R^2 \theta_{1c}\right)$$

$$B_{s11,1} = -\frac{1}{2} \rho ac \left(-\Omega^2 \mu_f R \beta_{pc}\right)$$

$$B_{s11,3} \quad = \quad -\frac{1}{2}\,\rho ac\,(-2\,\Omega^2 x\,R\,\mu_f)$$

$$B_{s11,4} \quad = \quad -\frac{1}{2}\,\rho ac\,(-\frac{1}{2}\,\Omega^2\,\mu_f^2\,R^2\,\theta_{1c})$$

$$B_{s11,5} \quad = \quad -\frac{1}{2}\,\rho ac\,(\frac{3c}{4}\,\Omega^2\,\mu_f\,R)$$

$$C_{s63} \quad = \quad \frac{1}{2}\,\rho ac\,(\frac{c}{4})^2\,(2\,\mu_f\,\Omega\,R)$$

$$C_{s10,2} \quad = \quad -\frac{1}{2}\,\rho ac\,\left[\,\Omega x\,\theta_{1s} - \mu_f\,\Omega R\,(\theta_c + \theta_t)\right]$$

$$C_{s11,1} \quad = \quad -\frac{1}{2}\,\rho ac\,\left[-2\Omega x\,\theta_{1s} + 2\,\mu_f\,\Omega R\,(\theta_c + \theta_t)\right]$$

$$C_{s11,2} \quad = \quad -\frac{1}{2}\,\rho ac\,\mu_f\,\Omega\,R$$

$$C_{s11,3} \quad = \quad -\frac{1}{2}\,\rho\,ac\,(\frac{3c}{4}\,\mu_f\,\Omega R)$$

For n = 2 ;

$$B_{c10,5} \quad = \quad -\frac{1}{2}\,\rho ac\,(\frac{1}{2}\,\Omega^2 x\,\mu_f\,R\,\theta_{1c} + \Omega^2\,\mu_f^2\,R^2\,\beta_{pc})$$

$$B_{c11,3} \quad = \quad -\frac{1}{2}\,\rho ac\,(\frac{1}{2}\,\mu_f^2\,\Omega^2\,R^2)$$

$$B_{c11,4} \quad = \quad -\frac{1}{2}\,\rho ac\,(-\Omega^2 x\,\mu_f\,R\,\theta_{1c} - \frac{1}{2}\,\Omega^2\,\mu_f^2\,R^2\,\beta_{pc})$$

$$C_{c10,2} \quad = \quad -\frac{1}{2}\,\rho ac\,(-\frac{1}{2}\,\mu_f\,\Omega R\,\theta_{1s})$$

$$C_{c11,1} \quad = \quad -\frac{1}{2}\,\rho ac\,(\mu_f\,\Omega R\,\theta_{1s})$$

$$B_{s10,3} \quad = \quad -\frac{1}{2}\,\rho ac\,(-\frac{1}{2}\,\Omega^2\,\mu_f^2\,R^2\,\beta_{pc})$$

$$B_{s10,5} \quad = \quad -\frac{1}{2}\,\rho ac\,\left[\frac{1}{2}\,\Omega^2 x\,\mu_f\,R\,\theta_{1s} - \frac{1}{2}\,\Omega^2\,\mu_f^2\,R^2\,(\theta_c + \theta_t)\right]$$

$$B_{s11,4} \quad = \quad -\frac{1}{2}\,\rho ac\,\left[-\Omega^2 x\,\mu_f\,R\,\theta_{1s} + \Omega^2\,\mu_f^2\,R^2\,(\theta_c + \theta_t)\right]$$

$$B_{s11,5} = -\frac{1}{2}\rho ac\left(-\frac{1}{2}\Omega^2\mu_f^2 R^2\right)$$

$$C_{s10,2} = -\frac{1}{2}\rho ac\left(\frac{1}{2}\mu_f\Omega R\ \theta_{1c}\right)$$

$$C_{s11,1} = -\frac{1}{2}\rho ac\left(-\mu_f\ \Omega R\ \theta_{1c}\right)$$

For n = 3 ;

$$B_{c10,5} = -\frac{1}{2}\rho ac\left(-\frac{1}{4}\Omega^2\mu_f^2 R^2\ \theta_{1s}\right)$$

$$B_{c11,4} = -\frac{1}{2}\rho ac\left(\frac{1}{2}\Omega^2\mu_f^2 R^2\ \theta_{1s}\right)$$

$$B_{s10,5} = -\frac{1}{2}\rho ac\left(\frac{1}{4}\Omega^2\mu_f^2 R^2\ \theta_{1c}\right)$$

$$B_{s11,4} = -\frac{1}{2}\rho ac\left(-\frac{1}{2}\Omega^2\mu_f^2 R^2\ \theta_{1c}\right)$$

APPENDIX D

ROTOR CONFIGURATIONS

Two rotor configurations have been considered in this investigation. The first is a uniform blade, and the second is typical of an operational blade with nonuniform properties.

The uniform blade has the following properties:

Radius, in 260

Linear twist, deg . . . . -10

Weight per unit length, lb/in 0.5796

Flapwise mass moment of inertia per unit length, lb-in 0.3476

Chordwise mass moment of inertia per unit length, lb-in 15.456

Flapwise bending stiffness, lb-in^2 . . . . 0.3x10^8

Chordwise bending stiffness lb-in^2 . . . . .0.1x10^{10}

Torsional rigidity, lb-in^2 . . . . 0.2x10^8

Mass axis offset, in. . . . . -0.6

Rotational speed, rpm 360

The nonuniform blade has the properties listed in the following table and illustrated in figures D-1 through D-6.

Radius, in 288

Root cutout, in 39

Precone, rad 0.1

Rotational speed, rpm 289

84
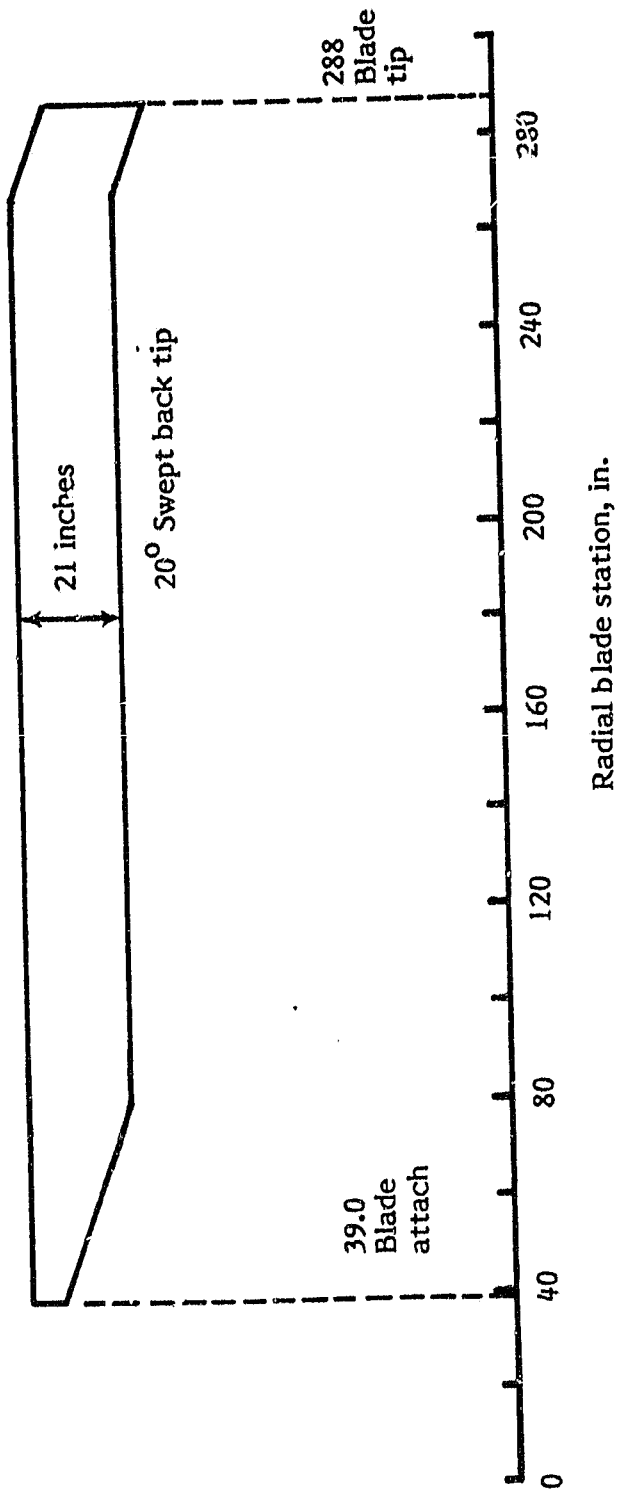
Figure D-1. - Blade planform.
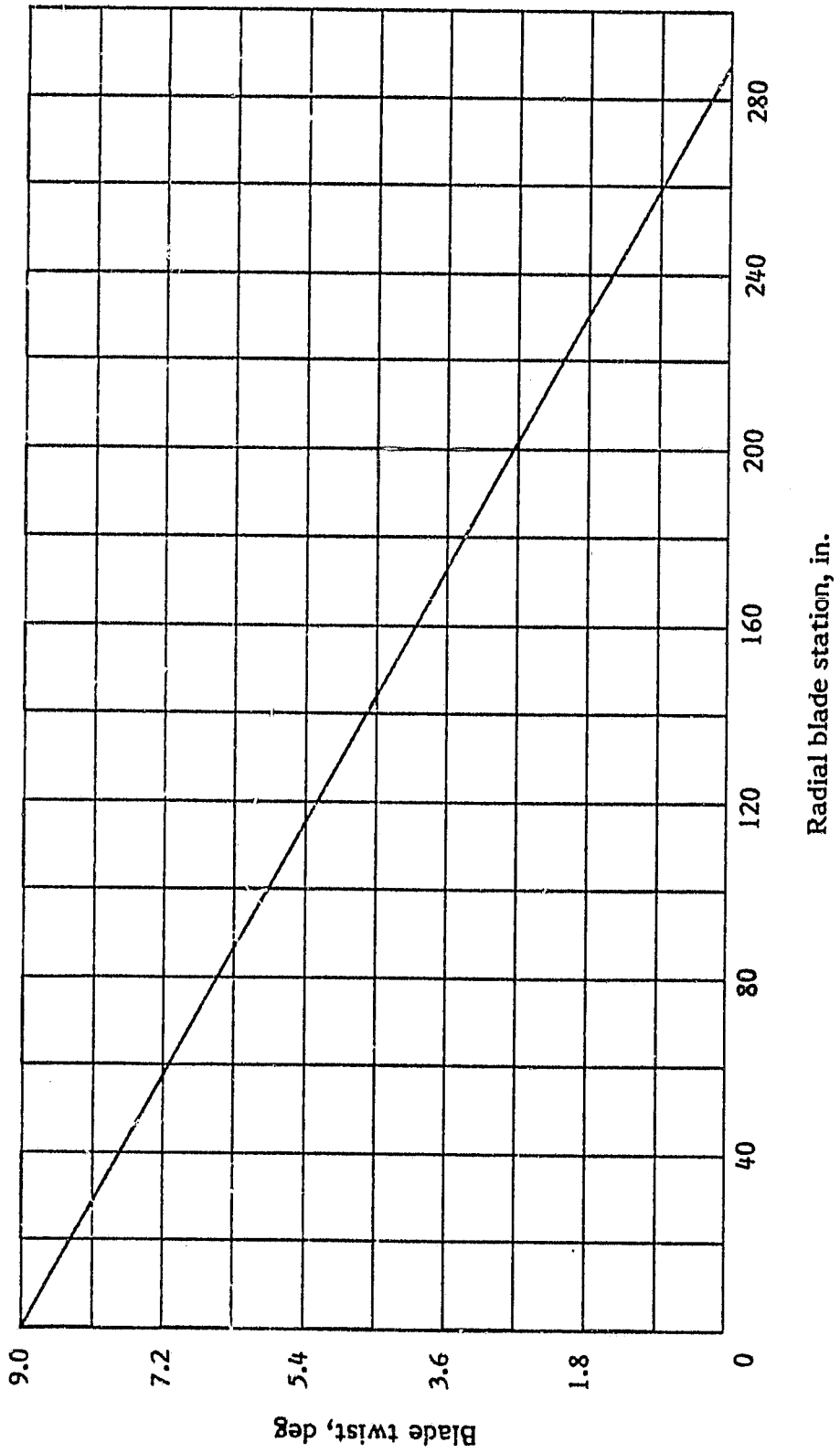
Figure D-2. - Rotor blade twist.
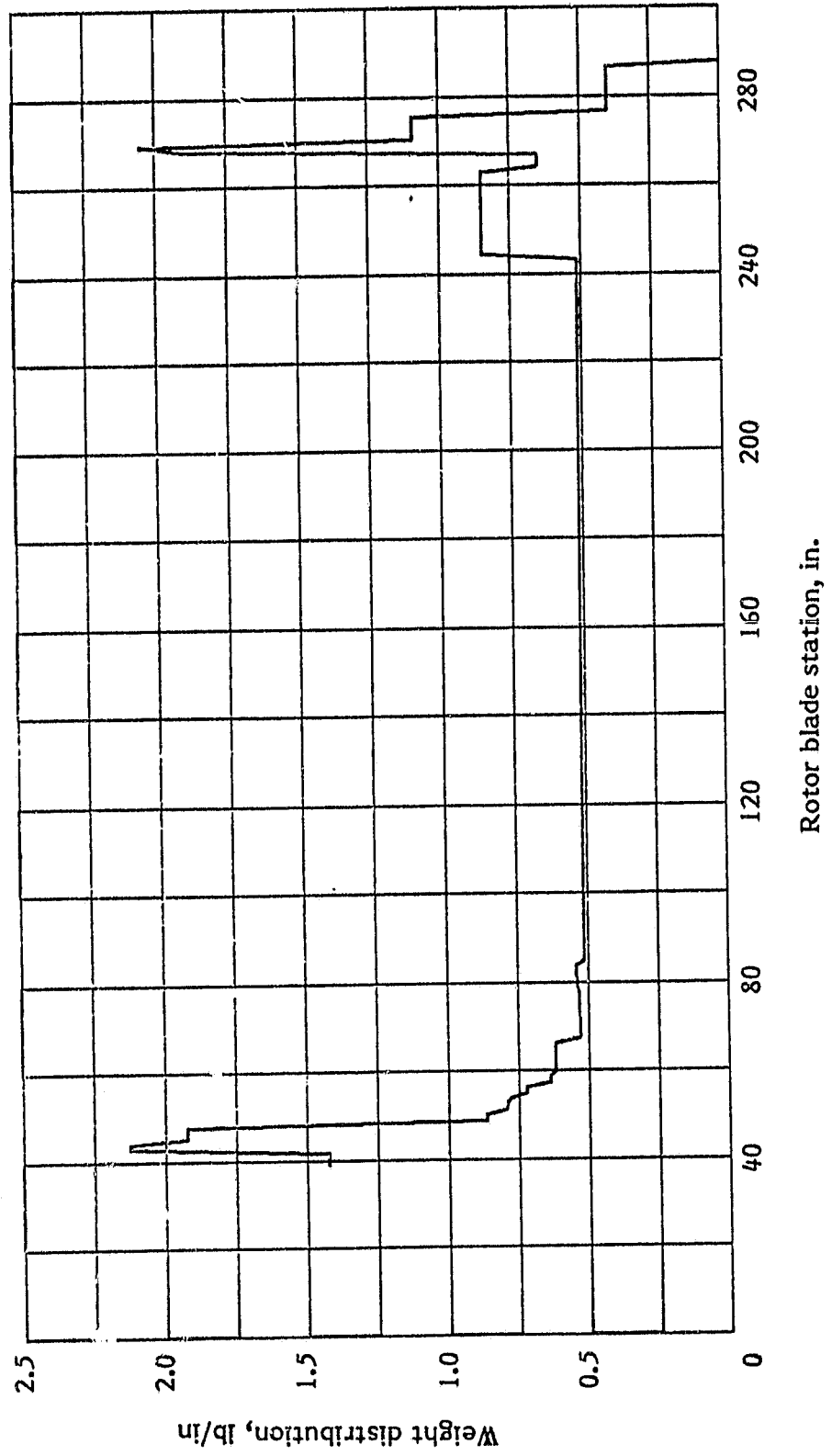
Figure D-3. - Rotor blade weight distribution.

87
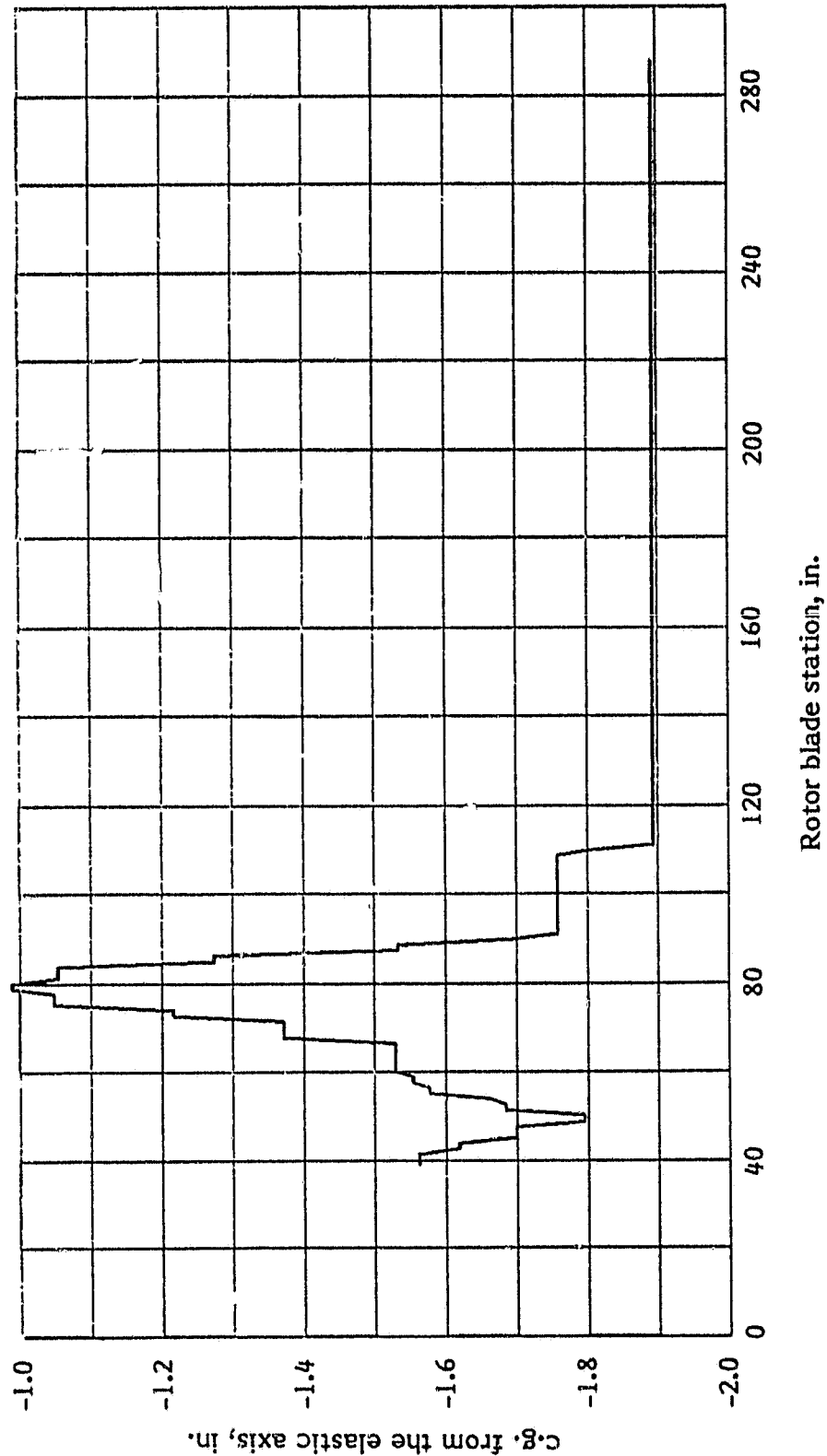
Figure D-4. - Rotor blade chordwise c.g. distribution.
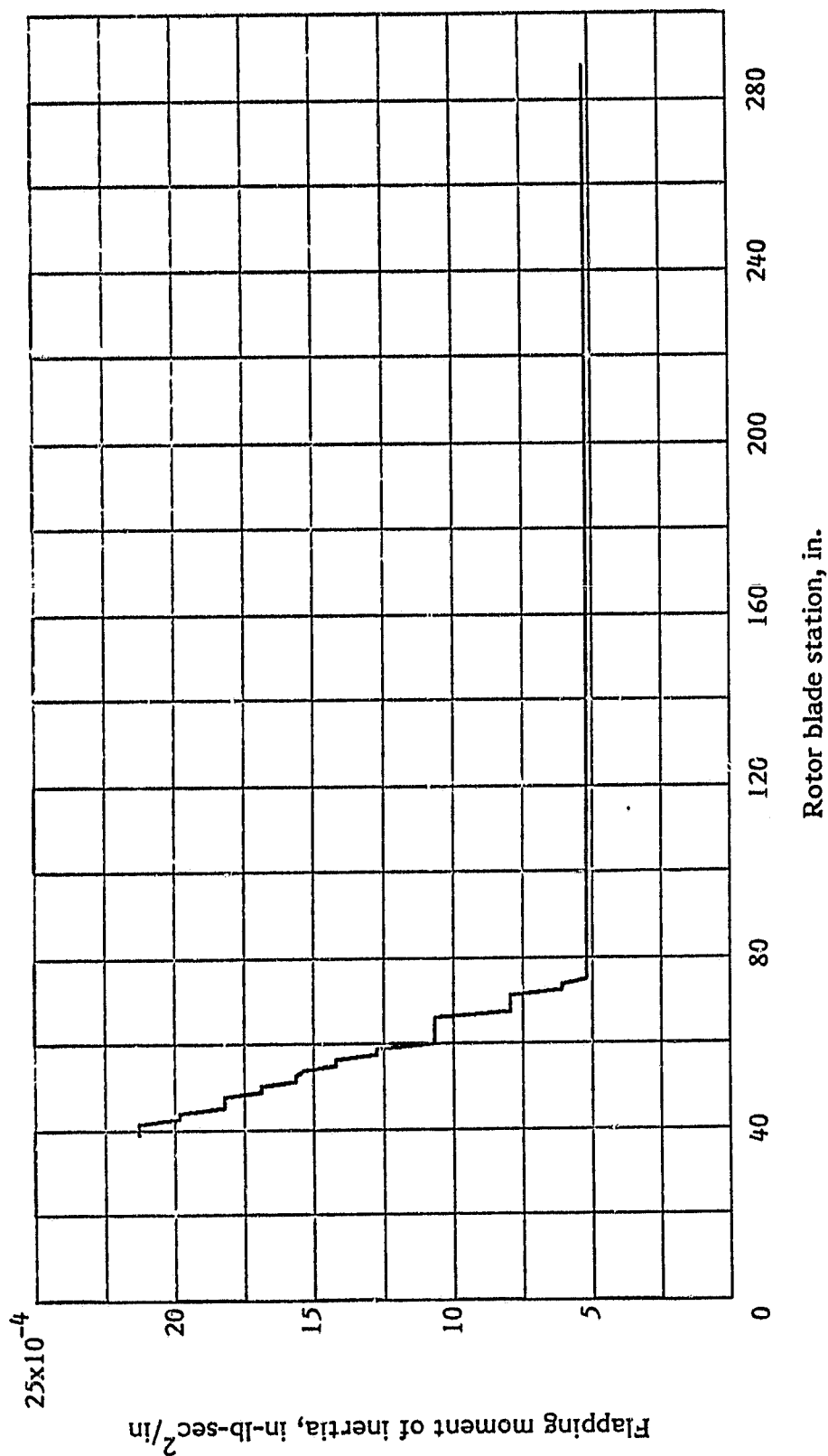
Figure D-5. – Rotor blade flapping moment of inertia.

89
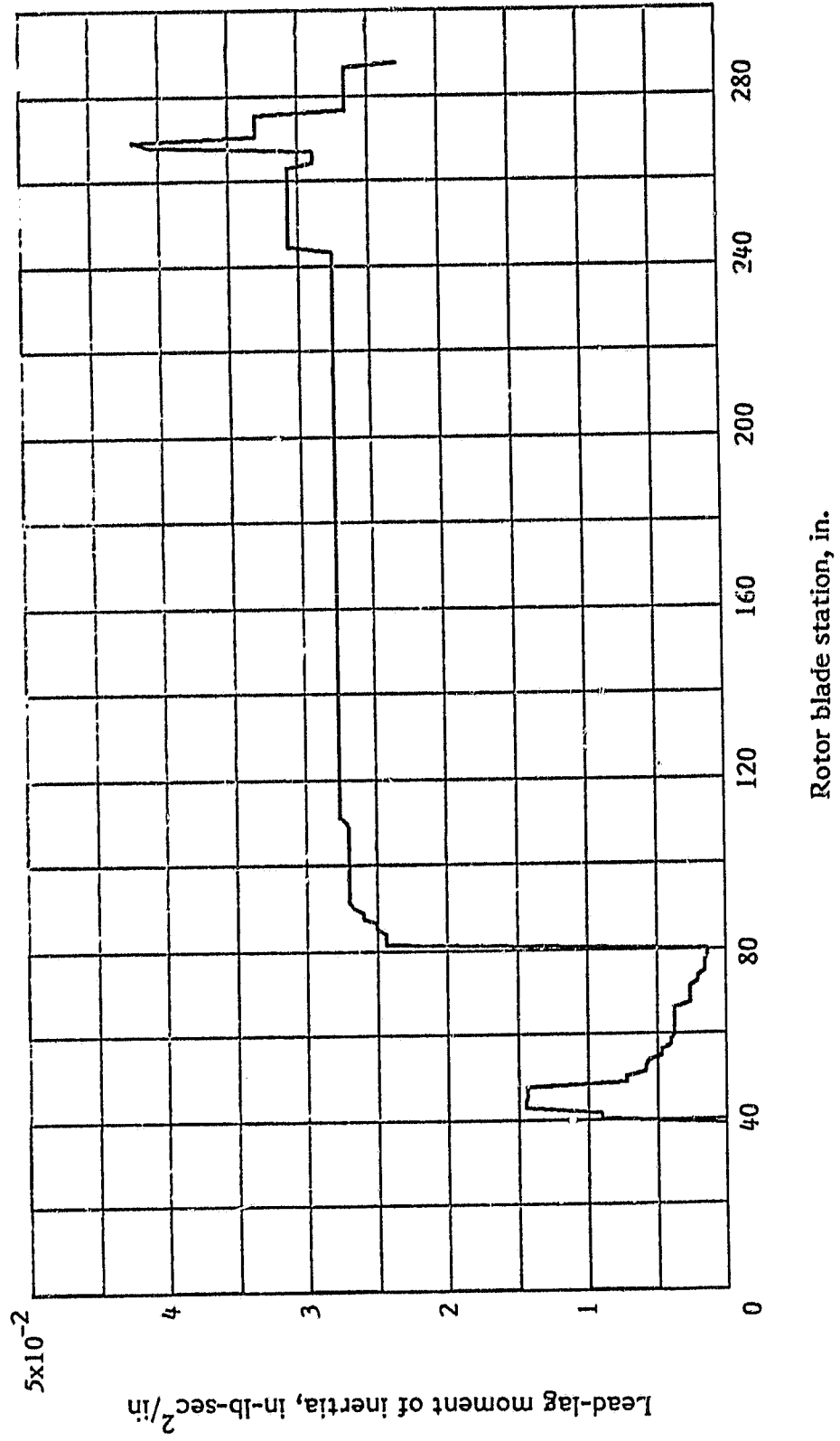
Figure D-6. – Rotor blade lead-lag moment of inertia.
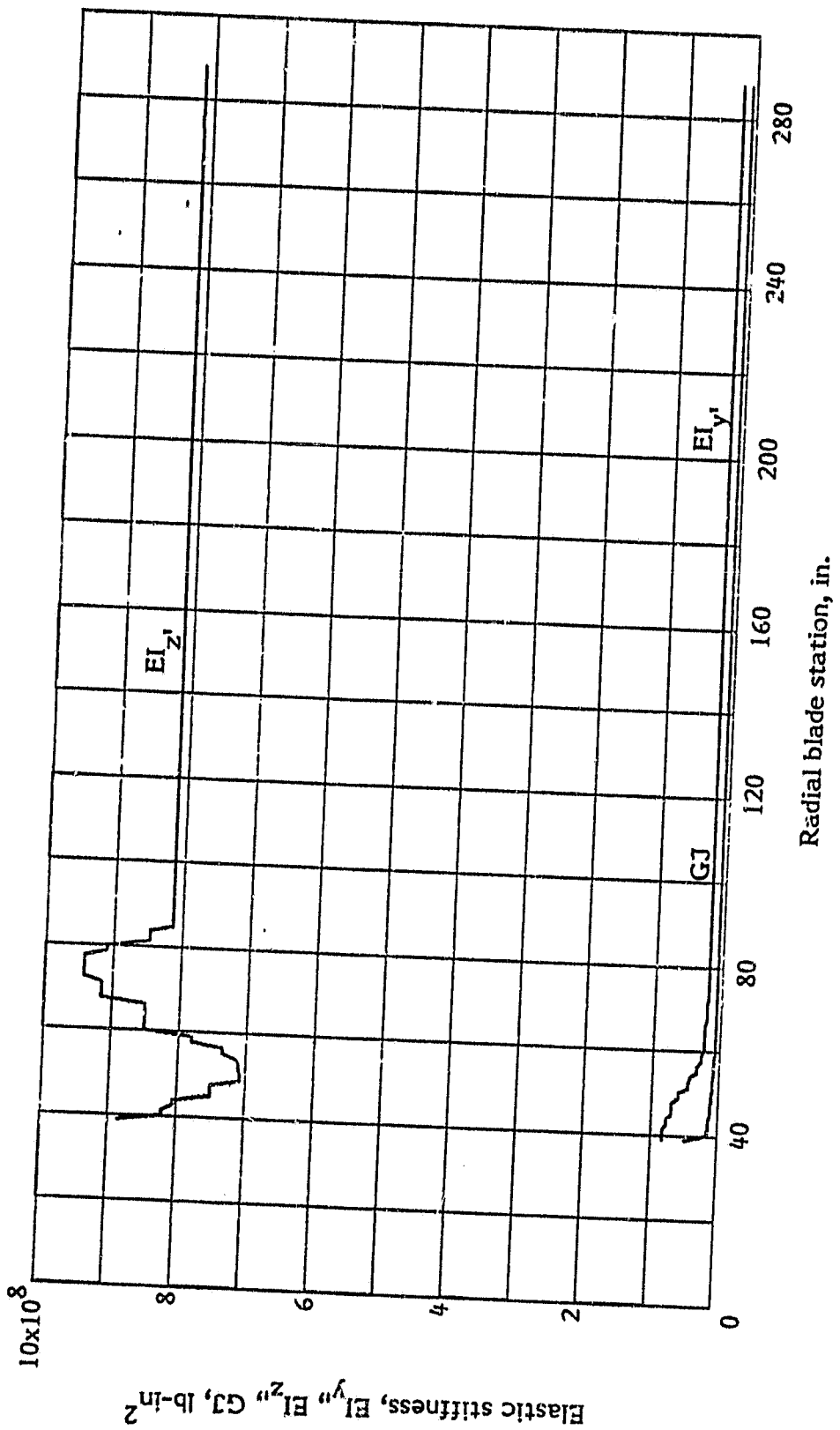
Figure D-7. – Rotor blade stiffness.

REFERENCES

1. McHugh, F. J.; and Shaw, J.: Helicopter Vibration Reduction with Higher Harmonic Blade Pitch. J American Helicopter Soc., vol. 23, October 1978, pp. 26-35.

2. Paul, William F.: Development and Evaluation of the Main Rotor Bifilar Absorber. 25th Annual National Forum of the American Helicopter Soc., May 1969.

3. Amer, Kenneth B.; and Neff, James R.: Vertical-Plane Pendulum Absorbers for Minimizing Helicopter Vibratory Loads. AHS/NASA-Ames Specialists Meeting on Rotorcraft Dynamics, February 1974.

4. Taylor, Robert B; and Teare, Paul A.: Helicopter Vibration Reduction with Pendulum Absorbers. 30th Annual National Forum of the American Helicopter Soc., May 1974.

5. Gabel, R; and Reichert, Gunther: Pendulum Absorbers Reduce Transition Vibration. 31st Annual National Forum of the American Helicopter Soc., May 1975.

6. Viswanathan, Sathy P.; and Myers, Alan W.: Reduction of Helicopter Vibration through Control of Hub-Impedence. J. American Helicopter Soc., vol. 25, October 1980, pp. 3-12.

7. Murthy, V. R.; and Hammond, C. E.: Vibration Analysis of Rotor Blades with Pendulum Absorbers. AIAA Paper 79-0730, April 1979.

8. Houbolt, J. C.; and Brooks, G. W.: Differential Equations of Motion for Combined Flapwise Bending, Chordwise Bending, and Torsion of Twisted Non-uniform Rotor Blades. NACA Rep. 1346, 1958.

9. Murthy, Vadrevu R.: Determination of the Structural Dynamic Characteristics of Rotor Blades and the Effect of Phase Angle on Multibladed Rotor Flutter. Ph.D. Thesis, Georgia Inst. of Tech., 1975.

10. Hodges, D. H.; and Dowell, E. H.: Nonlinear Equations of Motion for the Elastic Bending and Torsion of Twisted Nonuniform Rotor Blades. NASA TN D-7818, December 1974.

11. Greenberg, J. M.: Airfoil in Sinusoidal Motion in a Pulsating Stream. NACA TN 1326, 1947.

12. Kaza, K. R.; and Kvaternik, R. G.: Nonlinear Aeroelastic Equations for Combined Flapwise Bending, Chordwise Bending, Torsion, and Extension of Twisted Nonuniform Rotor Blades in Forward Flight. NASA TM 74059, August 1977.

13. Pestel, E. C.; and Leckie, F. A.: Matrix Methods in Elastomechanics. McGraw-Hill Book Co., 1963.

14. Murthy, V. R.: Dynamic Characteristics of Rotor Blades. J. Sound and Vib., vol. 49, no. 4, 1976, pp. 483-500.

15. Murthy, V. R.; and Hammond, C.E.: Vibration Analysis of Rotor Blades with Pendulum Absorbers. AIAA J. Aircraft, vol. 18, no. 1, January 1981, pp. 23-29.

16. Weller, W. H.; and Mineck, R. E.: An Improved Computational Procedure for Determining Helicopter Rotor Blade Natural Modes. NASA TM 78670, 1978.

17. Gessow, Alfred; and Myers, G. C., Jr.: Aerodynamics of the Helicopter. Frederic Ungar Publishing Co., 1967.
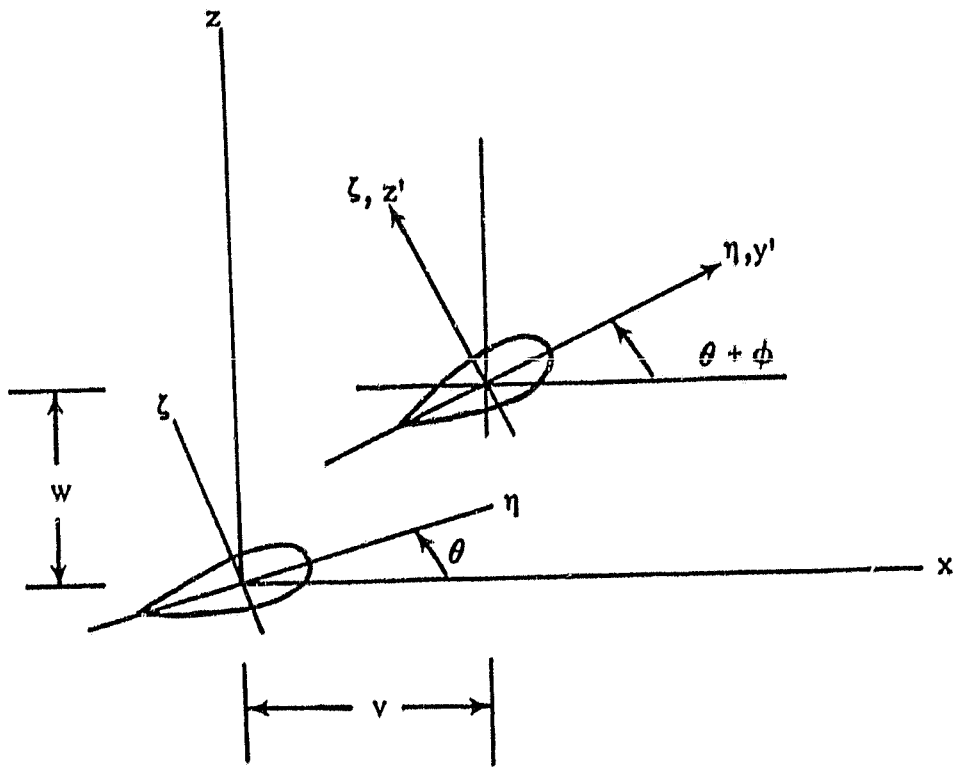
Figure 1. - Cross-section coordinates before
and after deformation.
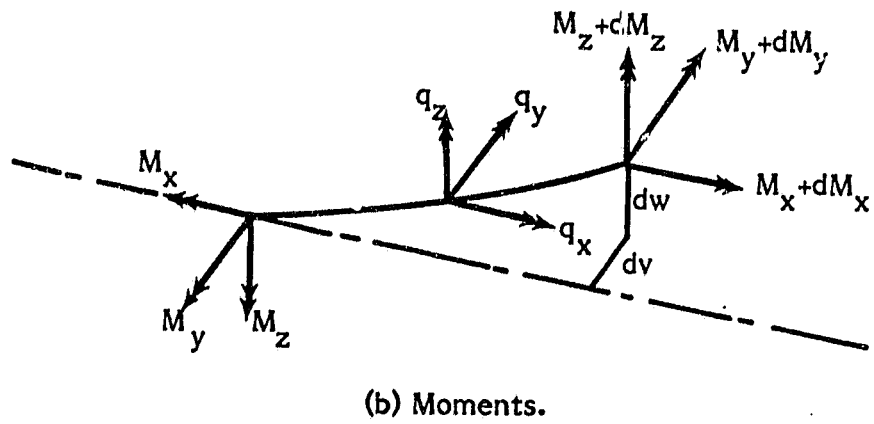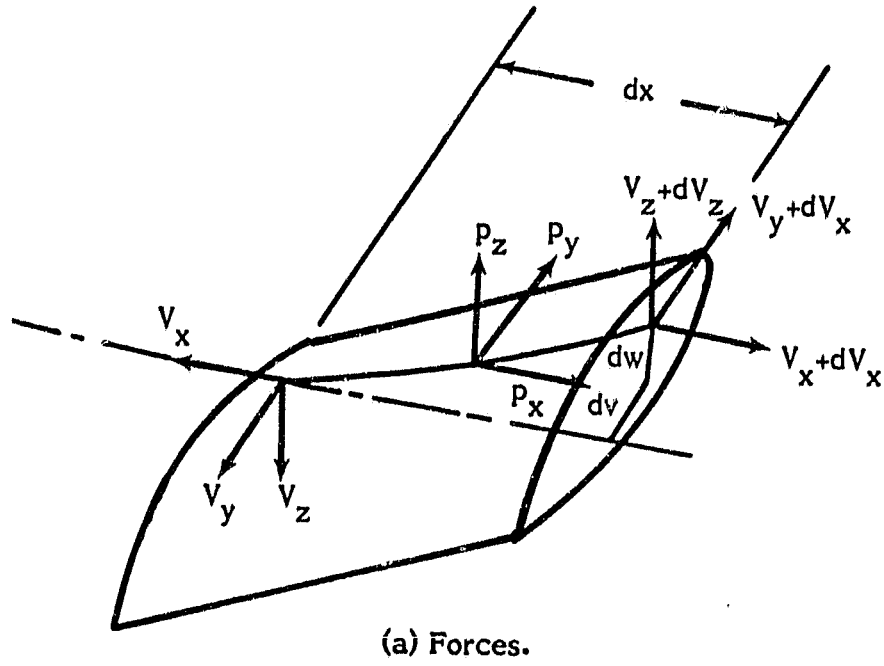
(a) Forces.

(b) Moments.

Figure 2. - Equilibrium forces and moments.

C-2
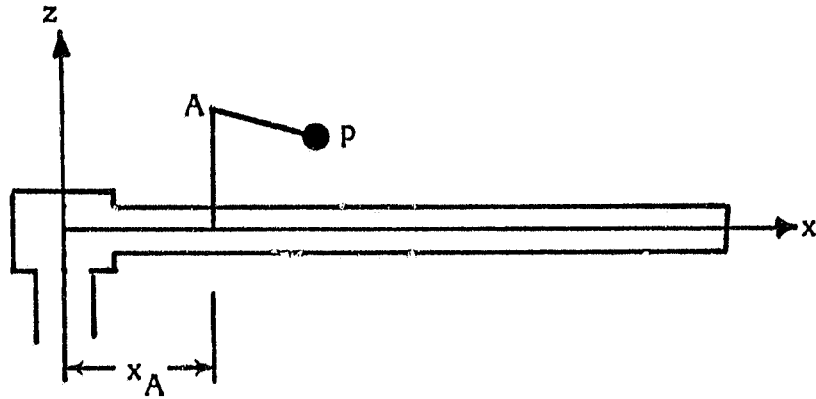
Figure 3. - Blade-mounted flapping pendulum
before deformation.
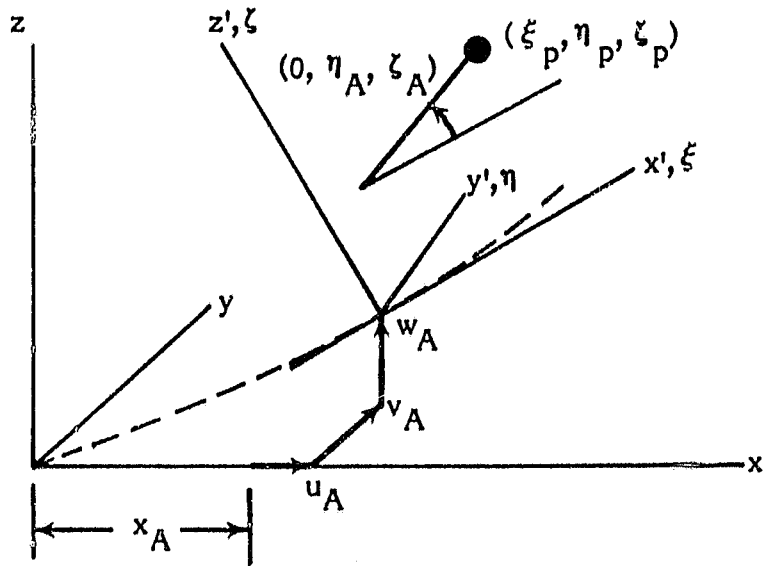
Figure 4. - Flapping pendulum location after deformation.
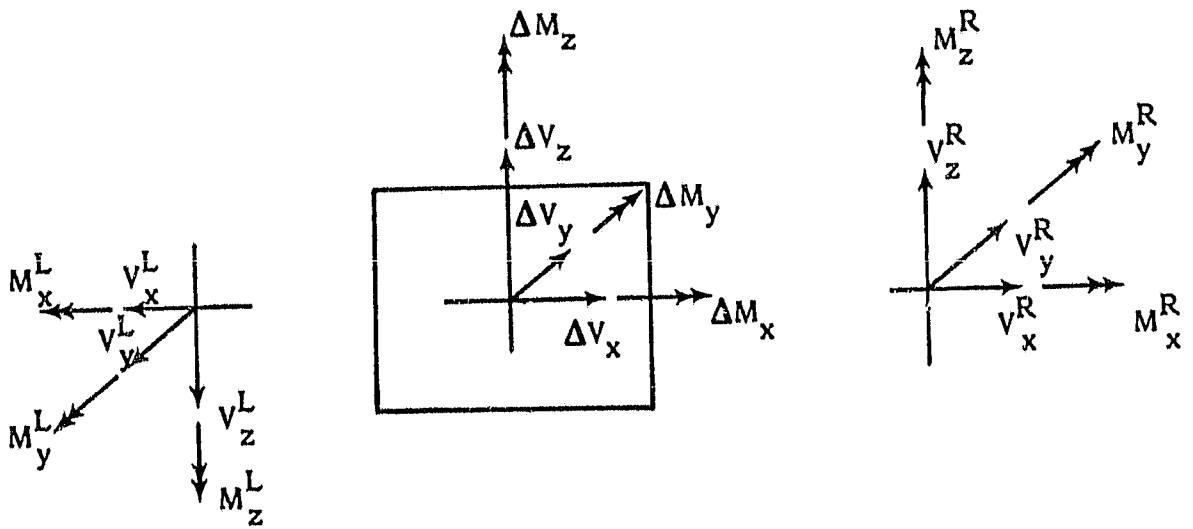
Figure 5. - Free-body diagram of the element containing flapping pendulum.
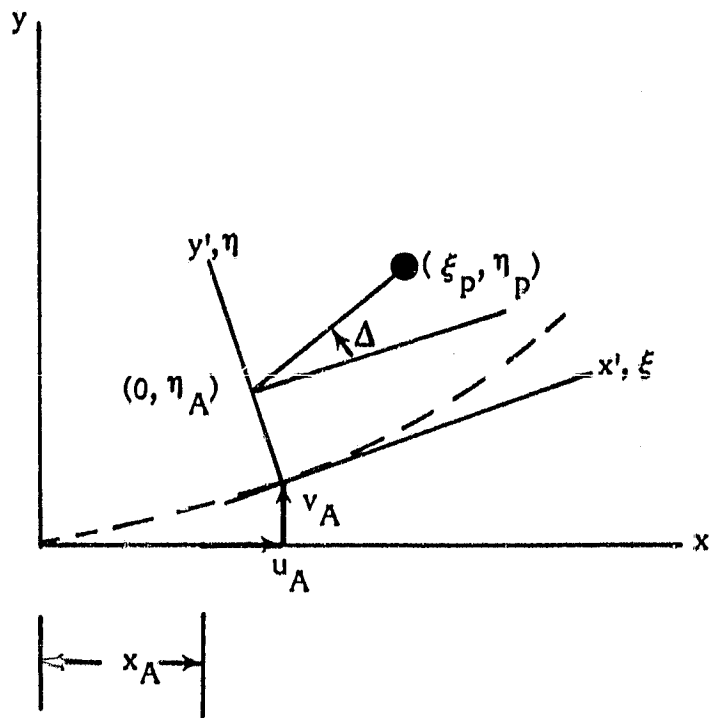
Figure 6. - Lead-lag pendulum after deformation.
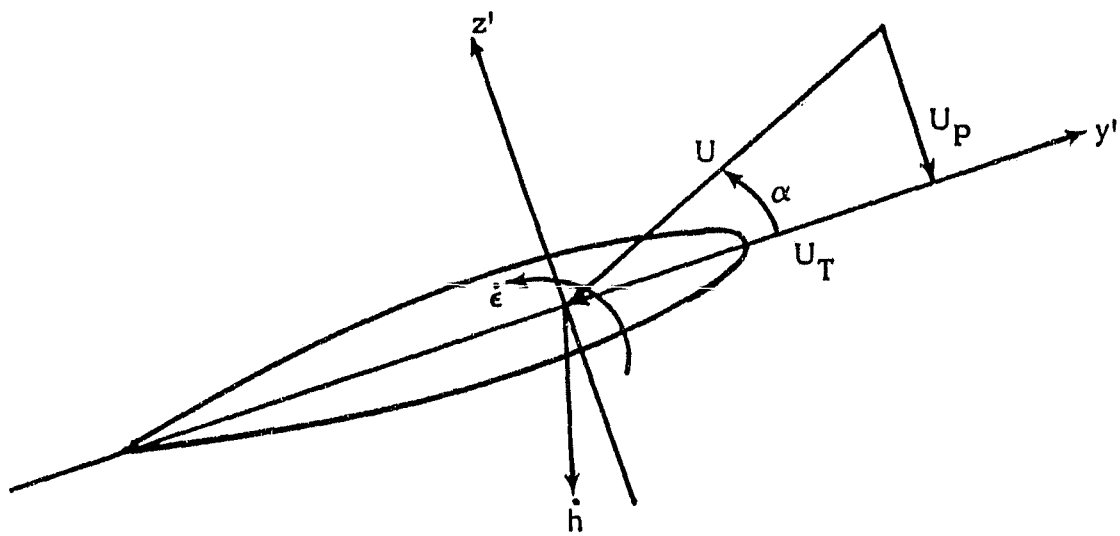
Figure 7. - Rotor blade airfoil inflow geometry.

$V \cos \alpha_s = \mu_f \Omega R$

$\mu_f \Omega R$

$\mu_f \Omega R \cos \psi$

$\mu_f \Omega R \sin \psi$

x_p

(b) Top view.

Tip-path plane

v_i

$\lambda \Omega R \equiv V \sin \alpha_s - v_i$

Vertical

α_s

Shaft Axis

$V \sin \alpha_s$

V

α_s

$V \cos \alpha_s$

(a) Side view.
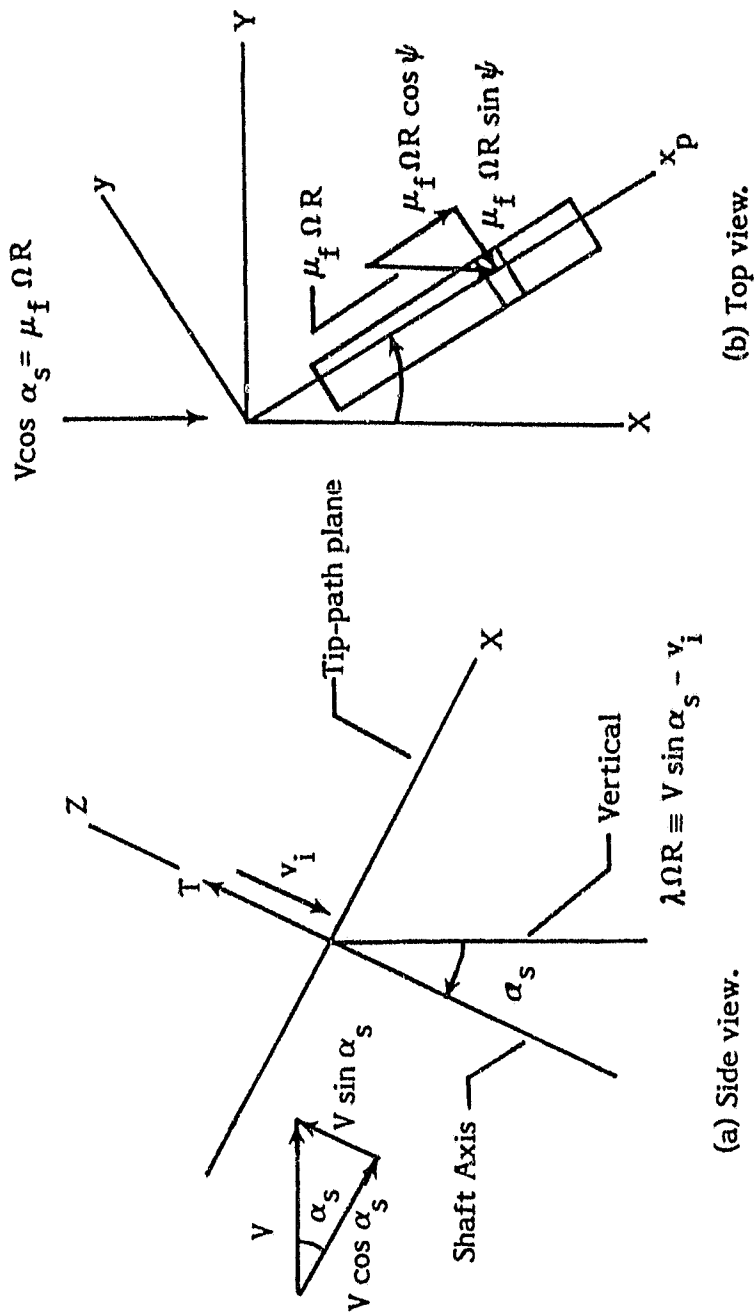
Figure 8. – Geometry for aerodynamic velocity components.
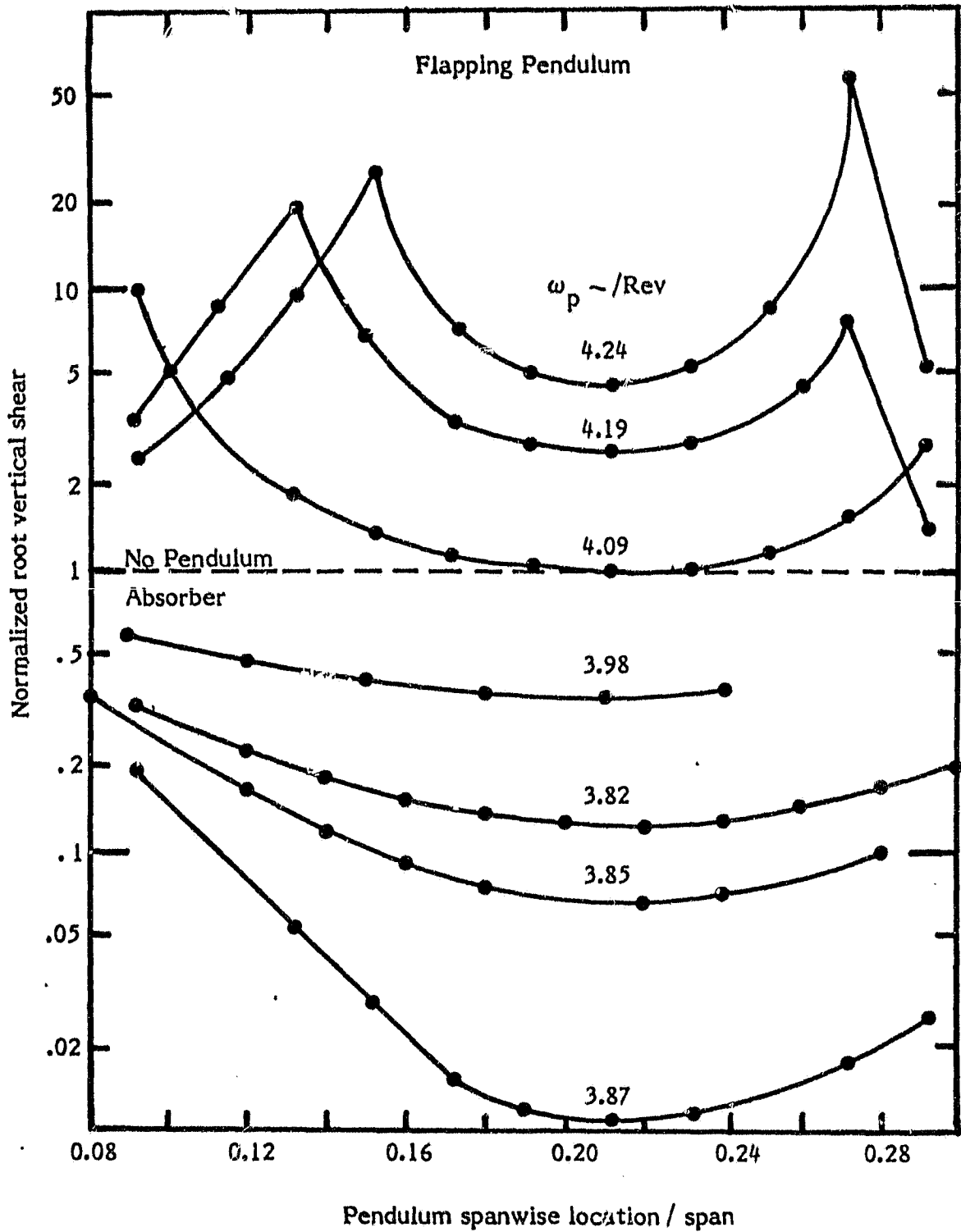
Figure 9. – Root vertical shear for 4/Rev concentrated excitation,
uniform blade, $W = 66.73$ N, $\eta_A = \zeta_A = 0$.
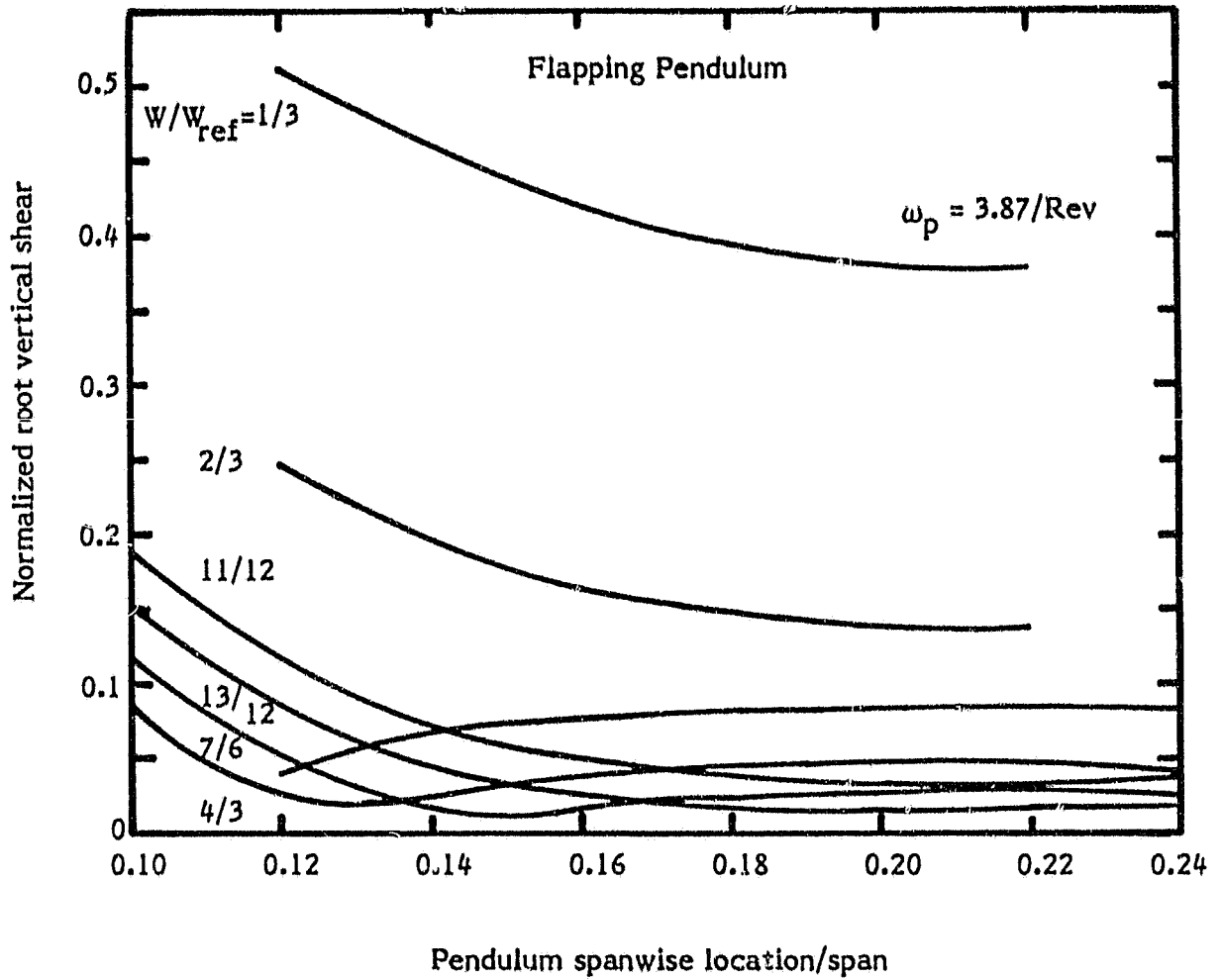
Figure 10 - Root vertical shear for 4/Rev concentrated excitation, uniform blade, $W_{ref} = 66.73$ N, $\eta_A = \zeta_A = 0$.
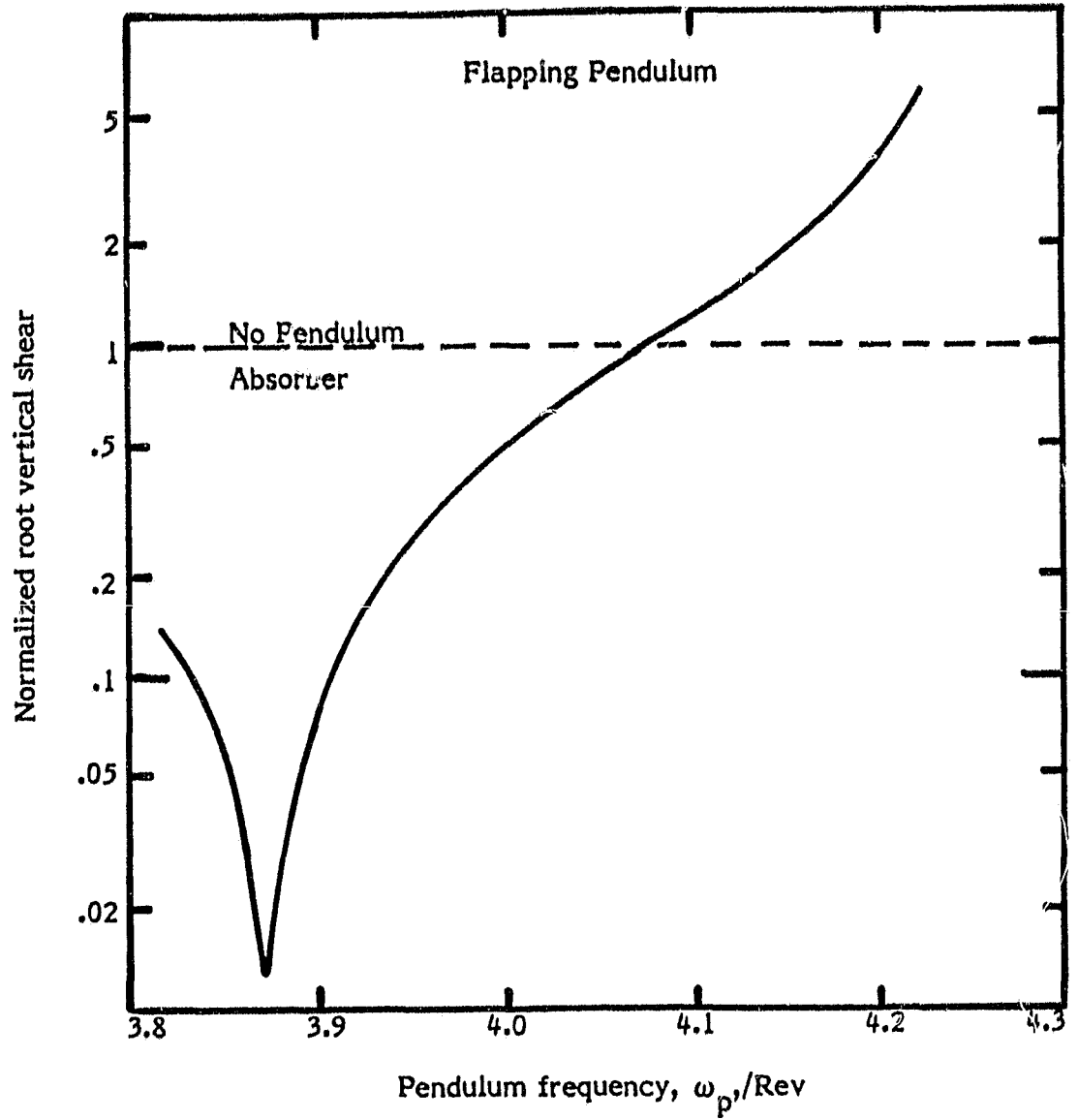
Figure 11. - Root vertical shear for 4/Rev concentrated excitation, uniform blade, $x_A/R = .18$, $W = 66.73$ N, $\eta_A = \zeta_A = 0$.
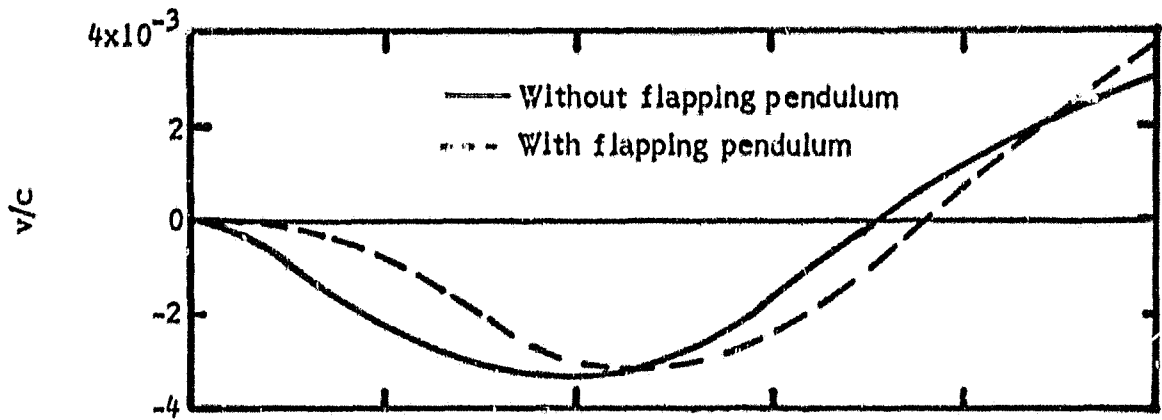
(a) Lead-lag deflection.
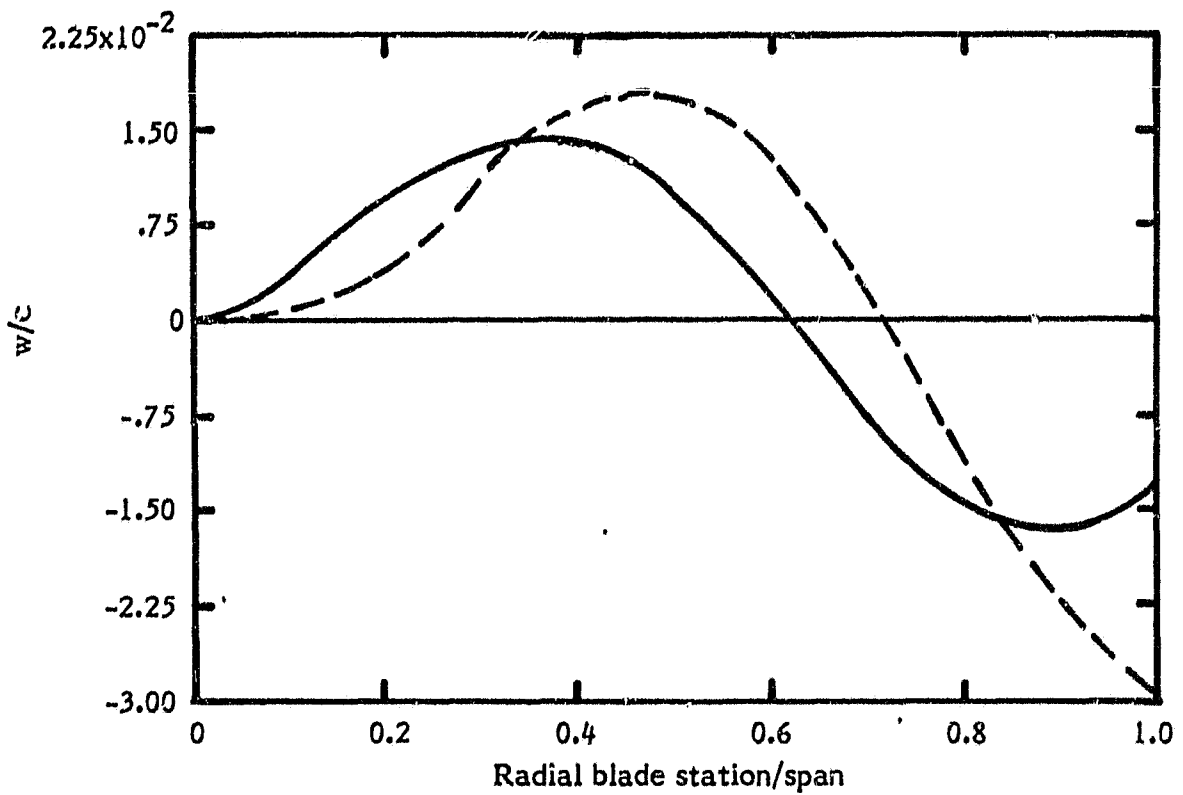
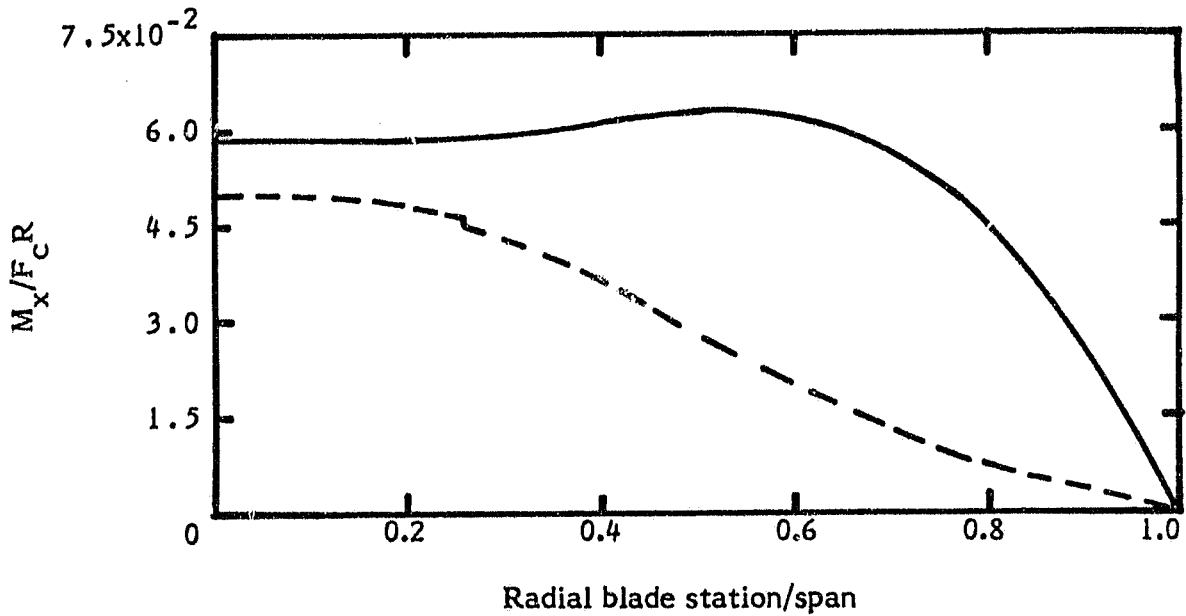

(b) Flapwise deflection.

Figure 12. - Deflections and loads for 4/Rev concentrated excitation, uniform blade, $x_A/R = .18$, $\omega_p = 3.87/Rev$.
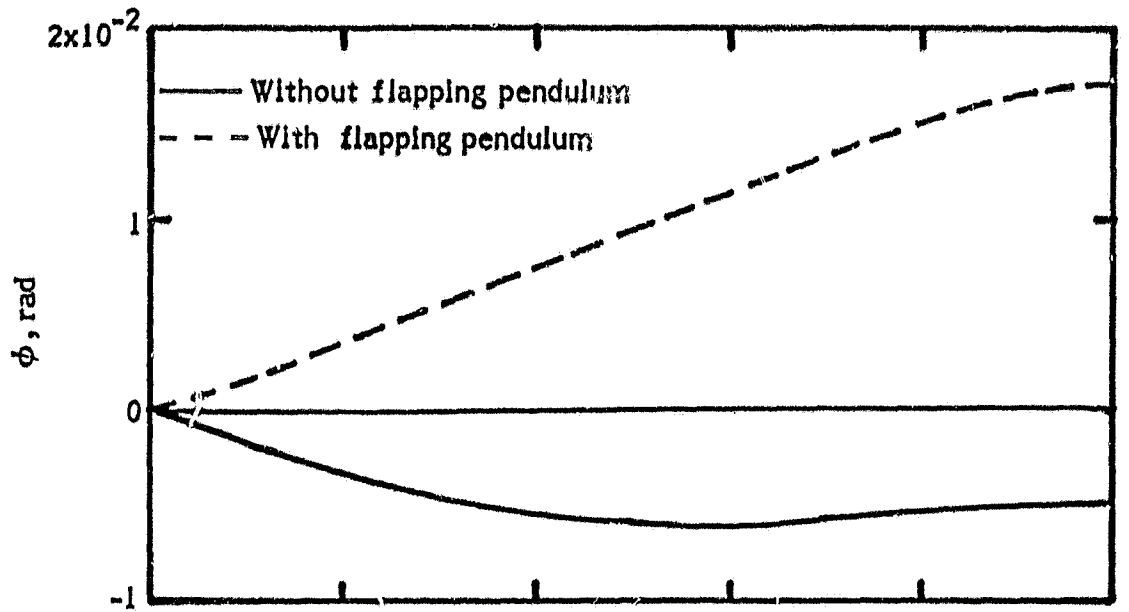
(c) Torsional deflection.
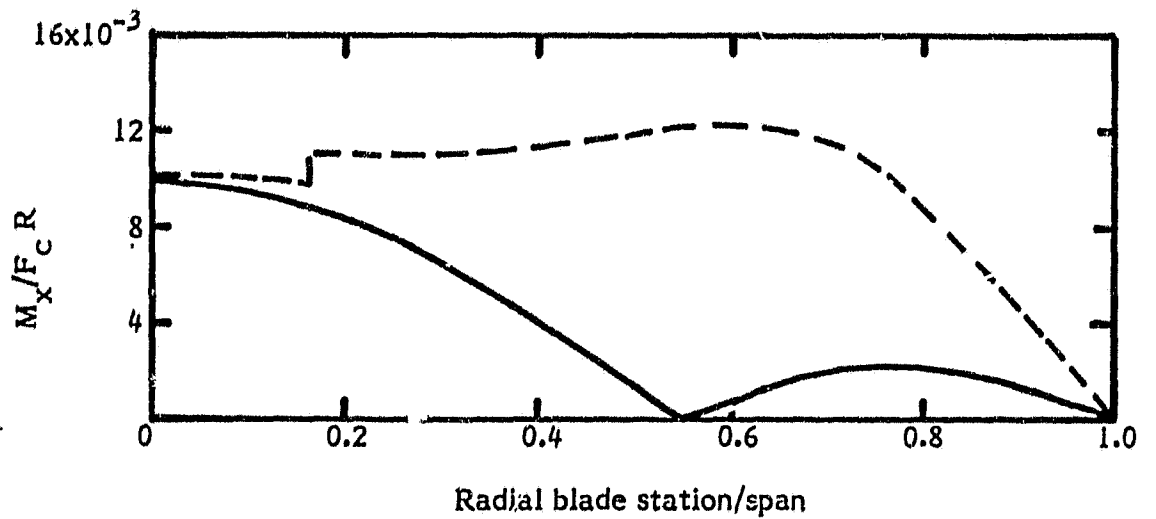
(d) Twisting moment (magnitude).

Figure 12. - Continued.
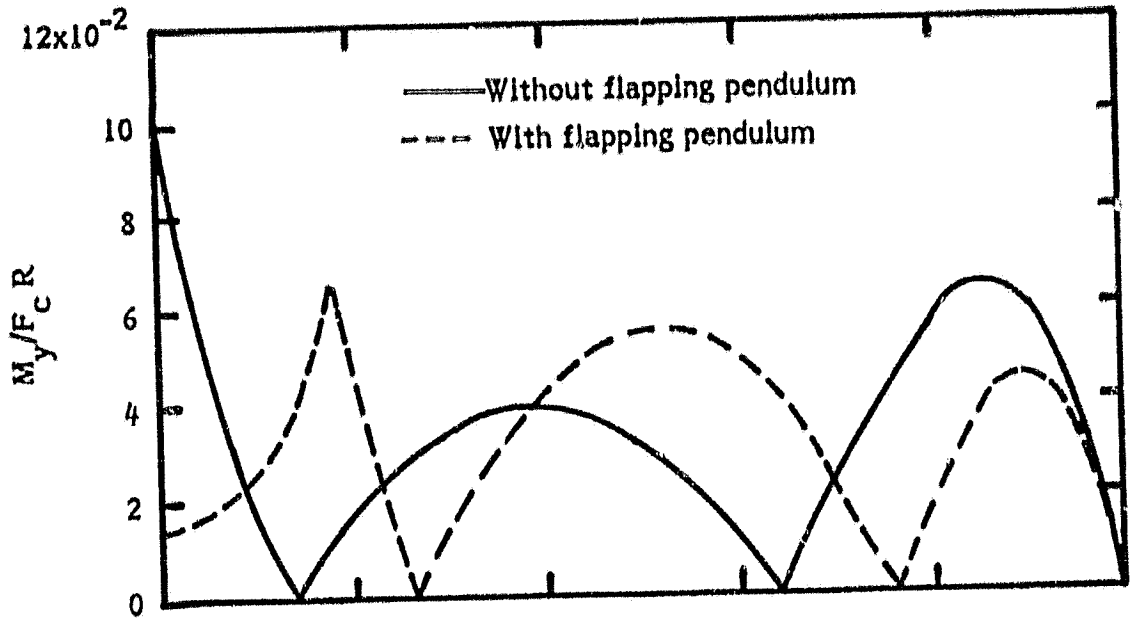
(e) Out-of plane moment (magnitude).
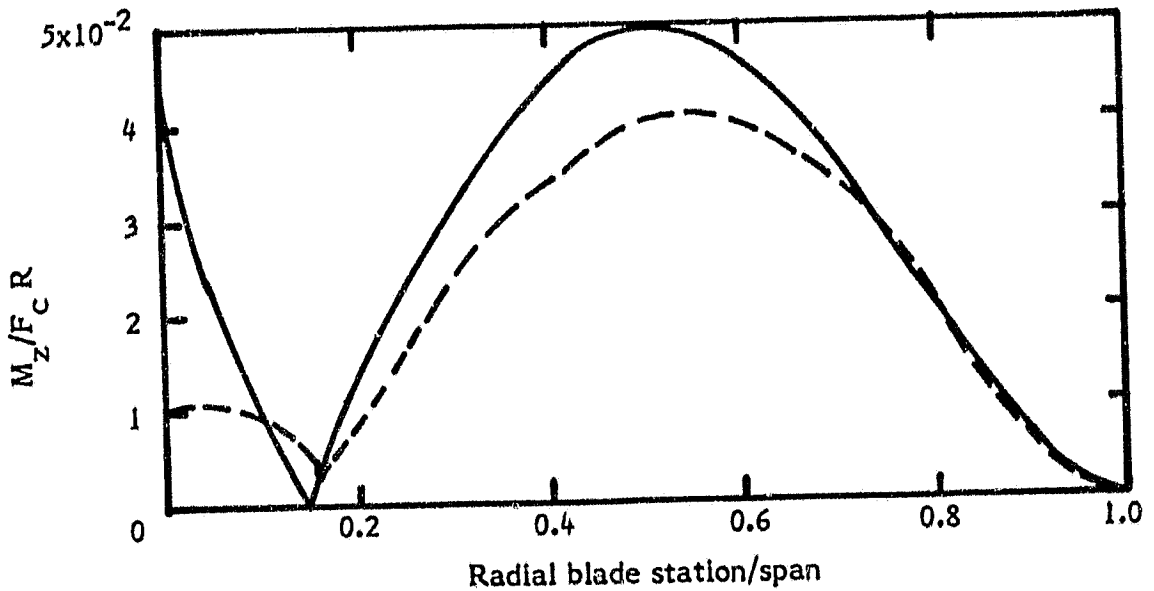
(f) In-plane moment (magnitude).

Figure 12. - Continued.
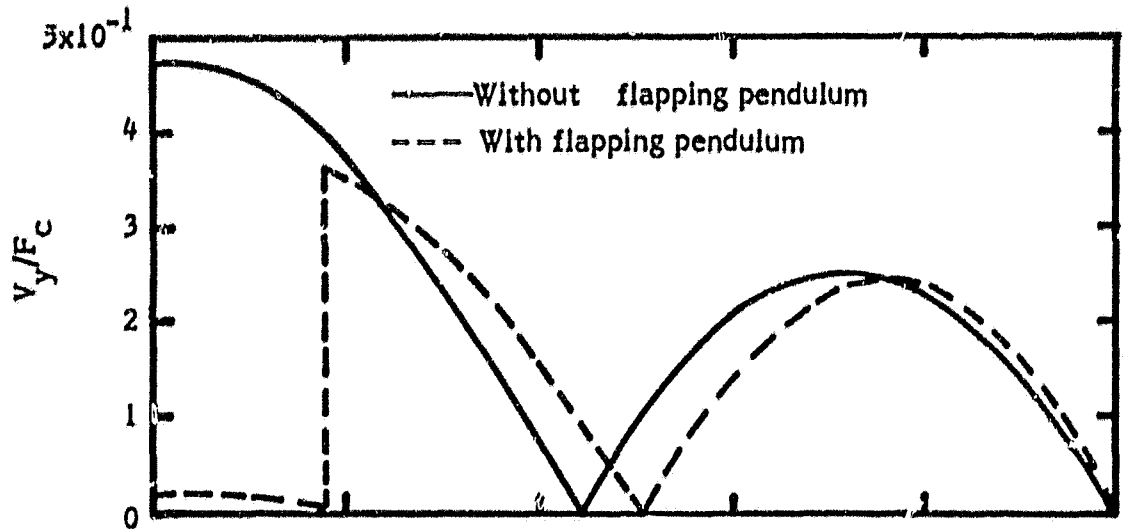
(g) In-plane shear (magnitude).
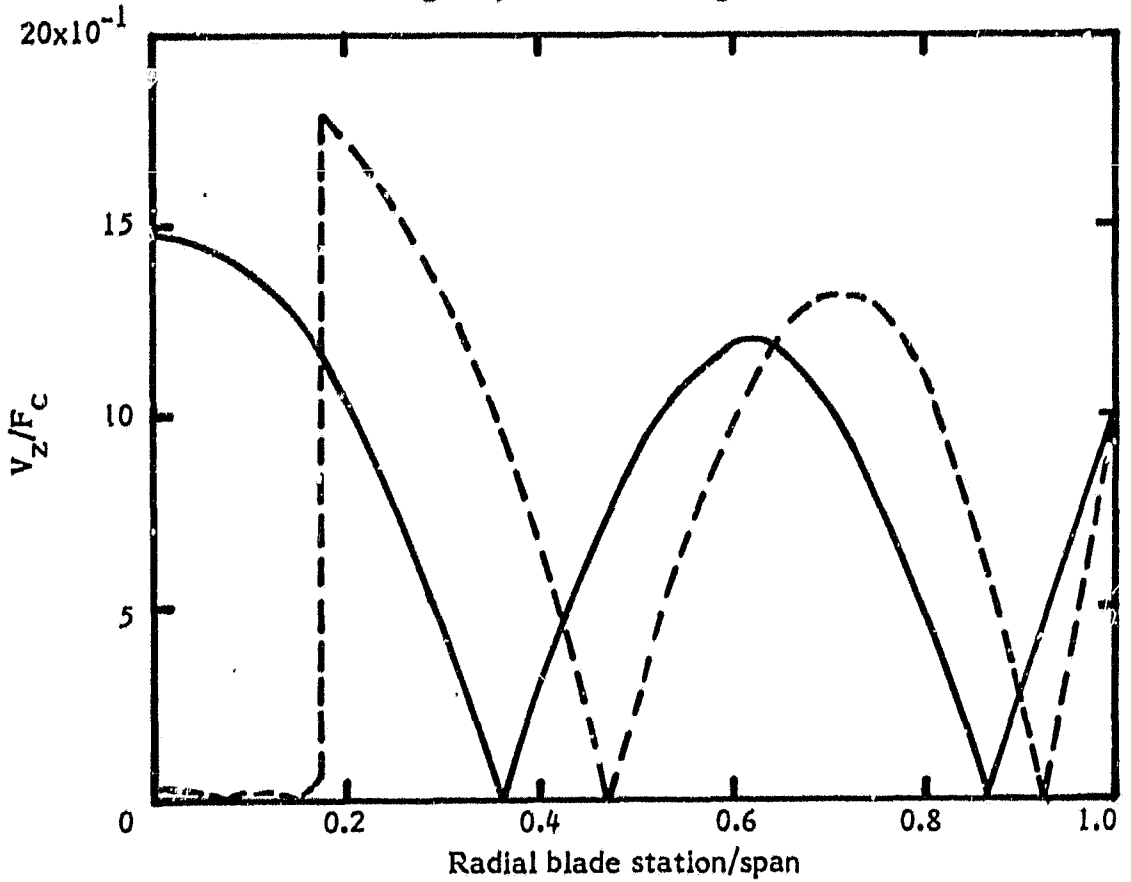
(h) Out-of-plane shear (magnitude).

Figure 12. – Concluded.
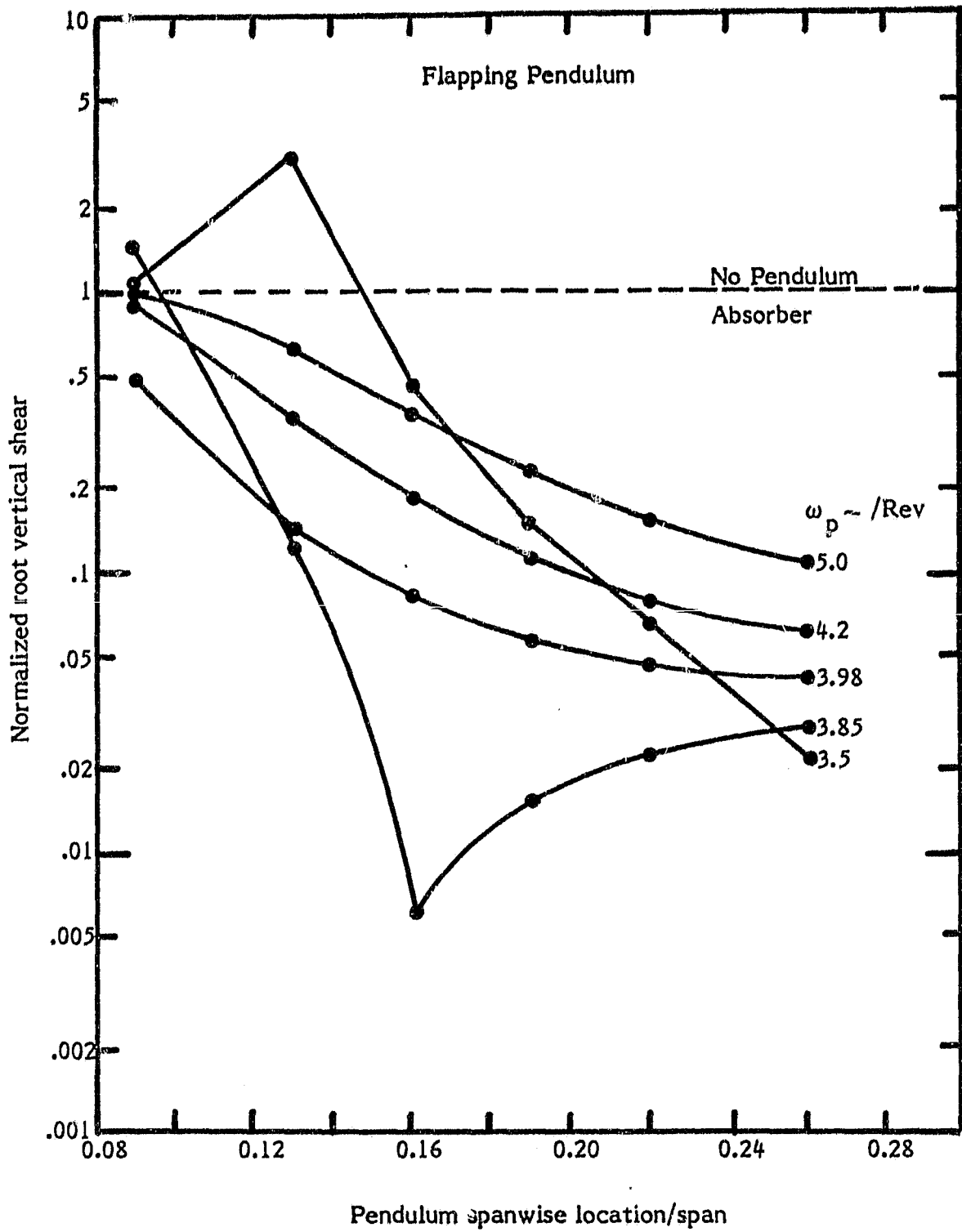
Figure 13. - Root vertical shear for 4/Rev concentrated excitation, nonuniform blade, $W = 133.45$ N, $\eta_A = \zeta_A = 0$.
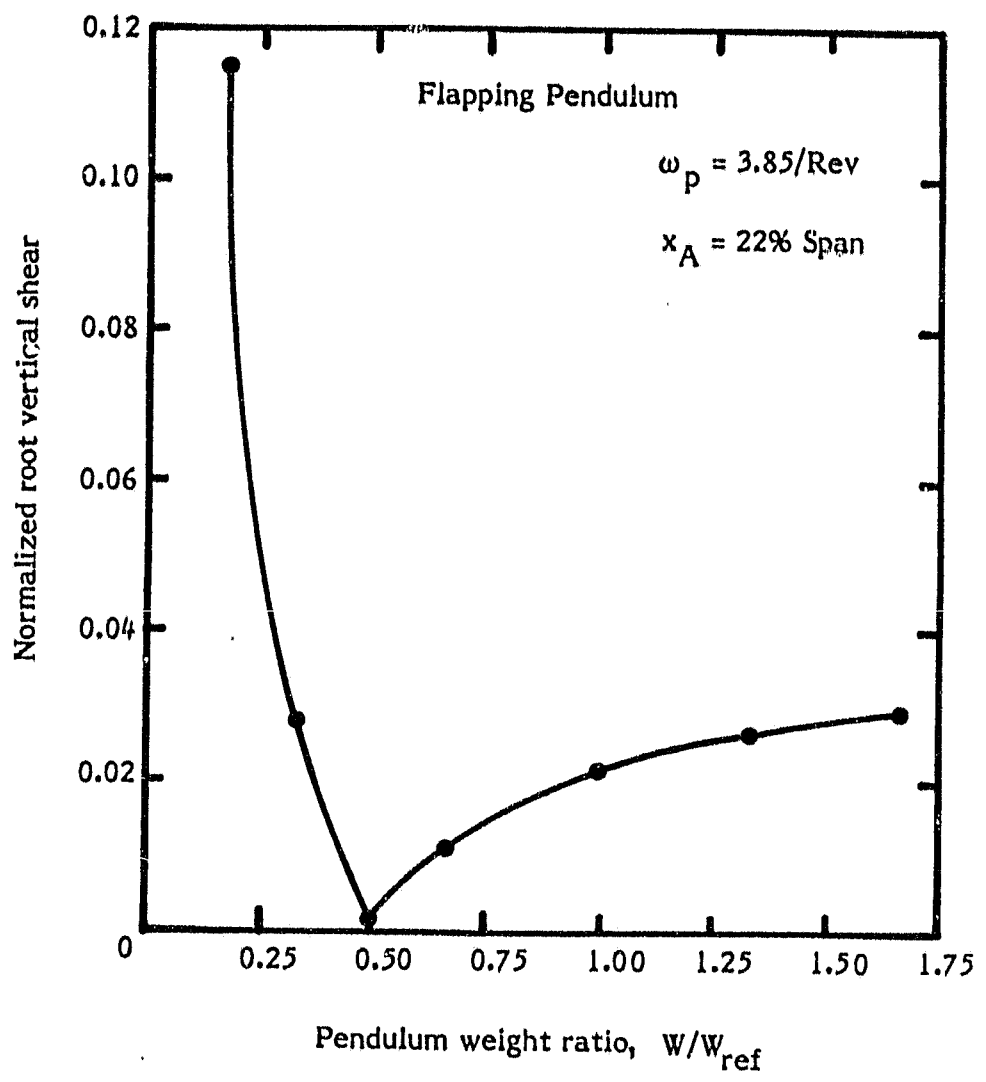
Figure 14. - Root vertical shear for 4/Rev concentrated
excitation, nonuniform blade,
$W_{ref} = 133.45$ N, $\eta_A = \zeta_A = 0$.
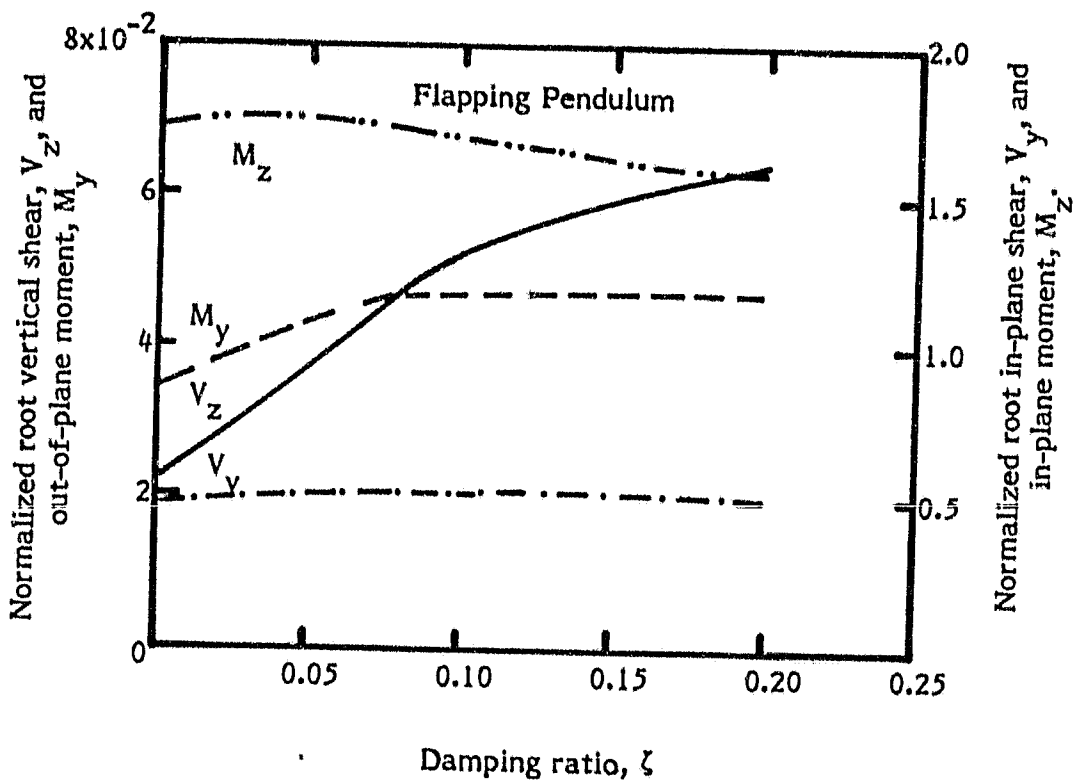
Figure 15. - Pendulum damping effect for 4/Rev concentrated excitation, nonuniform blade.
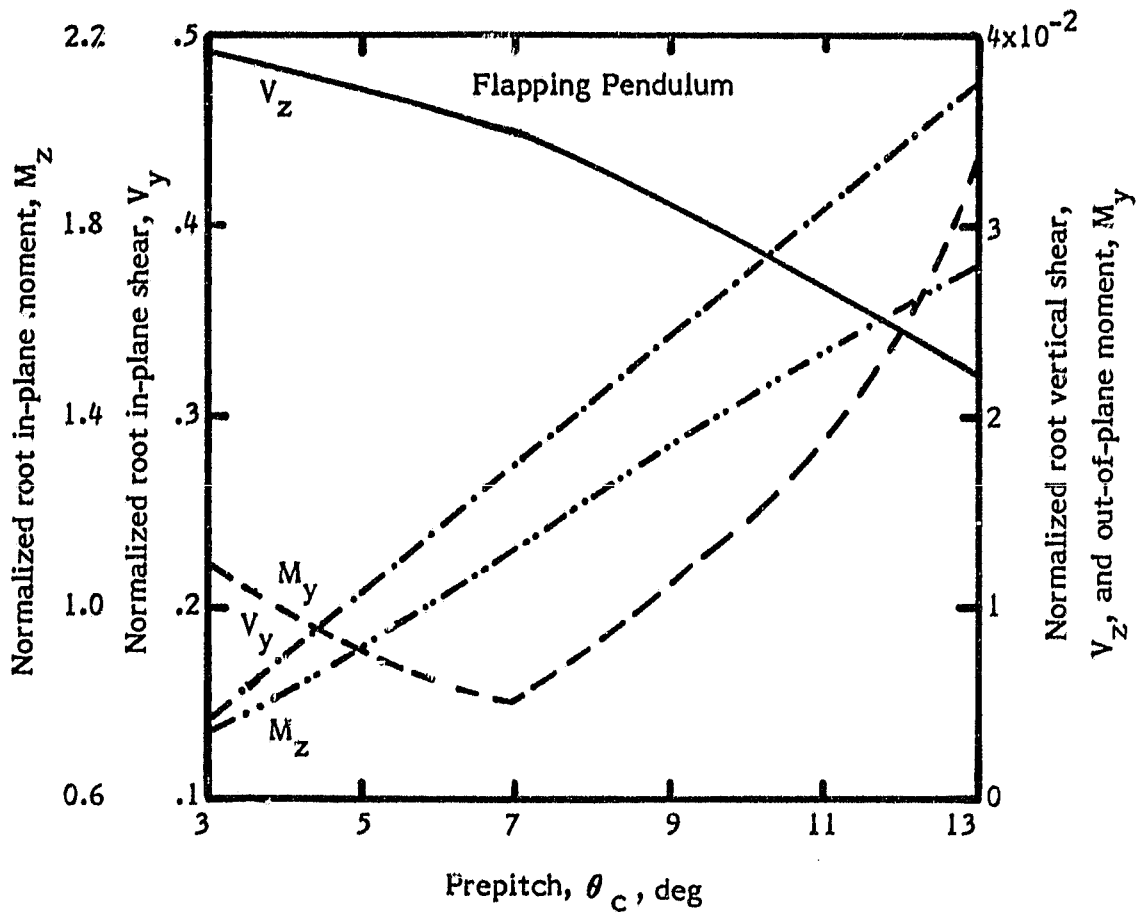
Figure 16 - Root collective pitch effect for 4/Rev concentrated
excitation, nonuniform blade.
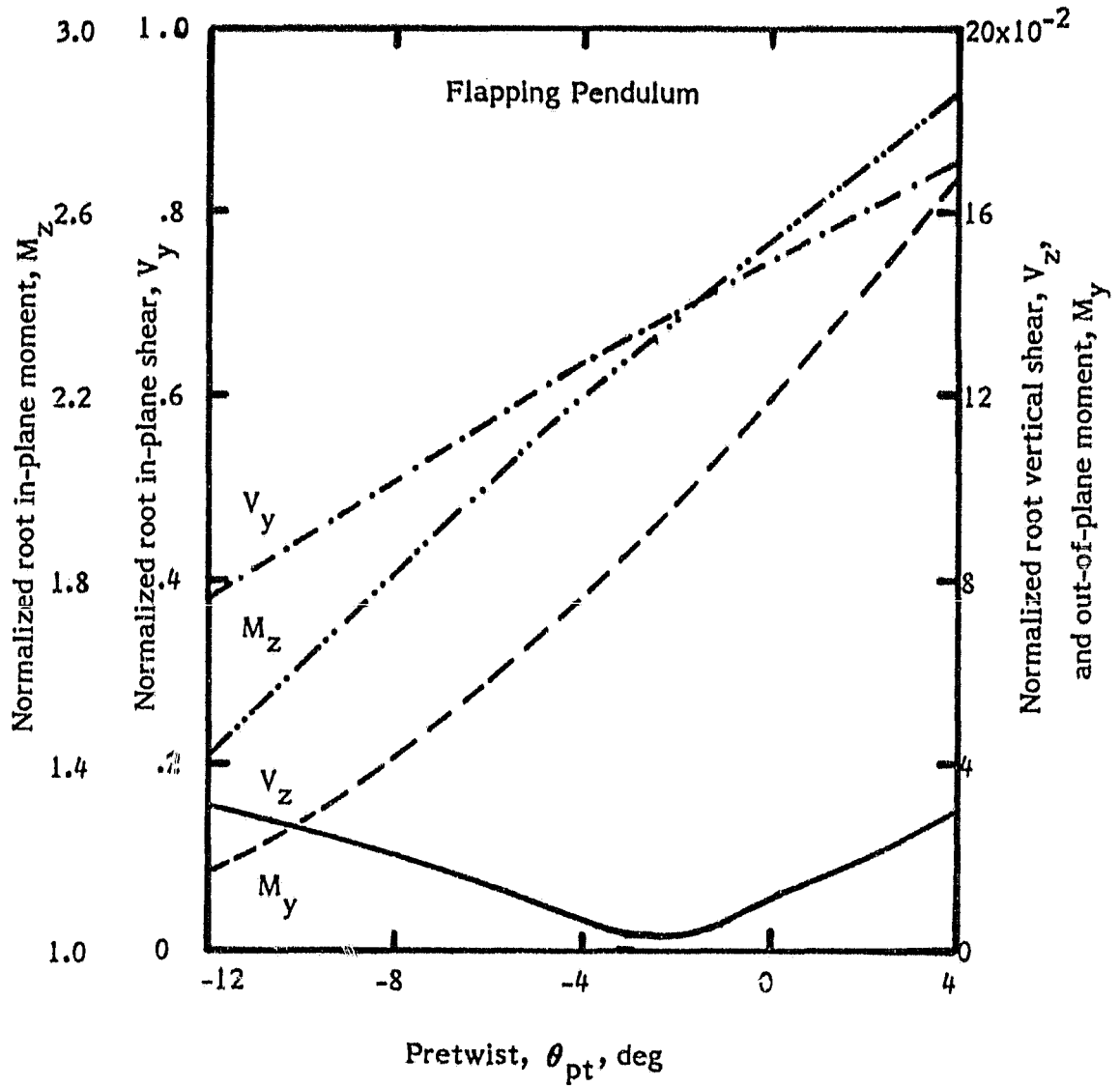
Figure 17. - Pretwist effect for 4/Rev concentrated
excitation, nonuniform blade.
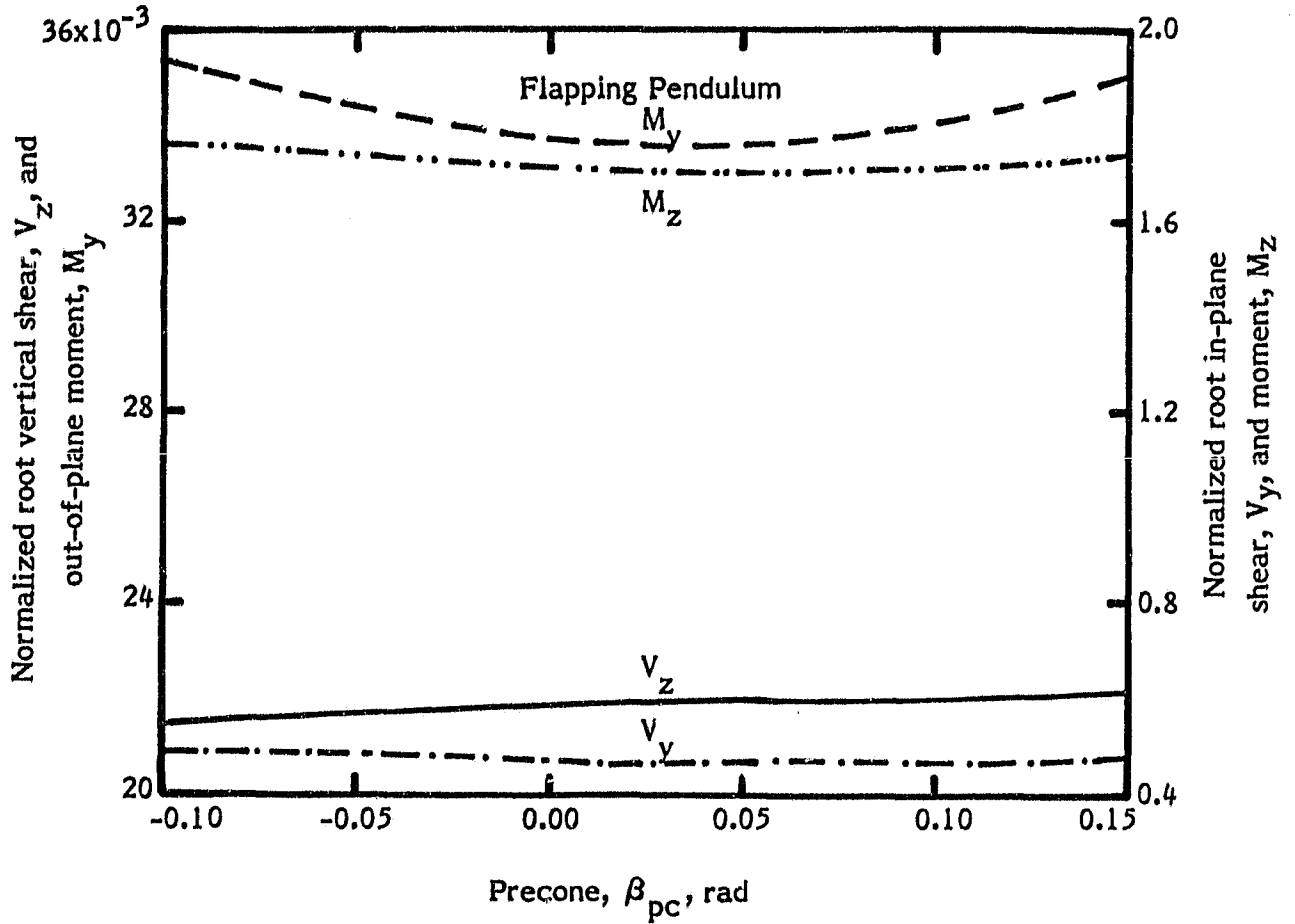
Figure 18. – Precone effect for 4/Rev concentrated
excitation, nonuniform blade.
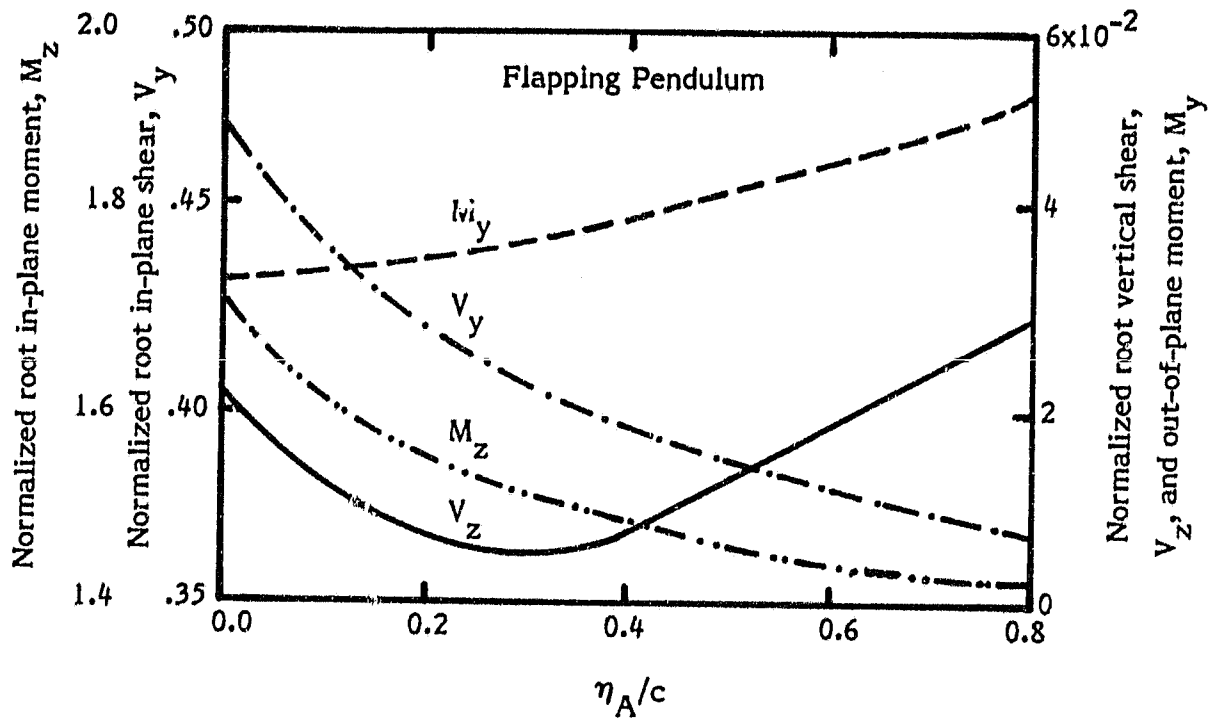
Figure 19. - Pendulum chordwise hinge offset, η_A, effect for 4/Rev
concentrated excitation, nonuniform blade.
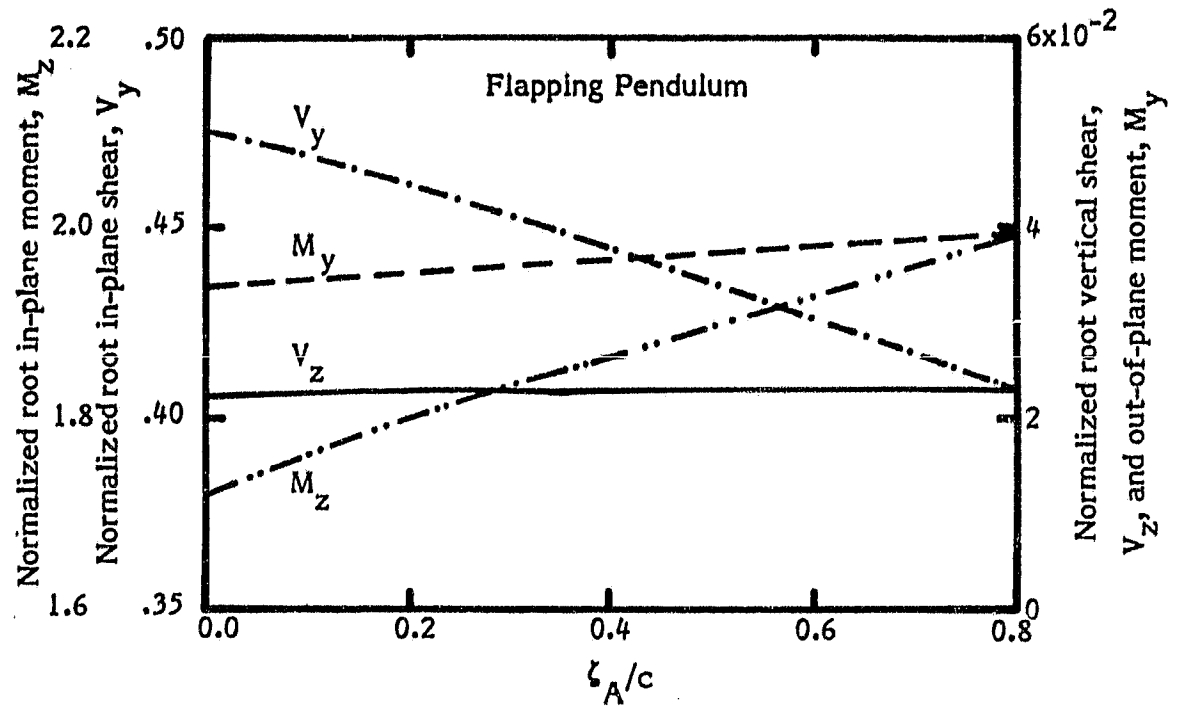
Figure 20. - Pendulum vertical hinge offset, ζ_A, effect for 4/Rev concentrated excitation, nonuniform blade.
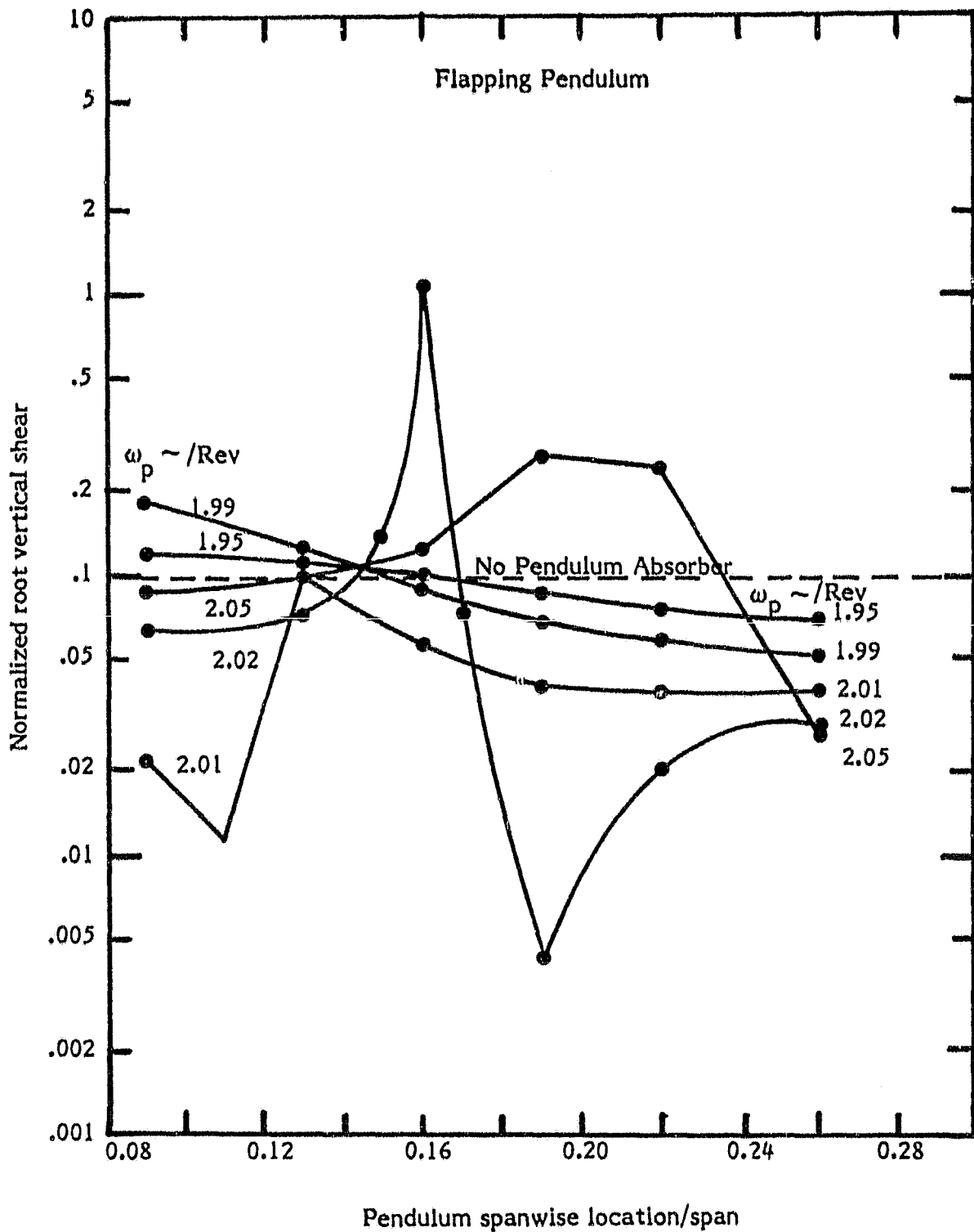
Figure 21. - Root vertical shear for 2/Rev distributed airload excitation,
nonuniform blade, $W = 133.45$ N, $\eta_A = \zeta_A = 0$.
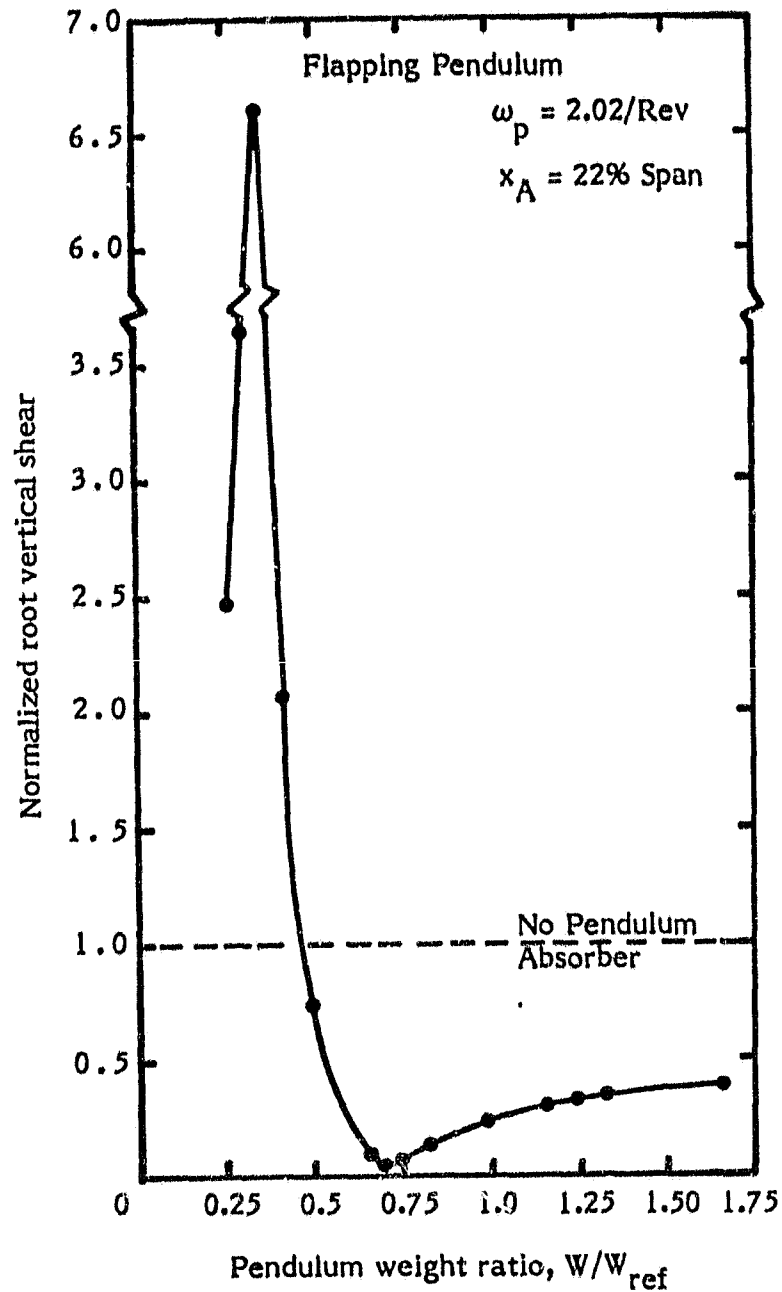
Figure 22. - Root vertical shear for 2/Rev distributed airload excitation, nonuniform blade, $W_{ref} = 133.45$ N, $\eta_A = \zeta_A = 0$.
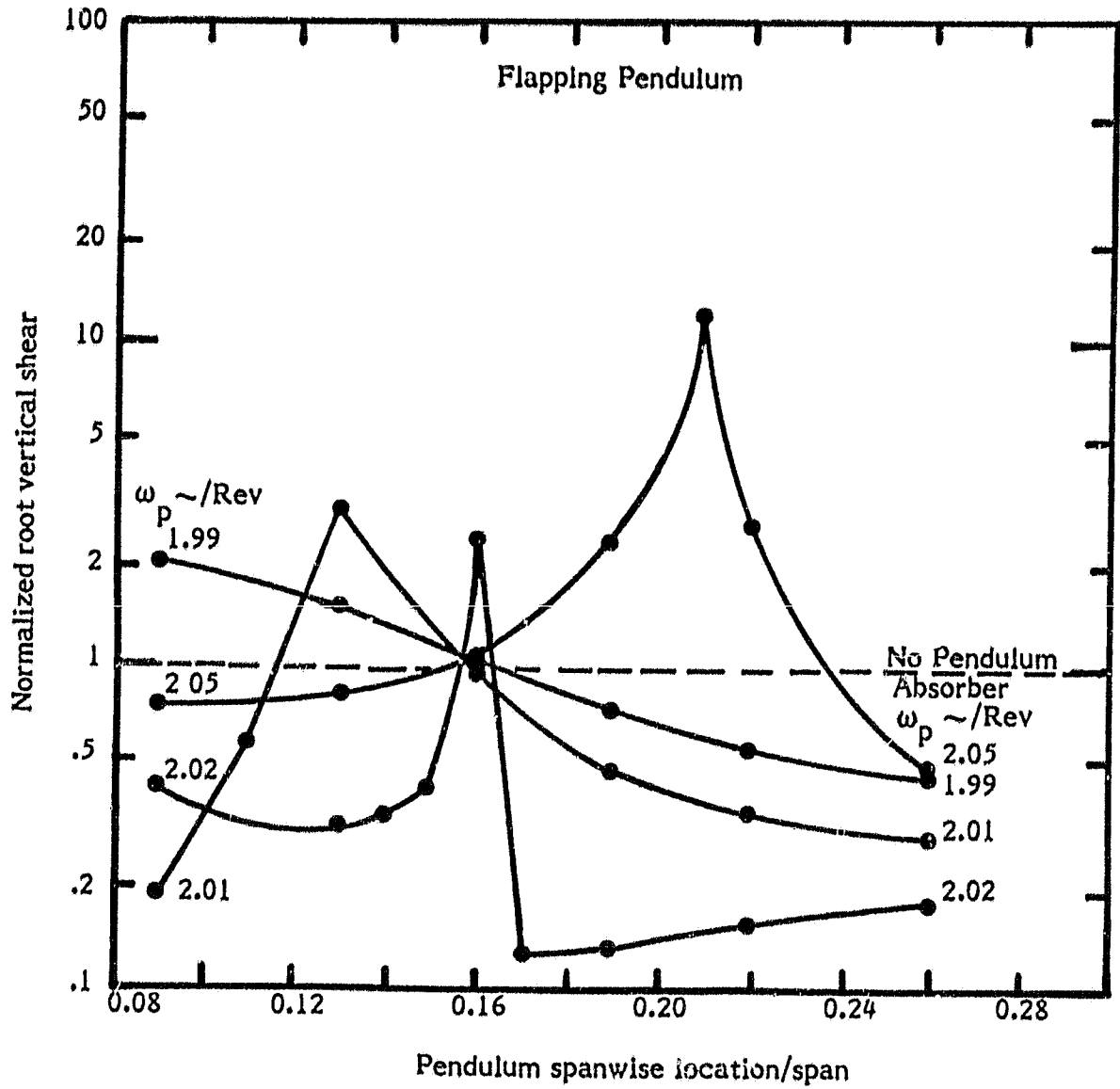
Figure 23. - Root vertical shear for 2/Rev concentrated excitation, nonuniform blade, $W = 133.45$ N, $\eta_A = \zeta_A = 0$.
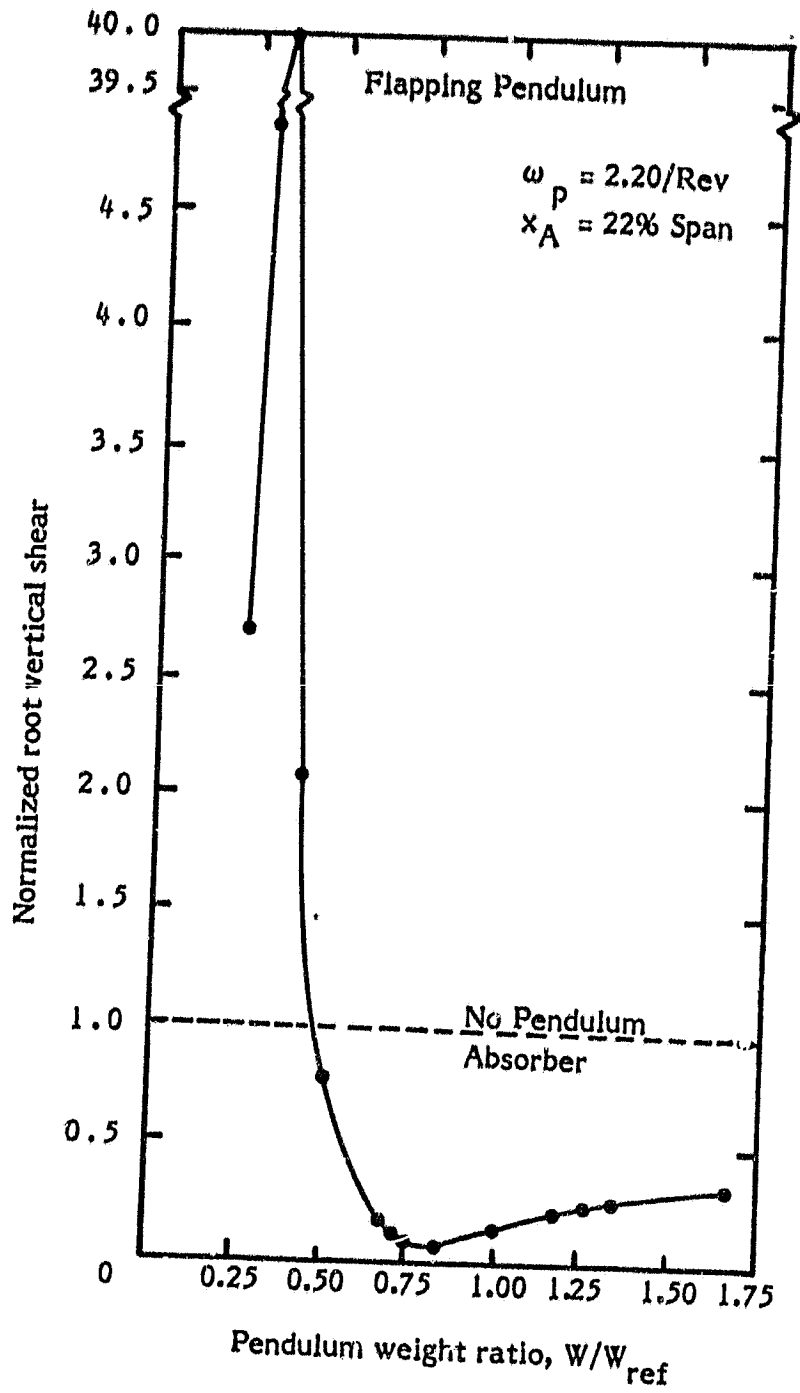
Figure 24. - Root vertical shear for 2/Rev concentrated
excitation, nonuniform blade,
$W_{ref} = 133.45$ N, $\eta_A = \zeta_A = 0$.
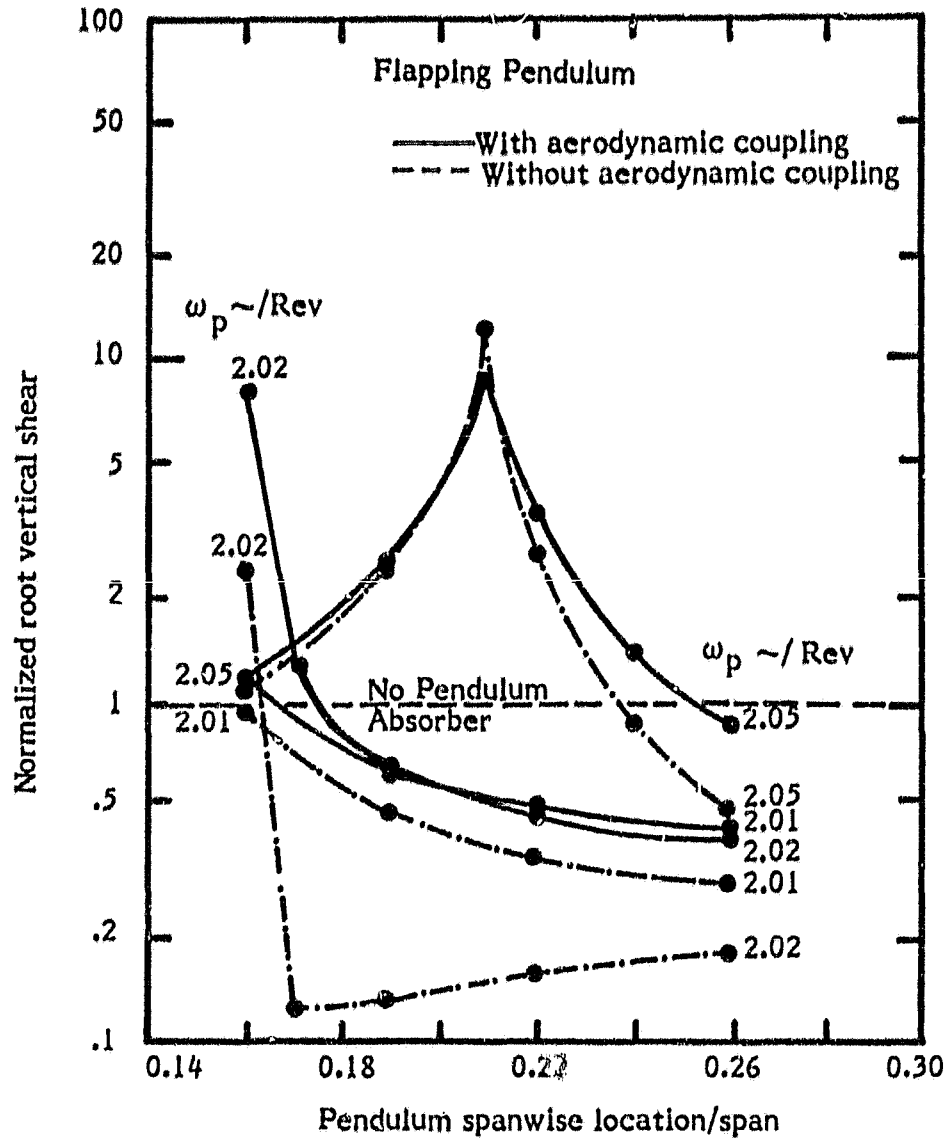
Figure 25. - Root vertical shear for 2/Rev concentrated excitation, with and without aerodynamic coupling, nonuniform blade, $W = 133.45$ N, $\eta_A = \zeta_A = 0$.
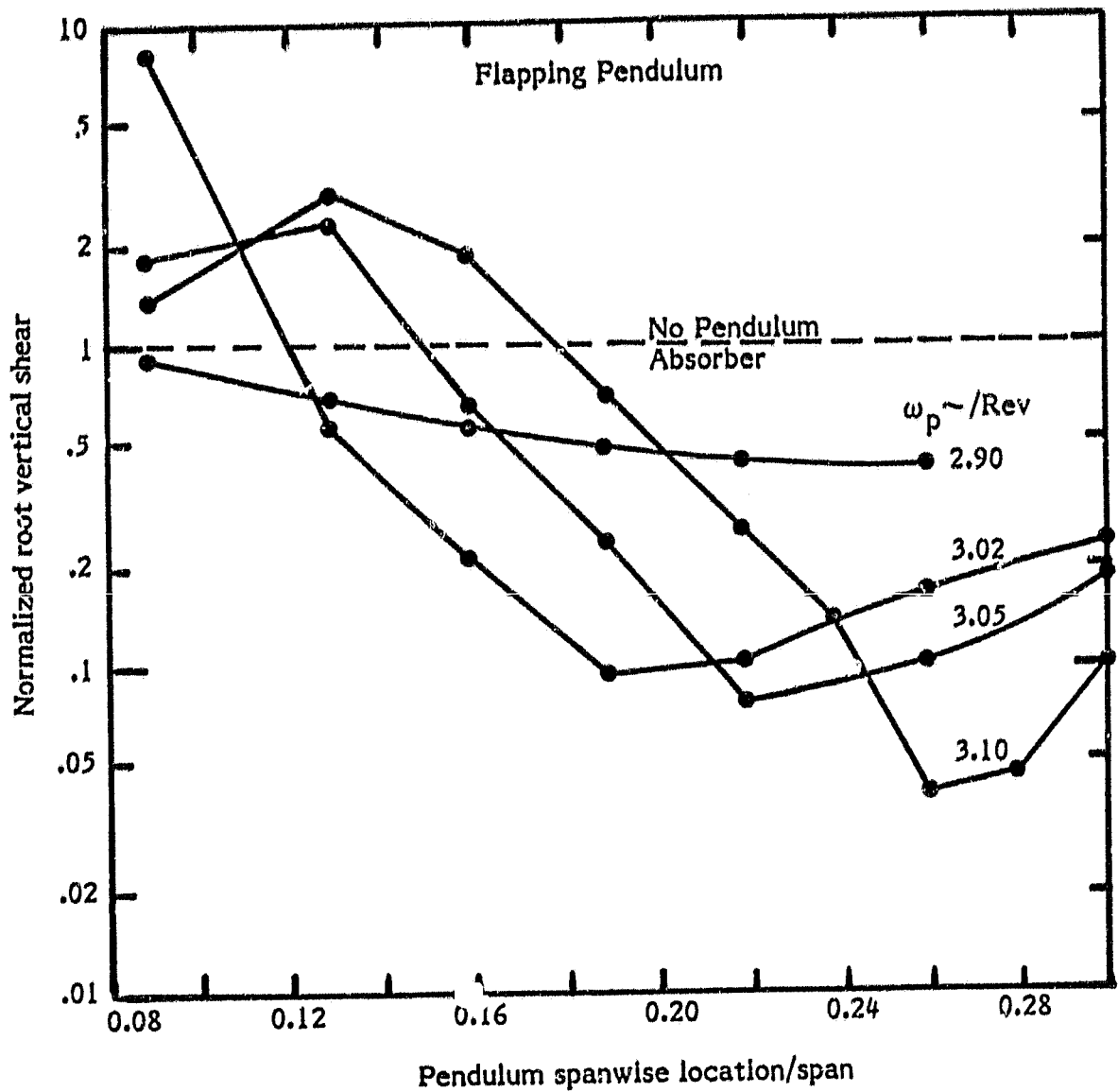
Figure 26. - Root vertical shear for 3/Rev distributed airload excitation, nonuniform blade, $W = 133.45$ N, $\eta_A = \zeta_A = 0$.
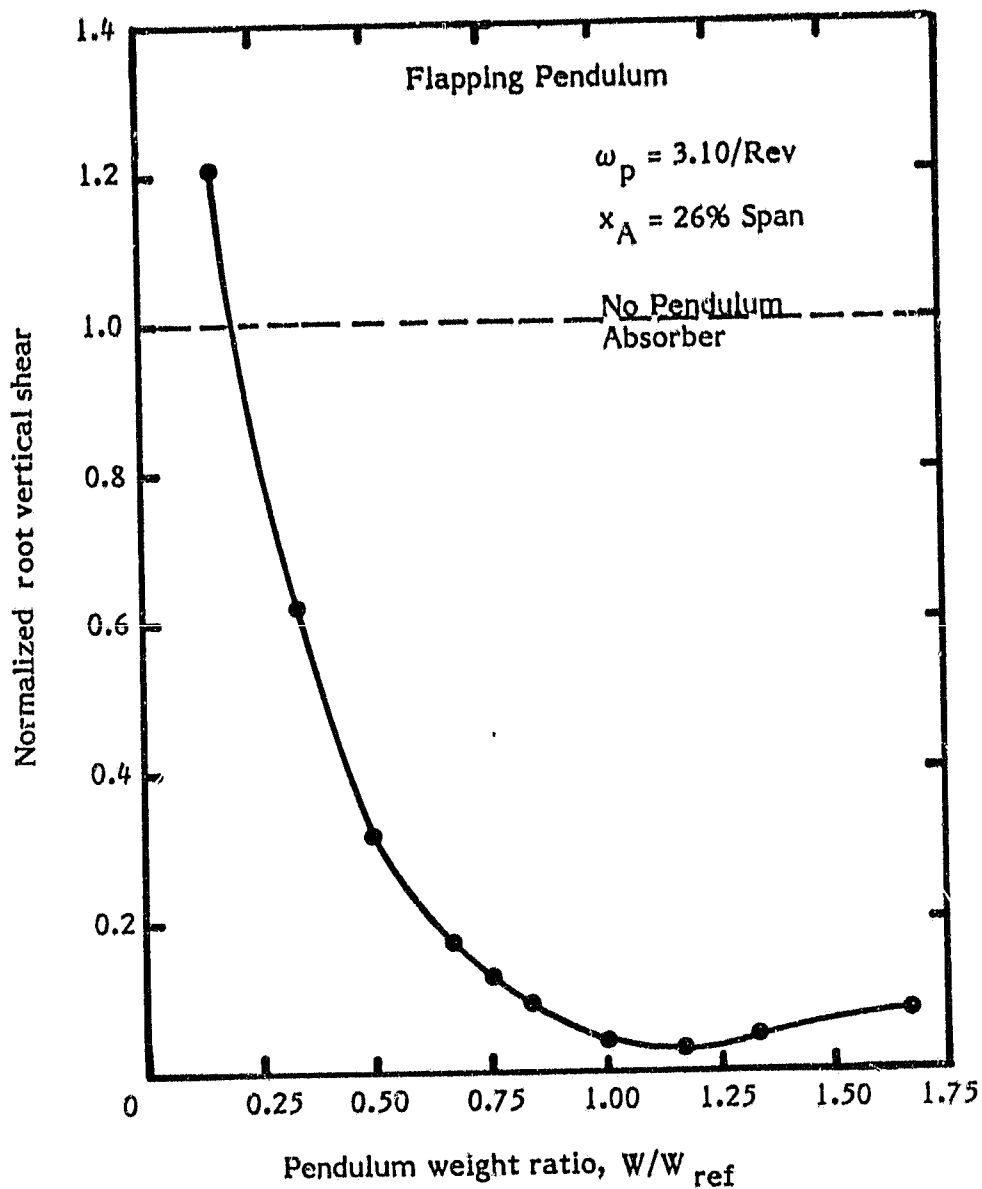
Figure 27. - Root vertical shear for 3/Rev distributed airload
excitation, nonuniform blade,
$W_{ref} = 133.45$ N, $\eta_A = \zeta_A = 0$.
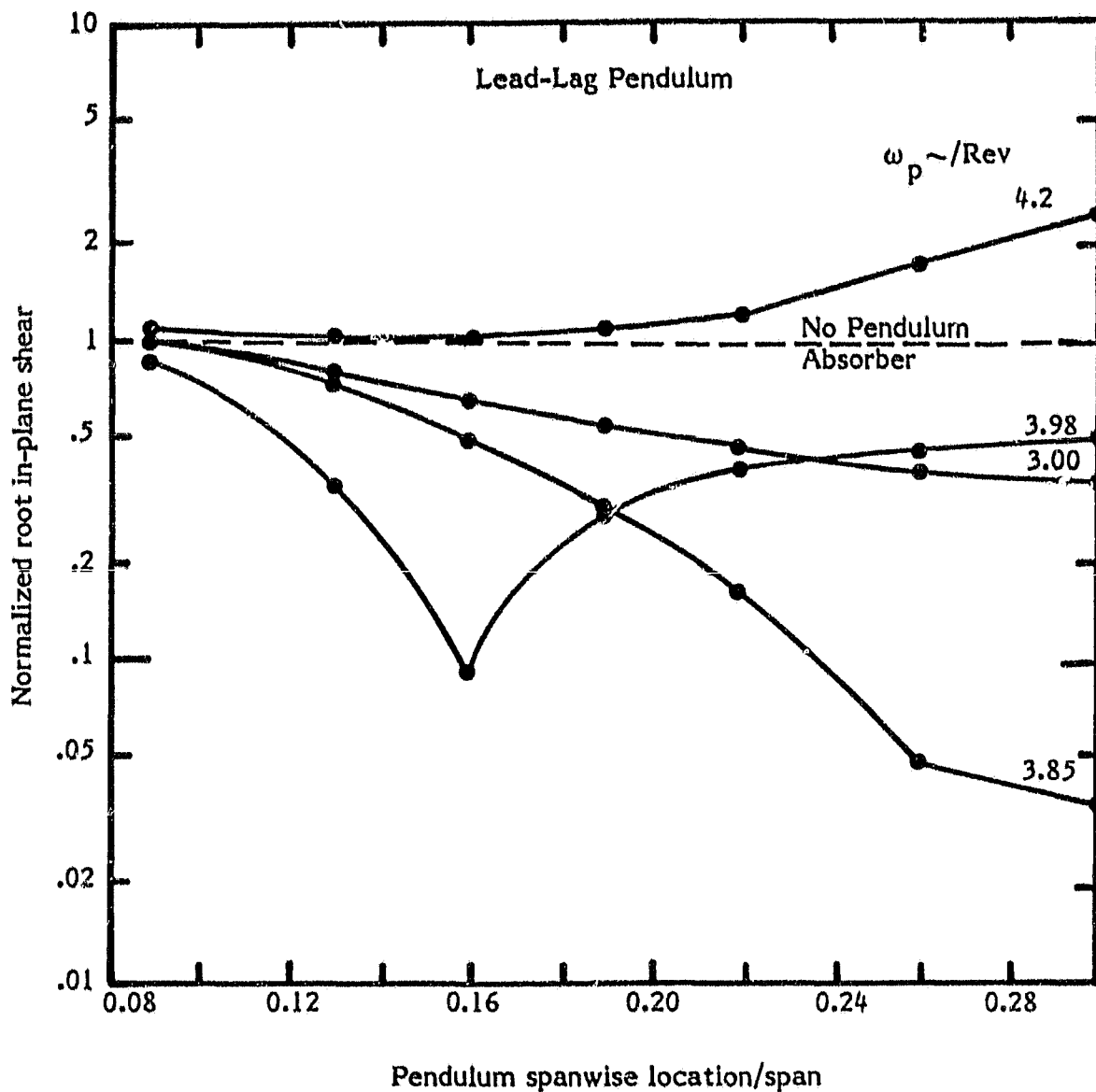
Figure 28. - Root in-plane shear for 4/Rev concentrated excitation, nonuniform blade, $W = 133.45$ N, $\eta_A = \zeta_A = 0$.

123
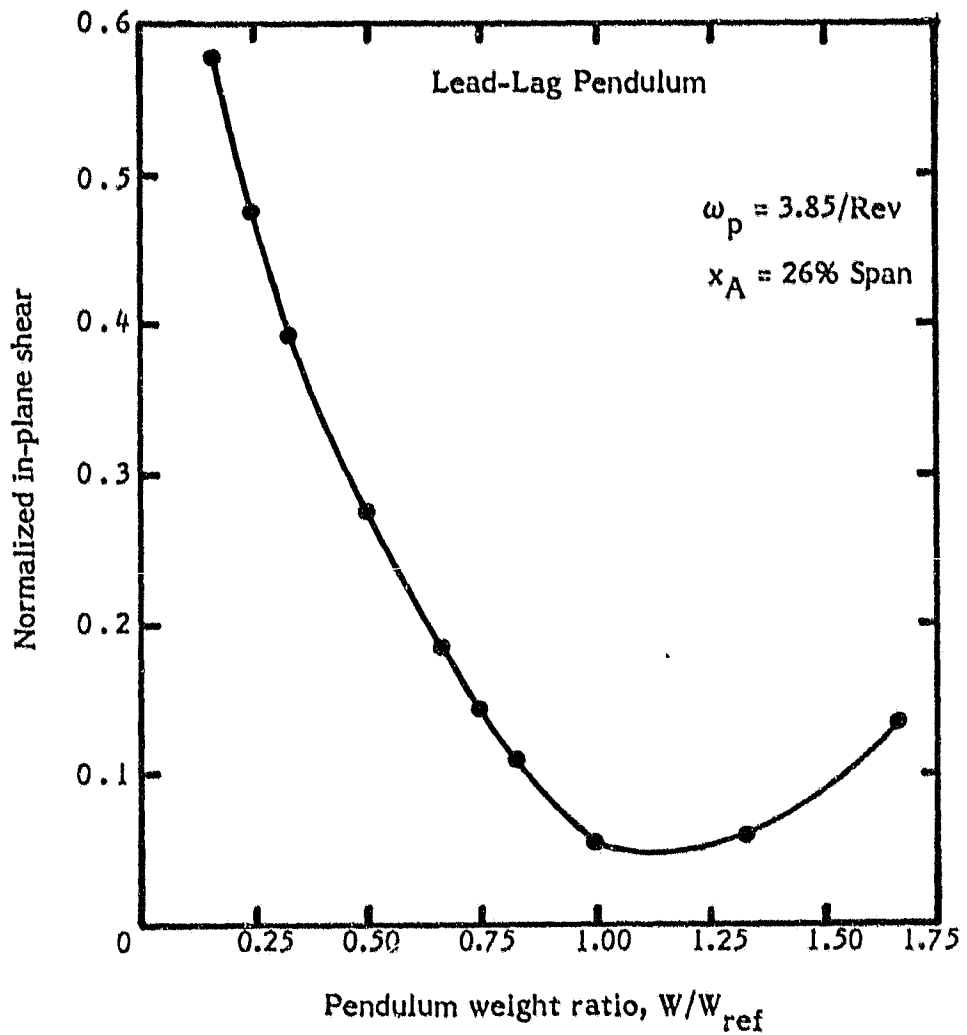
Figure 29. - Root in-plane shear for 4/Rev concentrated excitation, nonuniform blade, $W_{ref} = 133.45$ N, $\eta_A = \zeta_A = 0$.
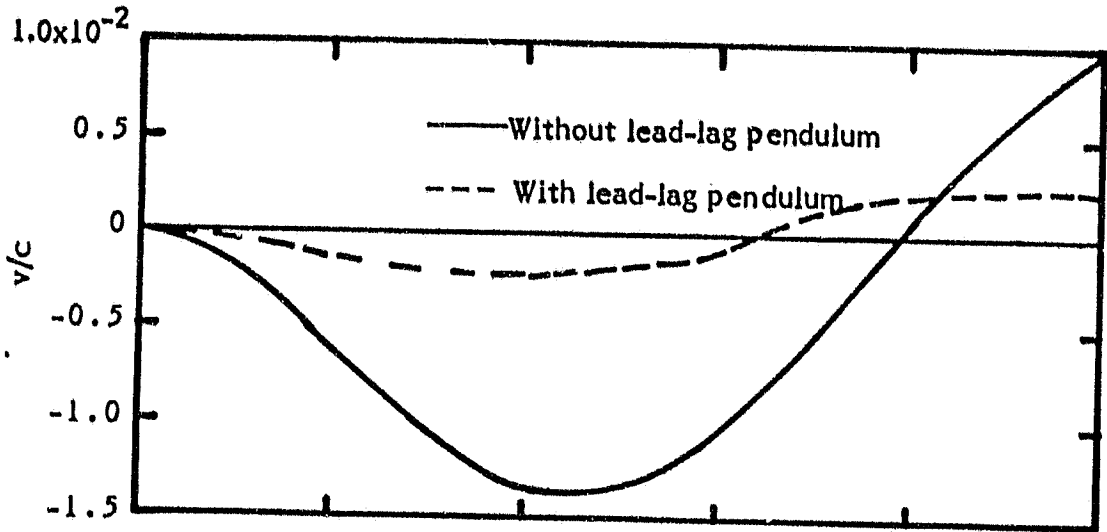
(a) Lead-lag deflection.
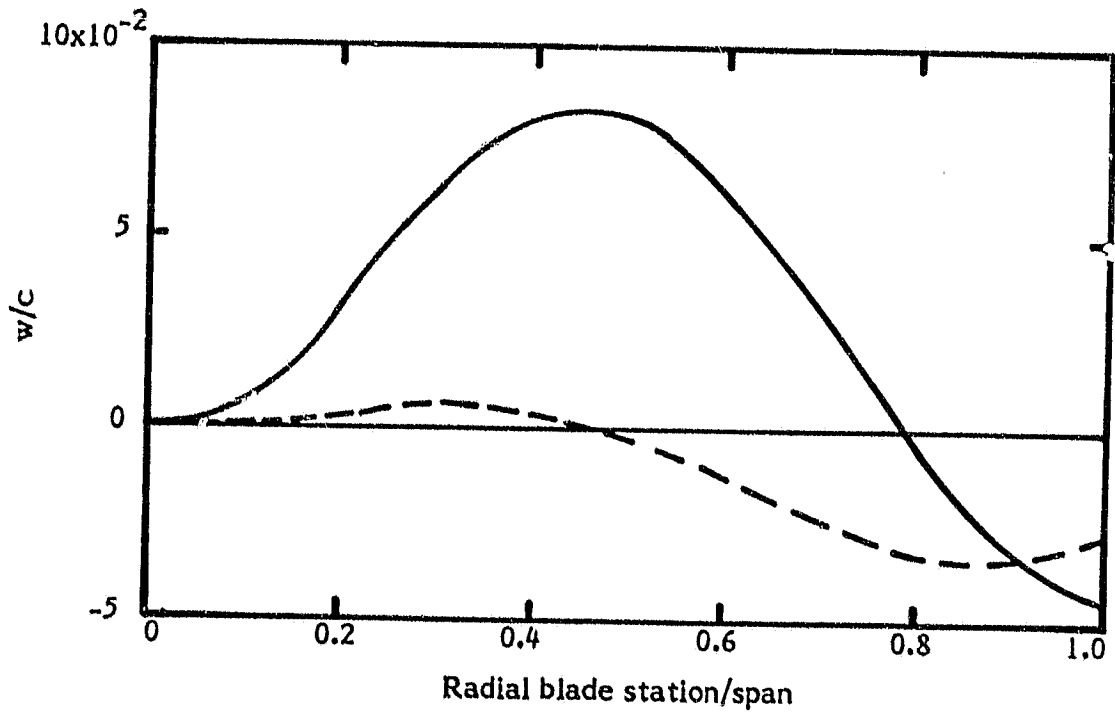
(b) Flapwise deflection.

Figure 30. – Deflections and loads for 4/Rev concentrated excitation, nonuniform blade, $x_A/R = .26$, $\omega_p = 3.85$/Rev.
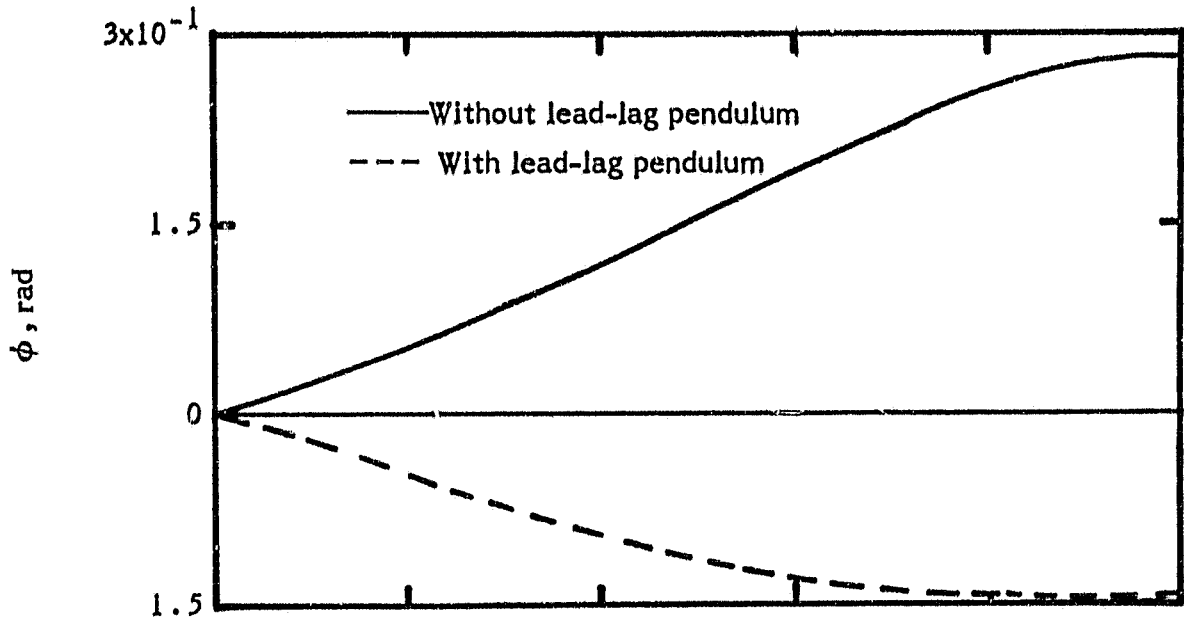
125

(c) Torsional deflection.

Radial blade station/span

(d) Twisting moment (magnitude).

Figure 30. - Continued.

(e) Out-of-plane moment (magnitude).

Radial blade station/span
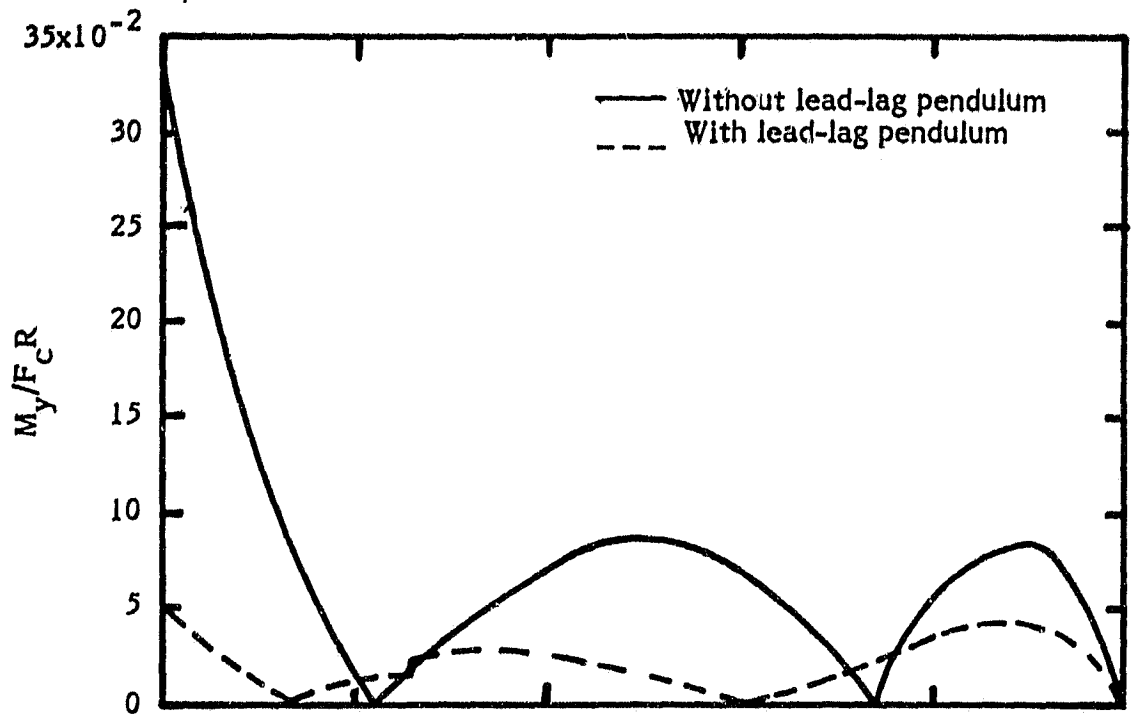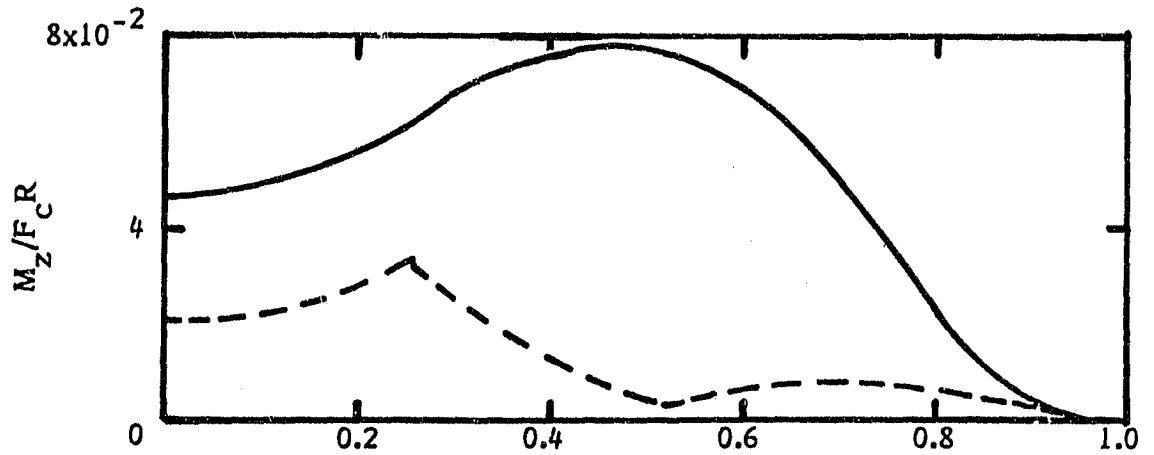
(f) In-plane moment (magnitude).

Figure 30. - Continued.
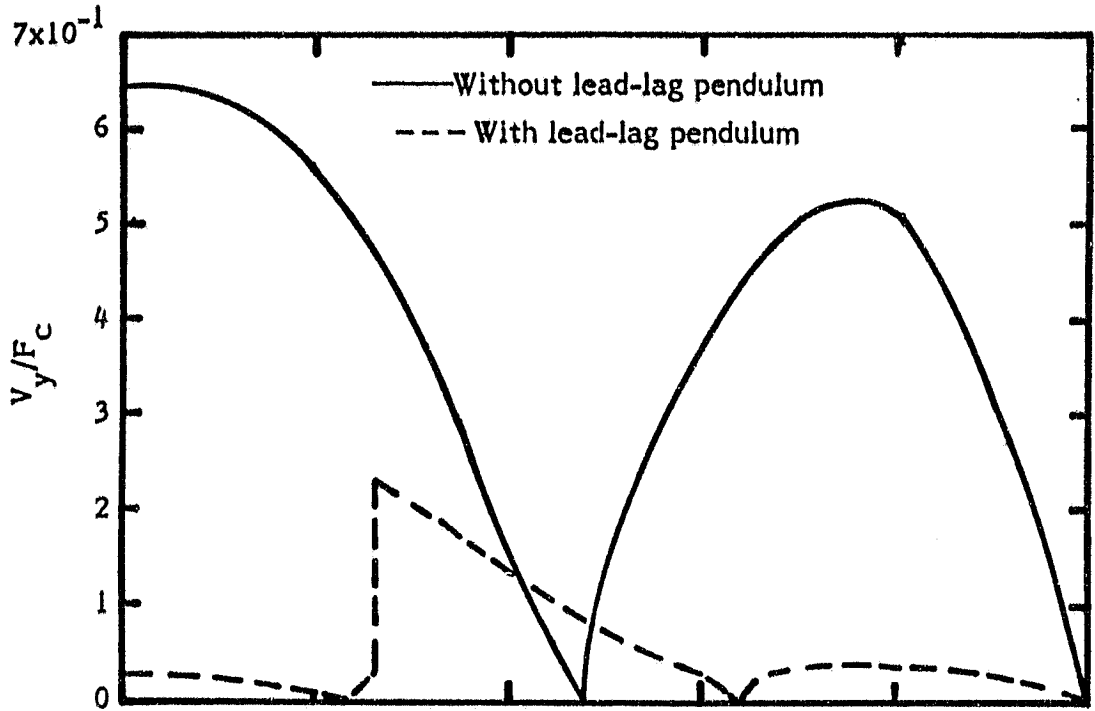
(g) In-plane shear (magnitude).
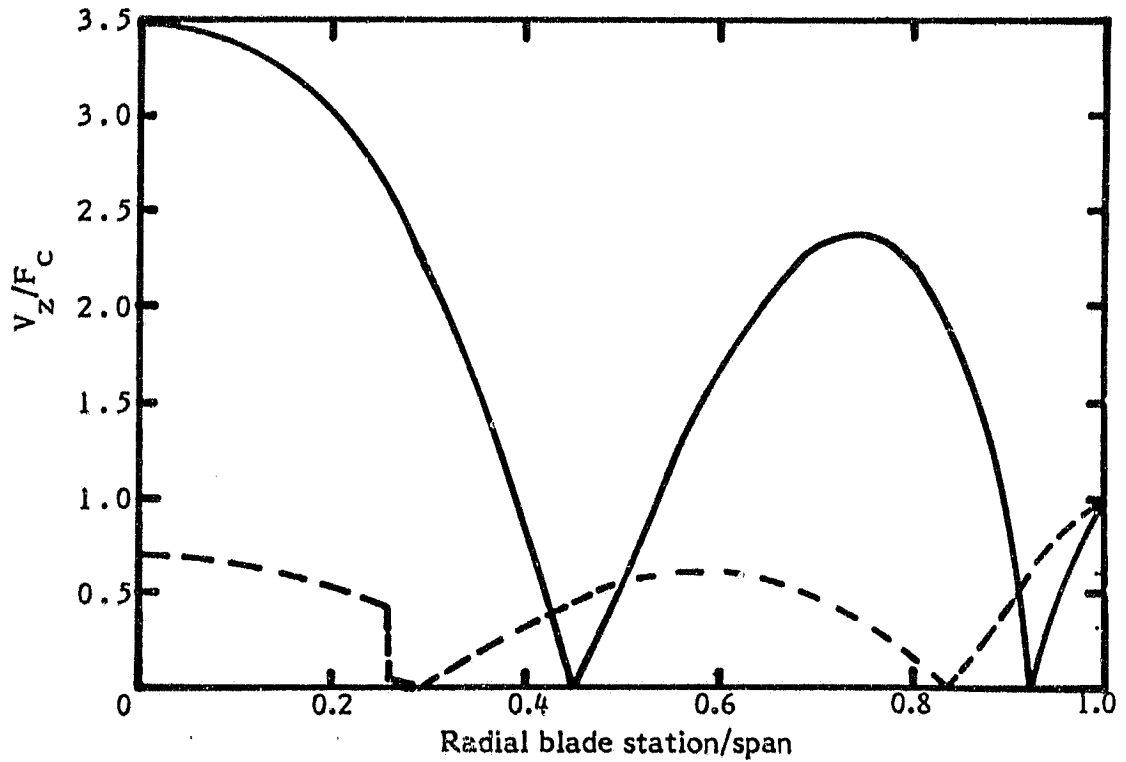
(h) Out-of-plane shear (magnitude).

Figure 30. – Concluded.
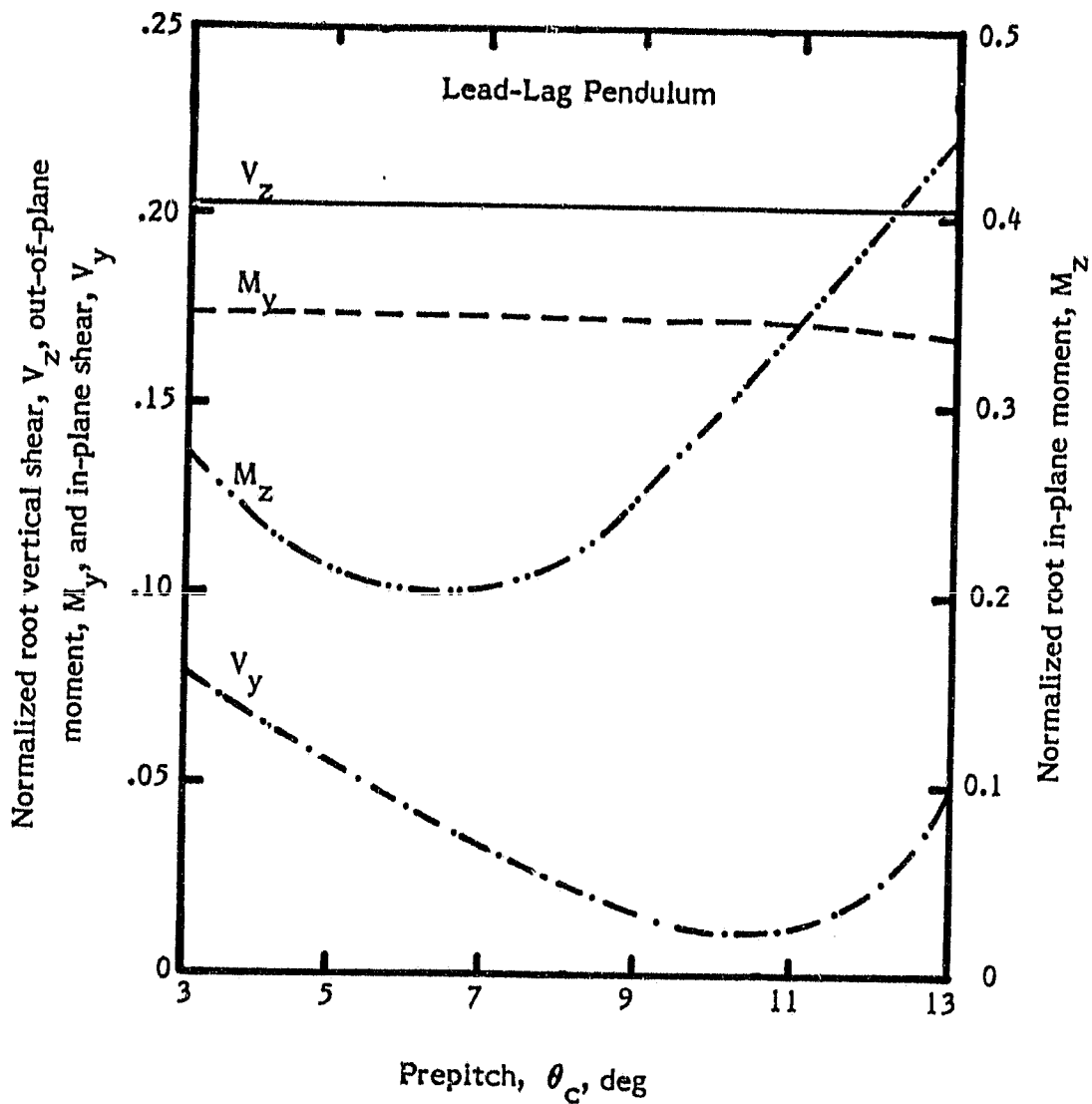
Figure 31. - Root collective pitch effect for 4/Rev concentrated excitation, nonuniform blade.
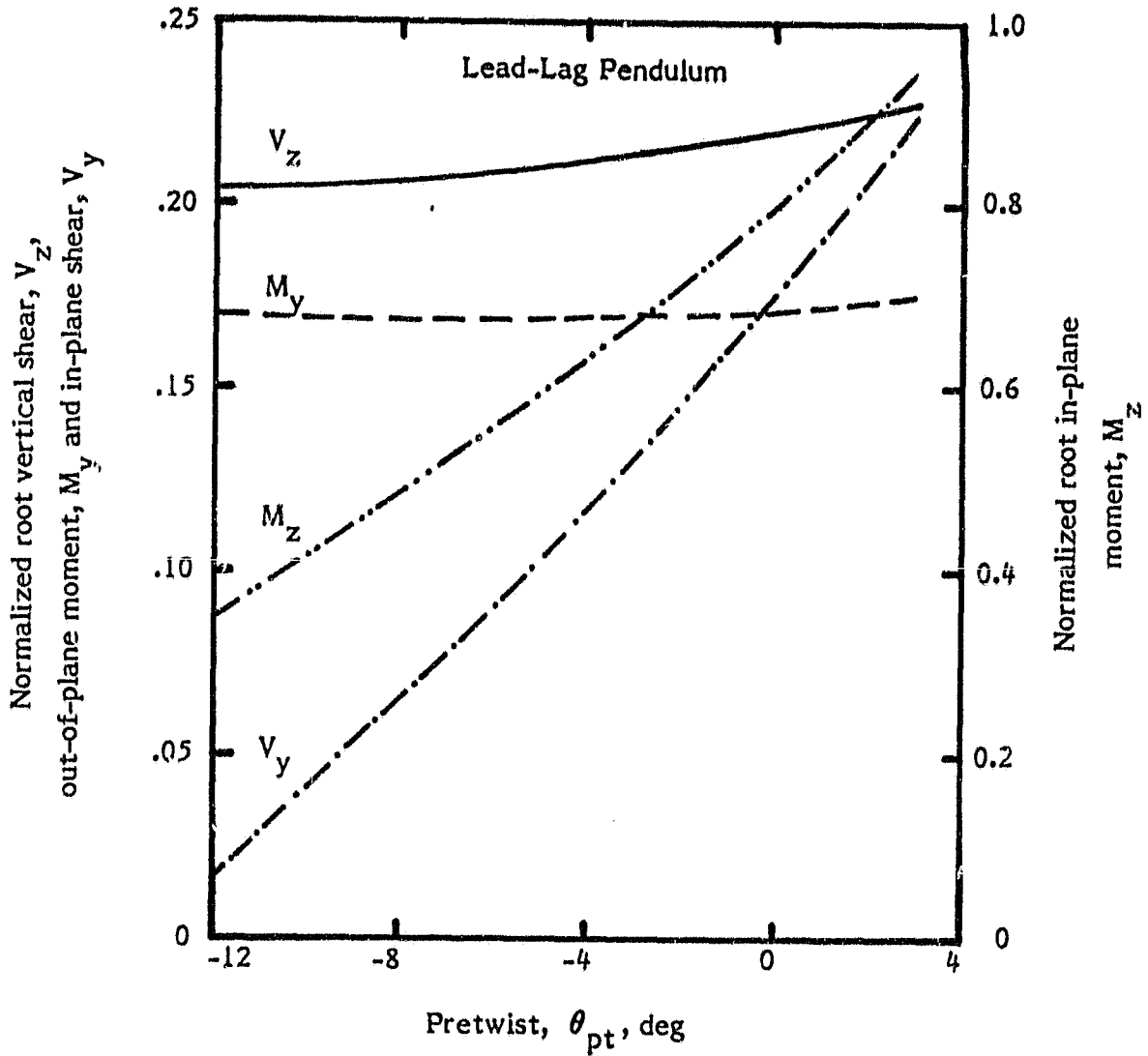
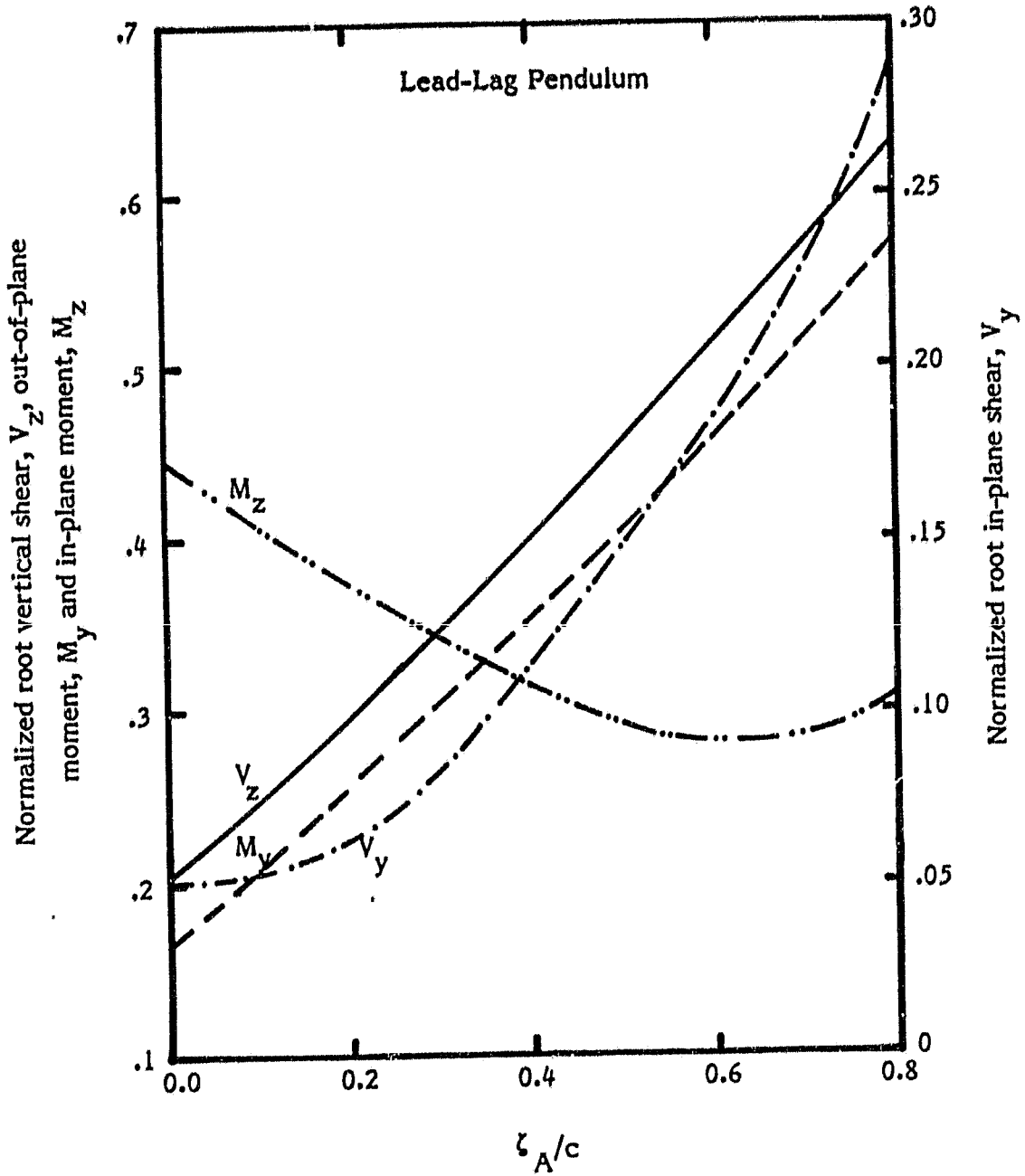Figure 32. - Pretwist effect for 4/Rev concentrated
exciation, nonuniform blade.
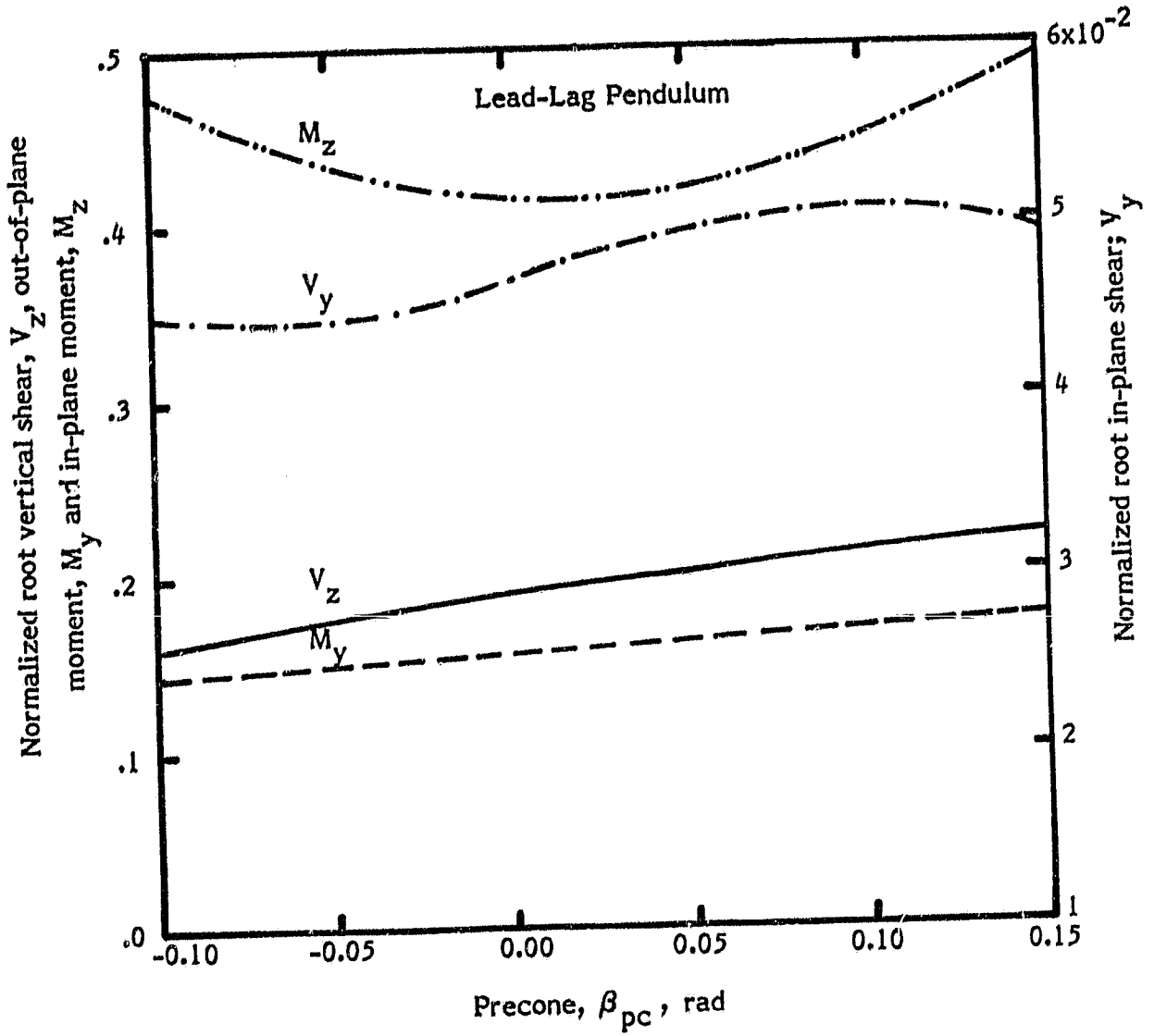
Figure 33. - Precone effect for 4/Rev concentrated
excitation, nonuniform blade.
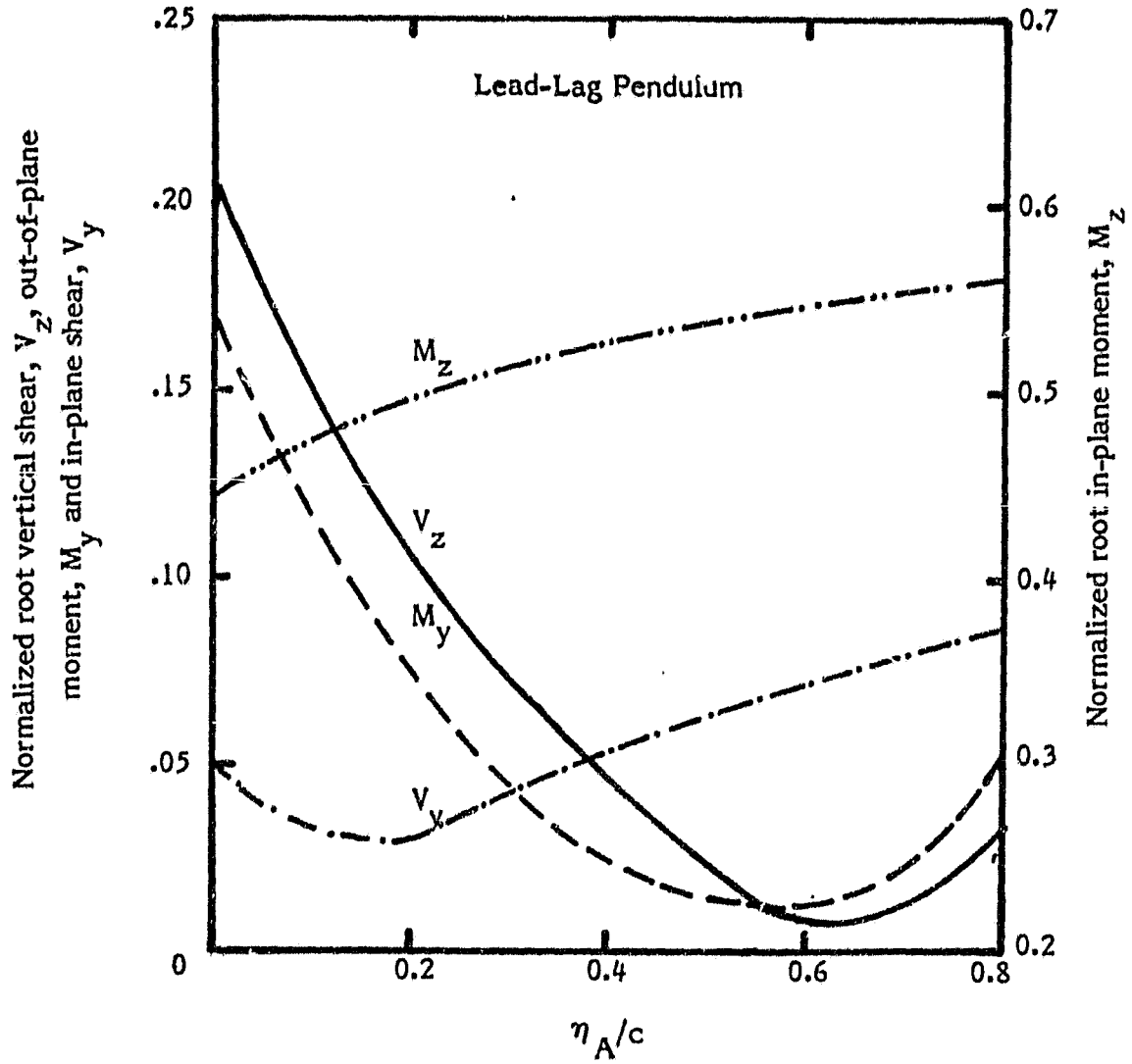
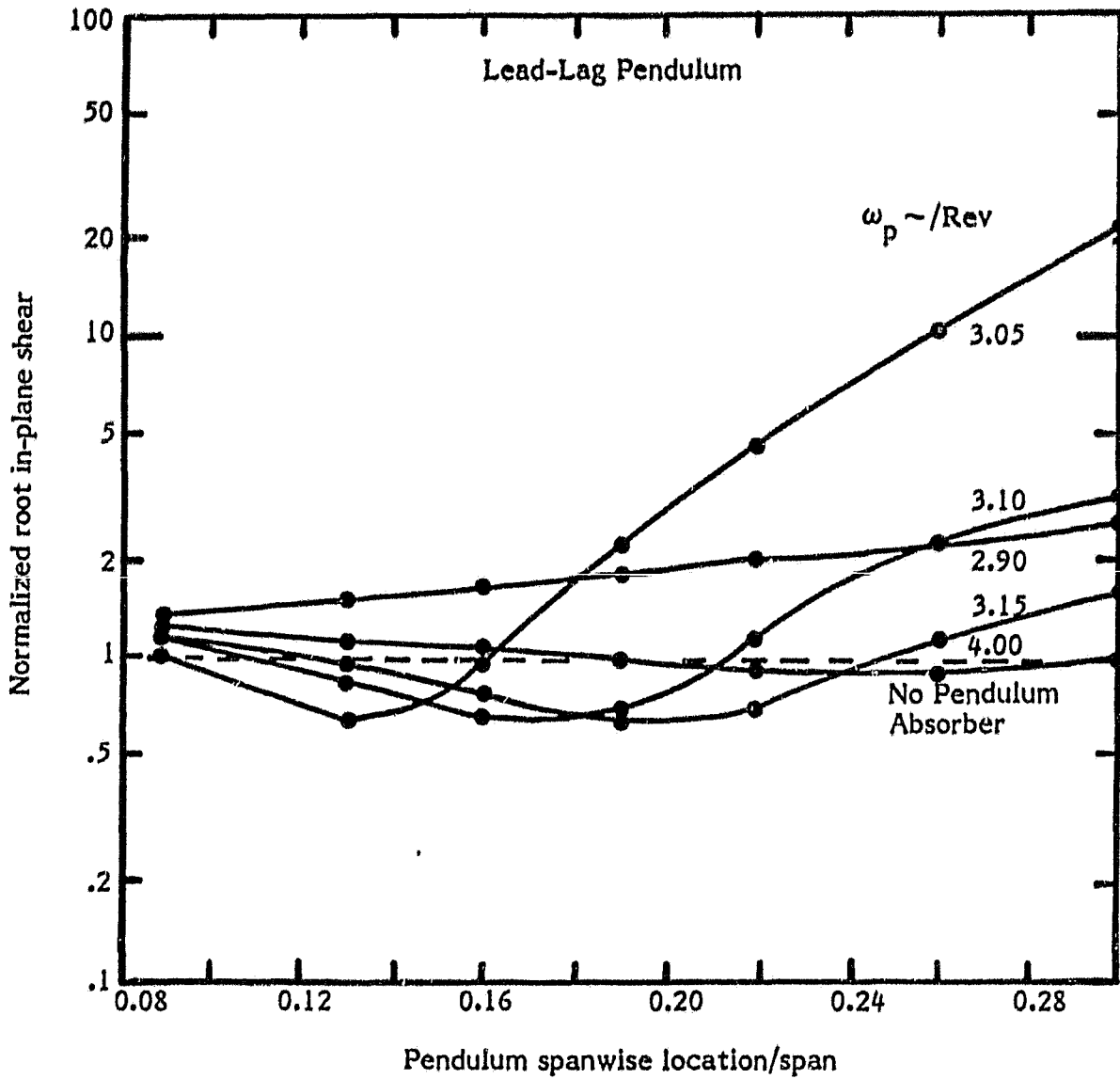Figure 34. - Pendulum chordwise hinge offset, η_A, effect for 4/Rev concentrated excitation, nonuniform blade.

Figure 35. – Pendulum vertical hinge offset, ζ_A, effect for 4/Rev concentrated excitation, nonuniform blade.

Figure 36. - Root in-plane shear for 3/Rev distributed airload excitation, nonuniform blade, W = 133.45 N, $\eta_A = \zeta_A = 0$.
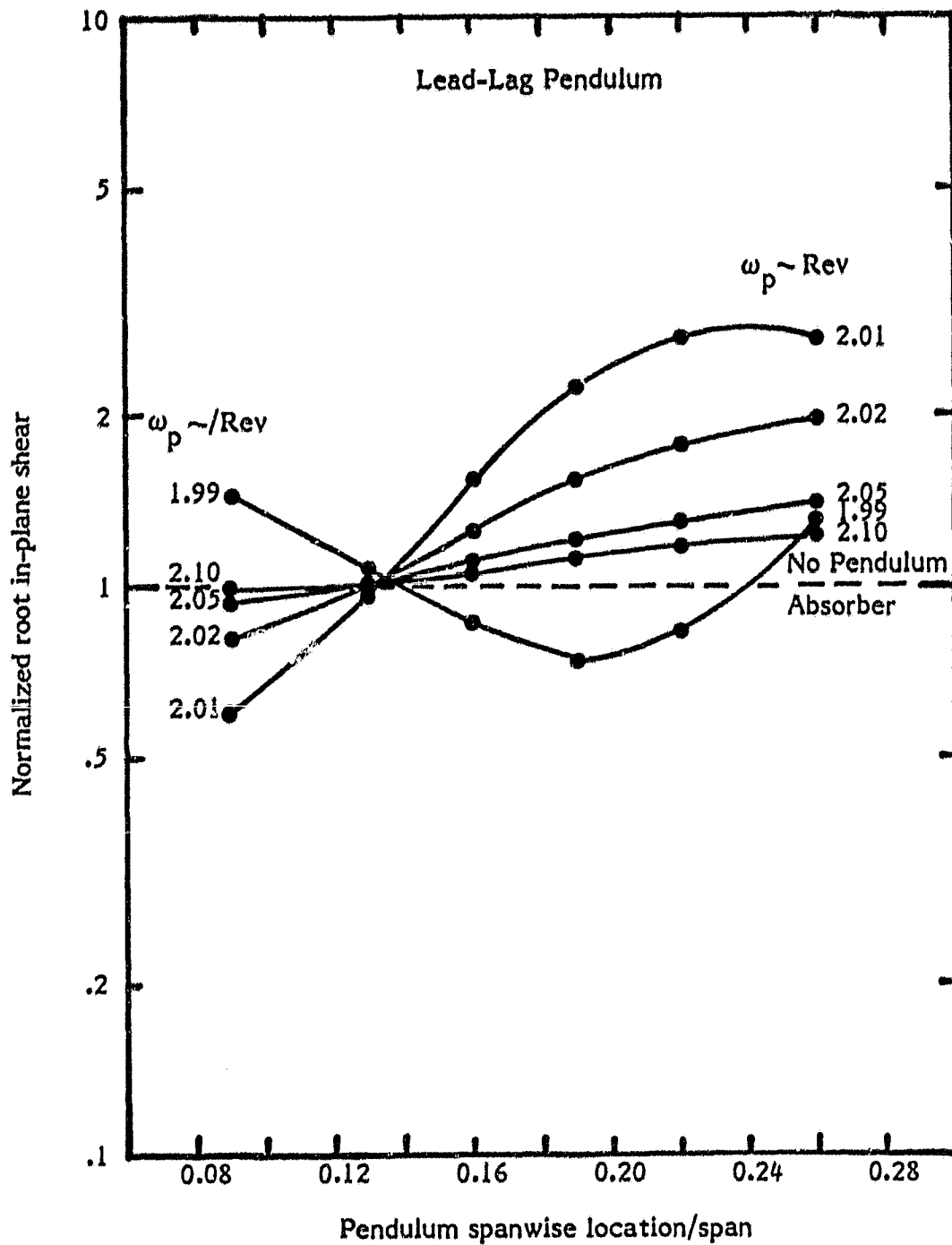
Figure 37. - Root in-plane shear for 2/Rev distributed airload excitation, nonuniform blade, $W = 133.45$ N, $\eta_A = \zeta_A = 0$.
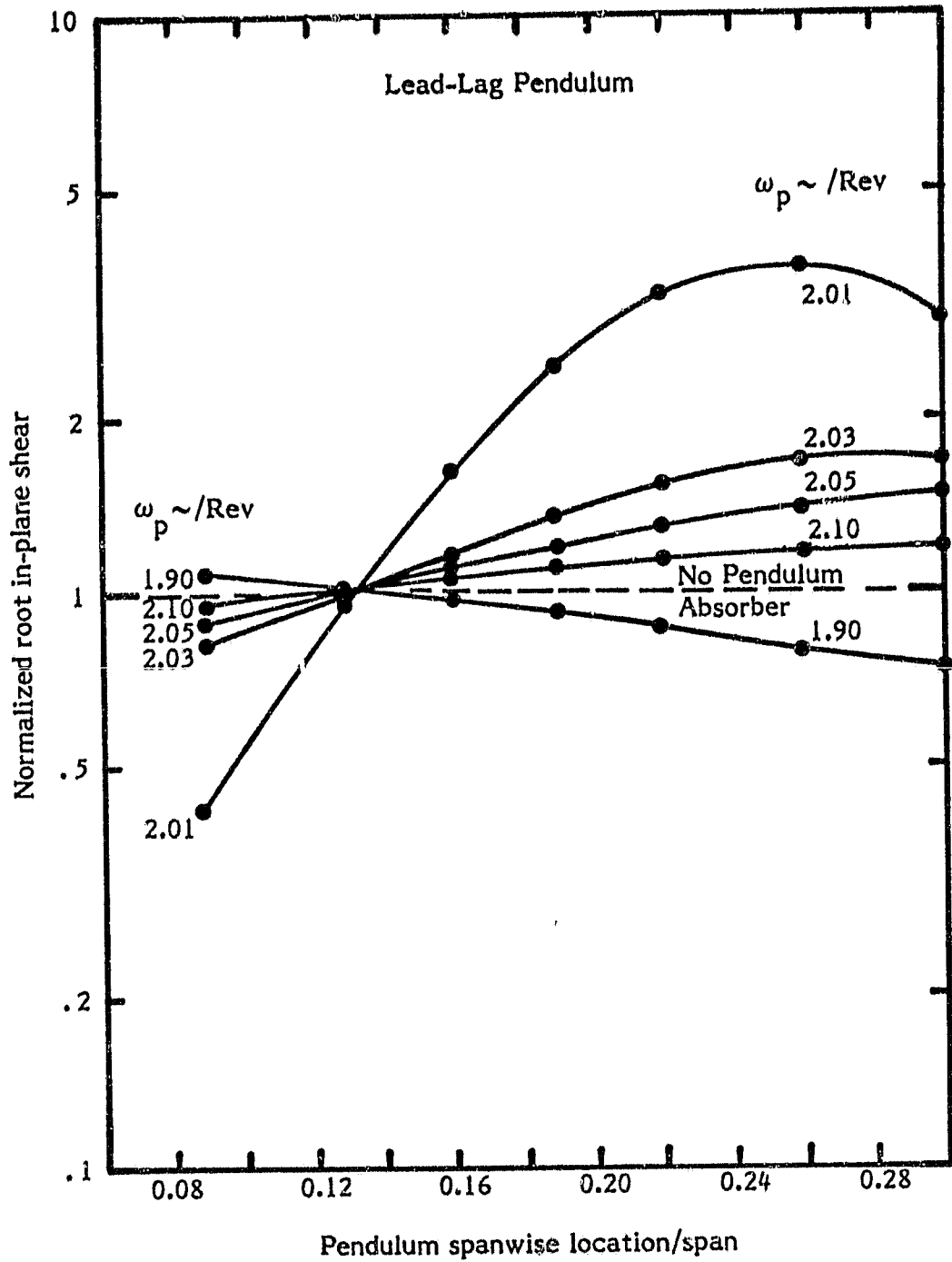
Figure 38. – Root in-plane shear for 2/Rev concentrated excitation, nonuniform blade, $W = 133.45$ N, $\eta_A = \zeta_A = 0$.